ANNUAL REPORT

SHEAR TRANSFER IN THICK WALLED REINFORCED CONCRETE STRUCTURES UNDER SEISMIC LOADING

NSF Grant AEN 73-03178 A01

January 1, 1974 to May 31, 1975

by

Richard N. White and Peter Gergely

December 1975 Report No. 75-10

This report was prepared with the support of the National Science Foundation, Grant No. AEN 73-03178 A01. However, any opinions, findings, conclusions, or recommendations expressed herein are those of the authors and do not necessarily reflect the views of NSF.

BIBLIOGRAPHIC DATA SHEET	1. Report No. NSF-RA-E-75-133	2.	3. Recipient's Accession No. PB 247 208
4. Title and Subtitle Shear Transfer in Thick Walled Reinforced Concrete Structures Under Seismic Loading (Annual Report-January 1, 1974-May 31, 1975)			5. Report Date December 1975 6.
7. Author(s) R.N. White, P. Gergely			8. Performing Organization Rept. No. 75-10
9. Performing Organization Name and Address Cornell University Department of Structural Engineering Ithaca, New York 14850			10. Project/Task/Work Unit No. 11. Contract/Grant No. AEN 7303178A01
12. Sponsoring Organization Name and Address Research Applied to National Needs (RANN) National Science Foundation Washington, D.C. 20550			13. Type of Report & Period Covered Annual 1/1/74-5/31/75 14.

15. Supplementary Notes

16. Abstracts The mechanism of membrane shear transfer under cyclic loading in thick-walled cracked reinforced concrete structures is studied. The specimens incorporate interface shear transfer and dowel action acting both alone and in concert. The results are used in a dynamic analysis program to predict nonlinear response of containment vessels. The work reported here includes: (1) experiments on specimens with 1/2 to 3/4 inch diameter reinforcing bars crossing a crack; (2) development of a mathematical model to predict stiffness characteristics of dowel action in thick concrete sections; (3) dowel action experiments (under cyclic loading) to correlate with the mathematical model predictions; (4) a dynamic analysis program that accounts for the non-linear load-slip behavior at a crack carrying reversing shear stresses; and (5) results of experiments on specimens with large bars (#14 maximum size) where shear is carried by combined dowel action and interface shear transfer.

17. Key Words and Document Analysis. 17a. Descriptors

Shear tests
Shear strain
Shear properties
Concrete structures
Dowels
Construction
Earthquake resistant structures
Structural design
Structural engineering

17b. Identifiers/Open-Ended Terms

Shear transfer
Seismic shear

17c. COSATI Field/Group

18. Availability Statement NTIS	19. Security Class (This Report) UNCLASSIFIED	21. No. of Pages 92
	20. Security Class (This Page) UNCLASSIFIED	22. Price PC A05/MF A01

1. SUMMARY

The mechanism of membrane shear transfer under cyclic loading in thick-walled cracked reinforced concrete structures is studied experimentally. The specimens incorporate interface shear transfer and dowel action acting both alone and in concert. The results are utilized in a dynamic analysis program to predict nonlinear response of containment vessels.

The work reported here includes:

a. experiments on specimens with 1/2 and 3/4 in. diameter reinforcing bars crossing a crack. Dowel action alone and combined interface shear transfer and dowel action are studied with external applied tension stress of 0 to 50 ksi on the bars. Cyclic shear stresses range from 150 to 400 psi.

b. development of a mathematical model to predict stiffness characteristics of dowel action in thick concrete sections.

c. dowel action experiments (under cyclic loading) to correlate with the mathematical model predictions.

d. a dynamic analysis program that accounts for the nonlinear load-slip behavior at a crack carrying reversing shear stresses. The program is used for 6 analyses of a typical reinforced concrete containment vessel subjected to different earthquake inputs. Stiffness characteristics at the cracks and soil conditions are also varied in the analysis.

e. results of experiments on specimens with large bars (#14 maximum size) where shear is carried by combined dowel

action and interface shear transfer.

2. APPLICATIONS TO ENGINEERING AND TECHNOLOGY

The results of this investigation will be used in the development of improved design and analysis techniques for treating the seismic behavior of thick-walled concrete structures. A major problem facing designers is the allocation of seismic shear to the various strength components that resist the shear, that is, how is the shear to be shared among the three mechanisms of: (a) interface shear transfer on the rough concrete surfaces at cracks, (b) dowel forces in reinforcing bars normal to the crack, and (c) inclined reinforcing?

The results of this research provide new insight into the shear transfer mechanism in cracked reinforced concrete and how it changes with the cyclic effect of seismic forces. The experimental studies furnish an improved basis for development of rational design criteria that properly account for the interface shear transfer mode of behavior, and for dowel action under cyclic load conditions.

The determination of internal seismic shearing forces in a cracked concrete structure (such as a nuclear containment vessel) is another major problem facing today's structural engineer. The dynamic analysis program described here provides an improved nonlinear analysis capability for cracked containment vessels and other cracked thick-walled concrete structures carrying seismic forces. The effects of earthquake characteristics, crack spacing and stiffness properties, and soil conditions may be assessed with this program.

Finally, the general understanding of shear transfer generated by this research will lead to better shear design methods for both seismic and non-seismic loadings in a variety of reinforced concrete structures.

3. RESEARCH RESULTS

Two completed studies on shear transfer are summarized in this report and preliminary remarks are made on a third major study that is nearly complete.

A. The first study is based on Eleiott's thesis in which he experimentally investigated shear transfer across cracks in reinforced concrete. The specimens were small scale (#4 and #6 reinforcing bars) and had combined dowel action and interface shear transfer.

B. The second study has several parts: (1) dynamic response of a typical containment vessel subjected to several different types of earthquakes, (2) formulation of a mathematical model of dowel action, and (3) experiments to measure dowel action and the effects of load cycling on dowel stiffness properties and cracking in the concrete.

C. The project nearing completion covers a number of experiments on large scale tests of specimens carrying shear by a combination of dowel action and interface shear transfer, along with analytical representations of the behavior.

A separate report on Subject B will be available in spring 1976 as a Departmental Report. Mr. Fajardo's thesis (Subject C) will form the basis for another separate report later in 1976. Interested readers may request copies of these reports directly from R.N. White.

In the following summaries the tables, figures and references for each subject are prefaced by the appropriate letter (A, B, or C).

4. PERSONNEL AND PUBLICATIONS

a. Personnel Involved in Research

The principal investigators, Richard N. White and Peter Gergely, received part-time academic year support and summer support in 1974. Prof. Gergely had the major responsibility for directing the research efforts of the graduate research assistants during the period September 1974-May 1975 while Prof. White was on sabbatical leave at the University of California, Berkeley. Prof. White was continuously involved in the project by correspondence during his leave and also planned and conducted a modest experimental program on dynamically loaded shear specimens while at Berkeley (to be reported in the next progress report).

Several graduate research assistants were supported by the grant Mr. Alan Eleiott received his M.S. degree in June 1974. Mr. Otto Fajardo completed the experimental phase of his Ph.D. thesis in shear transfer and will be completing his dissertation soon; he assumed a teaching position at the University of Texas (Arlington) in fall 1975. Mr. John Stanton concentrated on dowel action and on dynamic analysis of cracked concrete structures and is completing his M.S. thesis (May 1976 degree).

b. Publications

1. Eleiott, A.F., "An Experimental Investigation on Shear Transfer Across Cracks in Reinforced Concrete", M.S. Thesis, Cornell University, June 1974.

2. Laible, J.P., White, R.N., and Gergely, P., "An Experimental Investigation of Seismic Shear Transfer Across Cracks in Concrete Nuclear Containment Vessels", accepted for the ACI Seismic Symposium Volume.

3. Laible, J.P. and Gergely, P., "Nonlinear Dynamic Response of Cracked Reinforced Concrete Nuclear Containment Structures", Nuclear Design and Engineering, 30, September 1974, pp. 296-304.

4. Gergely, P., Stanton, J., and White, R.N., "Behavior of Cracked Concrete Nuclear Containment Vessels During Earthquakes", Proceedings, 1975 U.S. National Conference on Earthquake Engineering, June 1975.

5. Stanton, John, "The Dowel Action of Reinforcement and the Nonlinear Dynamic Analysis of Concrete Nuclear Containment Vessels", M.S. Thesis, Cornell University (May 1976).

c. Research Seminars

Prof. White presented seminars on "The Problem of Seismic Shear Transfer in Nuclear Containment Vessels" at the following universities:

University of Washington (Oct. 1974)

University of California (Nov. 1974)

Stanford University (April 1975)

A. REDUCED SCALE EXPERIMENTS ON COMBINED INTERFACE SHEAR TRANSFER (IST) AND DOWEL ACTION

A series of specimens with 3 in. by 5 in. shearing areas, reinforced with two different bar sizes (#4 and #6) were loaded in reversing shear to simulate a seismic shear loading. Behavior was determined for specimens carrying shear by (a) interface shear transfer (IST) alone, (b) dowel action alone, and (c) combined interface shear transfer and dowel action. In addition, the combination of cyclic shear and external tension applied to the bar crossing the crack was studied.

The experiments were conducted on a new form of specimen that presented some difficulties (one of the reasons for the study was to assess the adequacy of the specimen for large-scale tests). The results should be interpreted with this fact in mind; certainly the overall trends are valid but the precise values for some experiments may not be fully reliable.

Specimen Configuration and Loading

The specimen geometry and loading methods are shown in Fig. A1. The crack surfaces were formed in the intersection of the vertical members and the cross members to provide a total of 30 in^2 of shearing surface at each end of the specimen. Positive and negative shear loads across the two cracks were applied as shown in Figs. A1b, where the forces marked (+) and (-) indicate the loads and reactions for the two loading conditions. Slips and crack openings were measured with dial gages.

Specimens designed to study IST alone had no embedded reinforcing bars. Instead, they had external steel restraint rods across the cracks, as indicated in the upper part of Fig. A1b. With the nuts on the restraint rods in the loose position, the specimen was cracked by jacking metal plates into the V-shaped crack-initiating grooves case into the specimen. The desired initial crack width was then set by adjusting the nuts on the restraining system.

Specimens designed to study dowel action alone, and combined dowel action and IST, had embedded deformed reinforcing bars, one per shearing plane, as illustrated in the lower half of Fig. A1b.

Dowel action alone was achieved by casting greased steel plates in the shear planes with oversize holes at the reinforcing bar locations. No cracking was necessary in this specimen. For combined IST and dowel action, the specimens were cracked by tensioning the reinforcing bar against an independent external tubular steel frame.

In each test two shear planes were loaded simultaneously, and the resulting sets of displacements were averaged.

Interface Shear Transfer

Two tests were made to compare the IST mode behavior of the small scale specimens with that of the large specimens (300 in^2) used in all earlier tests. Specimen parameters were:

Concrete: f'_c	= 2920 psi with $\frac{1}{2}$ in. maximum aggregate
Restraint stiffness:	= 700 k/in on 15 in^2 shear surface
	= 46.7 ksi/in
Initial crack width:	= 0.030 in.
Shear stress:	= $\pm$ 150 psi
Load cycles:	= 15 full reversals of shear load

The behavior measured in the two tests was nearly identical and is shown for Test IST1 in Fig. A2. It is basically the same as that exhibited by the large scale specimens. The load-slip relationship is linear for loading in both directions during the first cycle. There is a pronounced "locking effect" during unloading and the neutral slip position can be reached only by reversing the load.

The slip increases with cycling but at a decreasing rate, increasing from 0.0135 in. in cycle 1 to 0.0175 in. in cycle 15. With each cycle, the "free slip" that occurs at low shearing stresses (less than 50 psi) increases, while the shear stiffness during the upper portion of the load cycle (from 50 to 150 psi) increases by a factor of nearly 4 from cycle 1 to cycle 15.

In the first cycle the shear resistance is provided primarily by bearing stresses between the particles projecting across the shear plane from one surface to the other. The loading and unloading action of the first cycle produces marked changes in behavior, and the free slip increases more between the 1st and 2nd

cycles than it does between the 2nd and 15th cycles. Once firm contact is made between the surfaces in the later cycles, the compacted concrete is stiffer and the sharply upward curving load-slip curve results.

Over-riding (and frictional resistance) becomes more prevalent as cycling wears down the surfaces. As the shear displacement increases, the over-riding action causes the crack to widen, thereby increasing the forces in the restraining bar which in turn increases the frictional resistance. Thus the restraint stiffness across the crack has substantially less influence in first cycle slip values than in later cycle slips. The results presented below verify this observation.

The results for large scale specimen J3 (from Laible) are shown in Fig. A2b for comparison. The J3 results are for $\pm$ 180 psi shear stress and a restraint stiffness of 7640 k/in on a 300 in^2 shearing surface; therefore direct comparisons of behavior are not possible.

The restraint stiffness for the small specimen was 83% higher than that for the large specimen. The small scale data are plotted in Fig. A3 along with a series of large scale test results. Specimen IST1 results appear to be consistent with the other data and no appreciable size effect is evident.

A summary of comparisons between specimens IST1 and J3 includes:

	Small scale specimen IST1	Large scale specimen J3
slip, cycle 1	0.016 in.	0.017 in.
slip, cycle 15	0.021 in.	0.031 in.
shear stiffness, cycle 1	11.1 ksi/in	9.9 ksi/in
shear stiffness, cycle 15		
free slip, cycle 1	0.0028 in.	0.0025 in.
free slip, cycle 15	0.014 in.	0.022 in.

Specimen IST1 results are scaled linearly from 150 psi shear up to 180 psi shear in the above comparisons. The higher shear stress level does produce more surface deterioration, however,

and these effects cannot be totally scaled. Thus it is expected that cycle 15 results will not compare as well as cycle 1 results. Also, the difference in restraint stiffness has more effect in the 15th cycle than in the 1st cycle.

Dowel Action

Several experiments were conducted to determine the behavior of specimens transferring cyclic shear by dowel action alone. Transfer of shear by dowel action is dependent upon preventing major dowel cracking along the bar, or by controlling such cracks with transverse reinforcement. Before cracking, slippage along the shear transfer plane is produced by bending of the bar and local deformation of the concrete under the very high local contact stresses. Consequently, the critical physical parameters are the diameter of the reinforcing bar and the concrete strength and stiffness.

The reinforcing across a crack ordinarily carries tension from either flexural action or membrane action. This tensile stress produces high localized bond stresses on each side of the shear plane that may lead to very small yet significant cracks around the bar and thus influence the shear stiffness.

The variables studied were:

1. diameter of reinforcing bar (1/2 and 3/4 in.)
2. axial stress applied to reinforcing bar, f_t = 0, 25, and 50 ksi.
3. level of shear stress - $\pm$ 150 psi and $\pm$ 180 psi for f_t = 0; $\pm$ 150 psi for f_t = 25 and 50 ksi. These shear stresses are computed on the basis of the concrete area. Actual average shear stresses on the dowel crossing the crack ranged from 5.1 to 13.5 ksi as detailed in Table A1.

In each specimen a single reinforcing bar was embedded at the center of the shearing plane. Interface shear transfer was prevented by casting greased plates in the specimen. Concrete strength varied from 2890 to 3130 psi.

Thirteen tests on four specimens are summarized in Table A1. Each specimen had two ends that were tested independently; they are marked with U (upper) and L (lower) in the table. Five tests (3a, 4a, 5a, 6a, and 8a) were done on specimens that had already been cycled according to the load history values given in Table A1 on the unlettered tests (3, 4, 5, 6, and 8). The number of specimens used to cover these parameters is inadequate, but again it must be realized that this program was designed to be exploratory and as an aid to planning large scale tests.

Dowel Action - Applied Axial Stress $f_t = 0$

Tests 1 and 2 on Specimen D1 resulted in early failure by dowel cracking because of twisting of the central loaded block around the reinforcing bar, and subsequent splitting produced by the wedging action of the deformed bars. The results of these tests are not meaningful and will not be reported here.

Specimen D2, with a #4 bar initially unstressed, was identical to Specimen D1 except the loading was changed to eliminate the twisting effects observed in D1. Discussion here will focus on tests 4 and 4a done on one end of the specimen.

The load-slip behavior for Tests 4 and 4a is summarized in Figure A4 and Table A2. The slip at $\pm$ 150 psi shear stress increased from 0.082 in. during cycle 1 to 0.0125 in. in the 15th cycle; the increase was negligible after 10 cycles. After 15 cycles at $\pm$ 150 psi shear, the loading was increased to $\pm$ 180 psi for 10 more cycles (Test 4a) with the response as shown in Fig. A4. The rate of increase of slip, which had become zero in Test 4, increased again when the shear stress level was raised. It appears that Test 4a behavior was not strongly influenced by the earlier 15 cycles at 150 psi, although the ratio of final maximum slips ($slip_{25}/slip_{10} = 1.42$) was greater than the ratio of shear stresses (180/150 = 1.2).

These load-slip curves have the same general shape as the curves for interface shear transfer except the first cycle loading in each direction has a slightly decreasing stiffness which must be due to localized concrete crushing from excessive bearing

stresses near the shear plane. There is also less free slip than in the IST mode, however, since the flexural stiffness of the reinforcing bar tends to return the specimen to a neutral slip value as it is unloaded. The free slip increased from 0.0008 in. on cycle 1 to 0.0052 in. in cycle 15, but the rate of increase decreased with cycling. In Test 4a the free slip increased by 35% in the 10 loading cycles, with 3/4 of this increase occurring in the first 5 cycles (16-20). The shear stiffnesses after free slip were essentially identical for cycles 10 and 25 in the two tests, which indicates that the shear stiffness approaches a constant value after a certain amount of cycling. If the shear stress level is then increased, the shear stiffness may initially decrease but subsequent cycling will bring it back to the previous level.

Tests 3 and 3a should have given the same results as 4 and 4a, but instead showed slips about twice as great as in the latter tests. Dowel cracking terminated the test on the 26th load cycle (19 at $\pm$ 150 psi and 7 at $\pm$ 180 psi shear). Since there is no feasible extraneous mechanism that could have enhanced the shear resistance in Tests 4 and 4a, and since the 3a test led to failure while the 4a test did not, it is concluded that some twisting action must have been present in Tests 3 and 3a to reduce the performance in shear.

Specimen D4 had a #6 reinforcing bar across each shear plane but was identical to D2 in all other respects. Tests 7 and 8 were done at $\pm$ 150 psi for 10 cycles and 5 cycles, respectively. The behavior is summarized in Fig. A5 and Table A3 where it is seen that the two tests gave essentially identical results.

The effect of bar size on shear stiffness is difficult to quantify because of the variable results achieved for the two #4 bar tests (3 and 4). The post-free slip stiffnesses at various cycles for the #6 bar tests were about 40 to 60% higher than those of Test 3 (#4 bar with highest slips). This agrees well with Baumann's prediction in Ref. A1 that the dowel shear stiffness varies as the diameter of the bar. On the other hand, Test 4 results for the #4 bar gave higher stiffnesses than measured in Tests 7 and 8 with the #6 bar.

The first cycle shear stiffness of the #6 bar (405 k/in) may be compared with results obtained by Baumann (A1) and Teller and Cashell (A2) on similar size bars. Baumann tested two 0.786 in. diameter bars in a concrete beam with f'_c = 5200 psi and obtained K = 619 k/in. This result is extrapolated to one 0.75 in. bar with f'_c = 3130 by

$$K = \left(\frac{3130}{5200}\right)^{\frac{3}{8}} \left(\frac{1}{2}\right)^{\frac{1}{4}} \left(\frac{0.75}{0.786}\right) (619) = 410 \text{ k/in}$$

This value compares very well with the measured K of 405 k/in.

Teller and Cashell obtained K = 333 k/in per 0.75 in. dowel in a specimen with a 3/4 in. crack width. This value becomes K = 585 k/in after applying the Teller and Cashell adjustment for the effect of crack width and scaling back from their high concrete modulus of 7120 ksi. With these rather severe adjustments it is not surprising that a 42% difference exists between the two K values (585 vs. 405 k/in).

An approximate analysis of the first cycle shear stiffness was made, modeling the reinforcing bar as a beam on a semi-infinite elastic foundation. This analysis indicates that within the narrow range of bar size studied, the effective foundation modulus K' is nearly independent of bar size and the shear stiffness K is of the form

$$K = \frac{d(K')}{0.23} \; 0.75$$

where d is the bar diameter and K' is about 1000 k/in^2.

Second and subsequent cycle behavior differs considerably from that of the first cycle. A large increase in the free slip occurs because of the concrete crushing action of the first cycle. The initial stress concentrations in the concrete are reduced by localized failures; thus after the free slip occurs, the elastic curve of the bar has a better contact with the compacted concrete and the shear stiffness increases. In some tests this behavior held true to the peak shear stress of cycle 2; in others, there was some decrease in shear stiffness near the peak of cycle 2, indicating some further substantial crushing action in the concrete under the bar. In later cycles (say after 10) the bar can firmly bed itself in the concrete without producing any significant new concrete crushing.

Dowel Action with Applied Axial Stress f_t = 25 or 50 ksi

The effect of applied external bar tension on shear stiffness was examined with Specimen D3 (Tests 5, 5a, 6, 6a on a #4 bar) and with Specimen D4 (Test 8a on a #6 bar).

A #4 bar tensioned to 25 ksi was cycled at $\pm$ 150 psi for 15 cycles in Test 5. The axial stress was then increased to 50 ksi, and a single cycle of shear load (Test 5a) produced a dowel cracking failure. This behavior is summarized in Fig. A6. Tests 6 and 6a were then run on the other end of the specimen, with one cycle at f_t = 25 ksi and 4 cycles at f_t = 50 ksi before the specimen cracked along the reinforcement (Fig. A7).

The crack widths and slips at several critical cycles are given in Table A4. At f_t = 25 ksi, the average crack width doubled during 15 cycles of shear, with nearly all of the increase occurring during the first cycle, and the slip increased by about 50%. On cycle 16 (Test 5a) the crack width again doubled when f_t was doubled from 25 to 50 ksi. In Test 6a, where the tensile stress was doubled on cycle 2, the crack width again doubled (from 0.0038 to 0.0075 in.) and increased to 0.0095 in. during four more cycles with f_t = 50 ksi.

Several observations can be made from these tests on #4 bars:

a. Shear displacements with f_t = 25 ksi were about twice those at f_t = 0 (compare Figs. A4 and A6.) Shear stiffnesses were correspondingly lower in the axially stressed case. This comparison must be tempered by the fact that the two tests at f_t = 0 differed considerably.

b. When f_t was increased from 25 to 50 ksi, the shear stiffness after free slip decreased by about 30% in the next shear cycle. This decreased stiffness indicates the additional bond-induced cracking produced by increased bar stress, which opens the crack and decreases the integrity and stiffness of the concrete around the bar. The first cycle shear stiffness with f_t = 50 ksi decreased substantially in the stress range from 100 to 150 psi, thereby demonstrating the additional damage done to the concrete. Some inelastic action in the reinforcing

may also have occurred under the combined stresses of 50 ksi tension, 11.2 ksi average shear, and the local bending stresses near the shear plane.

c. The shape of the upper portion of the load-slip curve during the first cycle at f_t = 50 ksi was the same in Tests 5a and 6a, even though the earlier cycling history at f_t = 25 ksi was considerably different in the two tests (15 and 1 cycles, respectively). The total slip and free slip values were greater in 5a, of course, but the shear stiffness after free slip was nearly identical to that in 6a.

d. Both ends of the specimen failed from dowel-induced cracks when the axial stress level was 50 ksi; one end carried four cycles of shear and the other only one. The difference in cycle numbers to failure can be attributed to the extra degree of damage done to the concrete by more extensive prior cycling with f_t = 25 ksi in Test 5 (15 cycles). The severity of combined high tension and cyclic shear is rather evident from this behavior.

The influence of axial stress on dowel action with a #6 bar was examined with Test 8a, where 10 cycles of shear stress ($\pm$ 150 psi) were applied with f_t = 25 ksi after the specimen was cycled 5 times with f_t = 0. The response is shown in Fig. A8 as cycles 6-15. The first cycle with f_t = 25 ksi (cycle 6) produced an increase in slip of 15% and a decrease in shear stiffness (after free slip) of about 30%. The slip increased rather sharply in the first 5 cycles (cycles 6-11) but had leveled off by cycle 15. The total increase in slip during the 10 load cycles was the same as that shown in 10 cycles with f_t = 0 in Test 7 (compare cycles 1 and 10 in Fig.A5 with cycles 6 and 15 in Fig. A8). The shape of the load-slip curve and the shear stiffness after free slip remained essentially unchanged during cycles 6-15, with only the free slip component increasing because of continuing deterioration of the concrete surfaces adjacent to the bar.

It may be concluded that combined cyclic shear of $\pm$ 150 psi (measured in terms of the concrete surface area) and axial stress of 25 ksi on the #6 bar is not substantially more damaging to the

concrete than cyclic shear stress alone. The improved performance of the #6 bar over the #4 bar is at least partially due to the fact that the same shear load was applied to both types of specimens; hence the shear stress and the bending stresses and deformations were substantially lower in the #6 bar. No tests were made with #6 bars stressed higher than 25 ksi tension, and it is not known if the application of 50 ksi would produce as severe as results as were measured with the #4 bar specimen.

In Test 8a a procedure was evolved to establish the axial restraint stiffness of the internally embedded reinforcement and its variation with increased cycling. At various times during a test, when the shear load had been decreased to zero before reversing the load direction, the axial stress in the reinforcement was released. The stress was then reapplied in increments and the crack width was measured after each step. A typical plot of crack width vs. bar stress is given in Fig. A9. The data is approximated with the straight dashed line, and its slope, multiplied by the bar area of 0.44 in^2, gives the axial stiffness of the combined bar-concrete specimen. In Fig. A9 the stiffness is K = 30(0.44)/ 0.00366 = 3600 k/in. This type of stiffness measurement was used mainly in the combined interface shear transfer and dowel action tests that are described in the following section.

Combined Interface Shear Transfer and Dowel Action

Combined interface shear transfer and dowel action was investigated on a double-ended specimen with a single #4 bar passing through each shear plane. The interface shear mode is highly dependent upon the normal restraint stiffness supplied by the reinforcement crossing the shear plane. With internal reinforcement, this restraint stiffness is determined in part by the bond between the steel and surrounding concrete. As the shear cycling progresses, dowel action results in crushing of the concrete around the bars, destroying the bond and changing the restraint stiffness. This process, which was studied for dowel action alone, will be less severe when interface shear transfer is also included because the increased shear stiffness and lower slips will decrease the rate of deterioration of bond.

Cracking of the specimen was achieved by tensioning the reinforcement and, when necessary, forcing wedges into the V-shaped crack initiating grooves at the crack plane. Both ends were cracked on the same day; one end was tested immediately and the other two weeks later. One end of the specimen was subjected to 45 cycles of shear with four different combinations of axial stress and shear stress (Tests 9, 9a, 9b, and 9c in Table A5). The other end was loaded with 28 cycles and three different stress combinations (Tests 10, 10a, and 10b in Table A5).

Axial stress in the reinforcing bar at the peak shear stress is of major importance in these tests. High axial stresses produce slip between the reinforcement and concrete. This damages the concrete, resulting in larger dowel shear displacements. The axial stress in the reinforcement is increased by the overriding of surface irregularities. This not only decreases the dowel stiffness but may also result in yielding of the bars if the initial axial stress is high or the steel ratio is low. When the reinforcement yields, neither dowel resistance nor the frictional component of interface shear transfer can increase further until large shear displacements produce kinking of the reinforcement.

Measurement of the bar stress at the crack was done indirectly by first measuring the effective axial stiffness of the bar at the crack by the procedure described in the earlier section on dowel action. This stiffness, multiplied by the increase in crack width between zero shear load and peak shear load, was used to estimate the change in bar stress at the crack during shear loading. This method of stress measurement was felt to be better than the use of strain gages on the bar that might interfere with bond between concrete and reinforcing.

The load position was adjusted at the end of the first cycle to force the slips on each of the two shear planes to be equal. In some tests the two shear planes still had significantly different stiffnesses because the crack widths became different with cycling.

The two variables in this test series were:

1. axial stress level, f_t - 25 or 50 ksi
2. shear stress level of 150, 250, and 400 psi

Test results are summarized in Table A5. Test 9 was the only test made with f_t = 25 ksi. Ten cycles of $\pm$ 150 psi shear produced extremely small slips and crack widths (about 0.001 in. each) and essentially no damage to the concrete and bond strength of the bar. No load-slip curves were plotted for this test. The #4 bar stress increased about 2 ksi at peak shear load.

In Test 9a, the axial stress level was raised to 50 ksi and shear cycling at $\pm$ 150 psi was done for 15 cycles (cycles 11-26 in Fig. A10). It is seen in the figure that the shapes of the load-slip curves for cycles 15 and 25 are intermediate to those determined earlier for interface shear transfer alone and dowel action alone, and that the slips are smaller. After about five shear cycles, the slip stopped increasing and there was little further degradation of the shear transfer characteristics.

Test 9b consisted of 10 cycles at $\pm$ 250 psi shear with f_t held at 50 ksi. The slips increase rather sharply during the first seven cycles (Fig. A10b) and the shapes of the load-slip curves remained about the same as in Test 9a (Fig. A10a).

The final loading (Test 9c) was cycled ten times at $\pm$ 400 psi shear with f_t = 50 ksi. Again the slips increased quickly during the first three cycles and then leveled off at about 0.01 in. as shown in Fig. A10b.

Cracks widths and slips in each of the two shear planes in each test were quite nonuniform, particularly in the earlier load cycles. By the end of the 45 load cycles the two planes were responding nearly identically, as shown in Fig. A11a. The crack widths and slips and the incremental values are given in Table A5 (Cols. 4-9) for the first and last cycle of each test. Values are tabulated for each shear plane and the average of the two planes.

Restraint stiffness was determined at each shear plane from measurements such as those shown in Fig. A11b. The values are given in Col. 10 of Table A5. The right plane (marked R) showed a marked decrease in stiffness during cycling, decreasing from 373 ksi/in to 213 ksi/in, while the other plane (L) remained essentially constant at 111 ksi/in. The reason for the difference is not known. Bar stresses calculated from these stiffnesses and

the changes in crack width during shear loading are given in Col. 11 of Table A5. In both shear planes the bar stresses at the crack during peak shear increased over the applied force of 50 ksi during cycling, with the right plane showing significantly higher axial stress. The increase in bar stress is a measure of the normal forces developed between the two concrete surfaces as overriding occurs during shear loading.

Free slip values are given in Col. 12 of Table A5. The free slip increased from 0.0012 in. in the 5th cycle of Test 9a to 0.0054 in. in the 5th cycle of Test 9c. Shear stiffness after free slip had occurred remained nearly constant during cycling (Col. 13 in Table A5).

Tests 10, 10a, and 10b had the same stress levels as Tests 9a, 9b, and 9c. Since response had stabilized in Test 9a after 10 load cycles, Test 10 was sone with only 10 cycles. Results are summarized in Fig. A12 and in Table A5. The load-slip curves for Tests 10 and 10a in Fig. A12b are nearly identical to those for tests 9a and 9b in Fig. A10; in both cases the final slip after cycling at $\pm$ 250 psi shear is about 0.0075 in. There was good correlation between the two sets of tests.

A major difference in behavior was observed at $\pm$ 400 psi shear, where slips and crack widths increased dramatically in Test 10b and the specimen was near failure from excessive cracking at the end of eight cycles. This rather severe degradation in Test 10b is also evident in Fig. A13, which compares the slips at similar load cycles, and in Col. 13 of Table A5 where the shear stiffness was only half the usual value by cycle 5 of Test 10b. Such differences in behavior at this very high shear stress and axial stress level, where cracking is imminent and slight differences in the quality of the specimen, or in secondary effects introduced by loading position inaccuracies can be important.

An estimate of the relative contribution of dowel action and interface shear transfer in carrying shear may be made by comparing the stiffness of #4 dowel action alone with the stiffness of the combined mode. In dowel action Tests 5 and 6 the shear stiffness was about 250 k/in after cycling, or 250/30 = 8.3 ksi/in. This stiffness is not sensitive to the size of crack in this study and

thus may be used as a good estimate of the dowel stiffness in the combined mode, where the total stiffness was about 67 ksi/in. Thus it is concluded that for a #4 bar in 15 in^2 of concrete surface (ρ = 1.33%), and with a shear stress of $\pm$ 150 psi, about 12% of the shear stiffness is provided by dowel action and 88% by interface shear transfer on the concrete surfaces.

Summary

Several general observations can be made from this study:

1. Small-scale interface shear transfer specimens give results comparable to large-scale specimens.

2. It is not known if dowel effects can be scaled with reasonable accuracy; it is felt that they most likely cannot if the scaling is to go from small bars such as #4 or #6 up to prototype #18 bars.

3. The load-slip relationship for dowel action alone is qualitatively similar to that for interface shear transfer except the return to a neutral slip position after unloading is more complete for dowel action.

4. Dowel action during the first cycle of shear loading differs sharply from that in subsequent cycles.

5. The presence of applied axial tension of 25 to 50 ksi on a #4 bar prior to application of shearing forces produces a substantial decrease in shear stiffness and large increases in slip at the shearing plane. High levels of axial tension can also contribute to earlier splitting failures along the bar. The larger #6 bar was less sensitive to axial load effects.

6. Yielding of reinforcing may be a problem when high axial loads are superimposed on dowel-action shearing stresses in the rebars; this needs very careful study in future tests.

7. The general behavior modes and sensitivities to axial stress observed for dowel action alone also hold true for combined dowel action and interface shear transfer.

REFERENCES

A1. Baumann, T., "Versuch zum Studium der Verdubelungswirkung der Biegezugbewehrung eines Stahlbetonbalken," Bericht Nr. 77, Materialprufungsamt fur des Bauwesen der Technischen Hochscule Munchen, 1968.

A2. Teller, L. W. and Cashell, H. D., "Performance of Dowelled Joints Under Repetitive Loading", Public Roads, A Journal of Highway Research, Bureau of Public Roads, U.S. Department of Commerce, Washington, D.C., April 1958.

Specimen	Bar size	f'_c, psi	f_y, ksi	Upper or Lower end	Test no.	Axial stress	Average shear stress: On surface area psi	Average shear stress: On dowel ksi	Cycles
D1	4	2890	40	U	1	0	150	11.25	2
				L	2	0	150	11.25	5
D2	4	2980	40	U	3	0	150	11.25	19
				U	3a	0	180	13.5	7
				L	4	0	150	11.25	15
				L	4a	0	180	13.5	10
D3	4	3080	75	U	5	25	150	11.25	15
				U	5a	50	150	11.25	1
				L	6	25	150	11.25	1
				L	6a	50	150	11.25	4
D4	6	3130	60	U	7	0	150	5.1	10
				L	8	0	150	5.1	5
				L	8a	25	150	5.1	10

Table A1 - Dowel Action Specimens

Test	Cycle No.	Slip, in.	Free slip, in.	Shear stiffness, k/in.
3	1	0.0165	0.0015	280
	2	-	0.0067	340
	10	-	0.0103	260
3a	1	0.082	0.011	150
	5	0.124	0.015	140
4	1	0.0082	0.0008	600
	2	-	0.0025	650
	10	-	0.0052	500
	15	0.0125	-	-
4a	1	0.0135	0.0056	500
	5	-	0.0070	510
	10	0.0170	0.0076	500

Table A2 - Dowel Action, #4 bar with $f_t = 0$ (Tests 3,3a,4,4a)

Test	Cycle no.	f_t, ksi	Ave. crack width, in.	Slip, in.	Free slip, in.	Shear stiffness, k/in
7	1	0		0.0112	0.0015	410
	2	0		-	0.0050	450
	10	0		0.0159	0.0077	480
8	1	0		0.0110	0.0017	400
	2	0		-	0.0045	430
	5	0		0.0156	0.0075	470
8a	1	25		0.018	0.0070	340
	5	25		-	0.0115	365
	10	25		0.023	0.0126	365

Table A3 - Dowel Action, #6 bar (Tests 7,8,8a)

Test	Cycle no.	f_t, ksi	Ave. crack width, in.	Slip, in.	Free slip, in.	Shear stiffness, k/in
5	1	25	0.0026	0.021	0.0025	220
	10	25	-	-	0.0108	310
	15	25	0.0051	0.033	-	-
5a	16	50	0.0101	0.0393	0.0130	200
6	1	25	0.0038	0.0185	0.0032	240
6a	2	50	0.0075	0.0265	0.0048	180
	5	50	0.0095	0.0333	-	-

Table A4 - Dowel Action, #4 bar with f_t = 25 or 50 ksi (Tests 5,5a,6,6a)

Test	f_t, ksi (1)	shear, psi (2)	Cy-cycles (3)	Crack Width x 10^4, in 1st cycle (4)	Crack Width x 10^4, in last cycle (5)	Crack Width Δ (6)	Slip x 10^4, in 1st cycle (7)	Slip x 10^4, in last cycle (8)	Slip Δ (9)	Re-straint stiff-ness (10)	Peak bar stress, ksi (11)	Free slip x 10^4 in, at cycle no. (12)	Shear stiff-ness, ksi/in at cycle no. (13)
9	25	150	10	8	12	4	7	12	5	-	27		
9a	50	150	15	L=100 Ave= 58 R= 16	100 71 42	0 14 28	45 26 8	45 30 16	0 4 8	111 373	54 60-68	12 @ 5 15 @ 15	65 @ 5 78 @ 15
9b	50	250	10	100 73 46	100 88 76	0 14 28	57 42 26	67 71 75	10 28 -	111 213	56 70	27 @ 5 40 @ 10	66 @ 5 67 @ 10
9c	50	400	10	75	95	17	90	119	29	111 191	62-68 73-82	51 @ 5	70 @ 5
10	50	150	10	180 96 12	180 120 60	- 24 -	42 21 4	42 31 20	0 10 16	100 130	60 50	13 @ 5 23 @ 10	104 @ 5 111 @ 10
10a	50	250	10	136	136	0	50	80	30	78 186	62 50-69	32 @ 5 39 @ 10	67 @ 5 67 @ 10
10b	50	400	8	148	268	120	115	335	220	107 167	65 66	105 @ 5	33 @ 5

Table A5 - Combined IST and Dowel Action

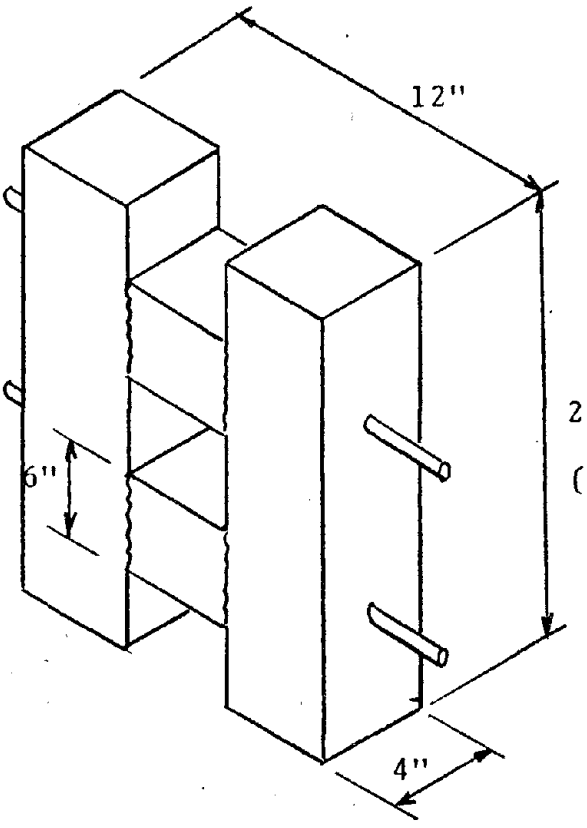

(a) specimen dimensions

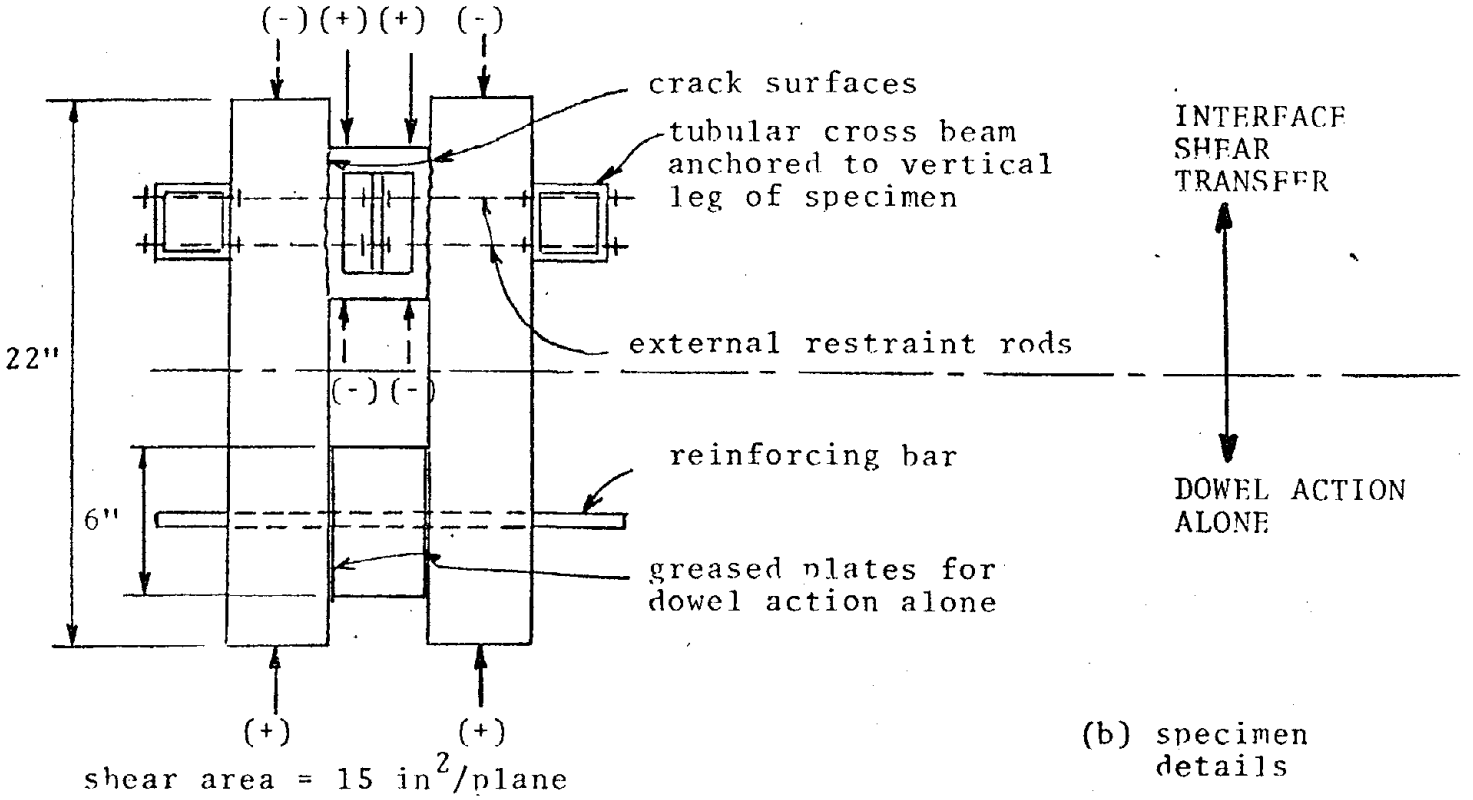

(b) specimen details

Fig. A1 - specimen geometry

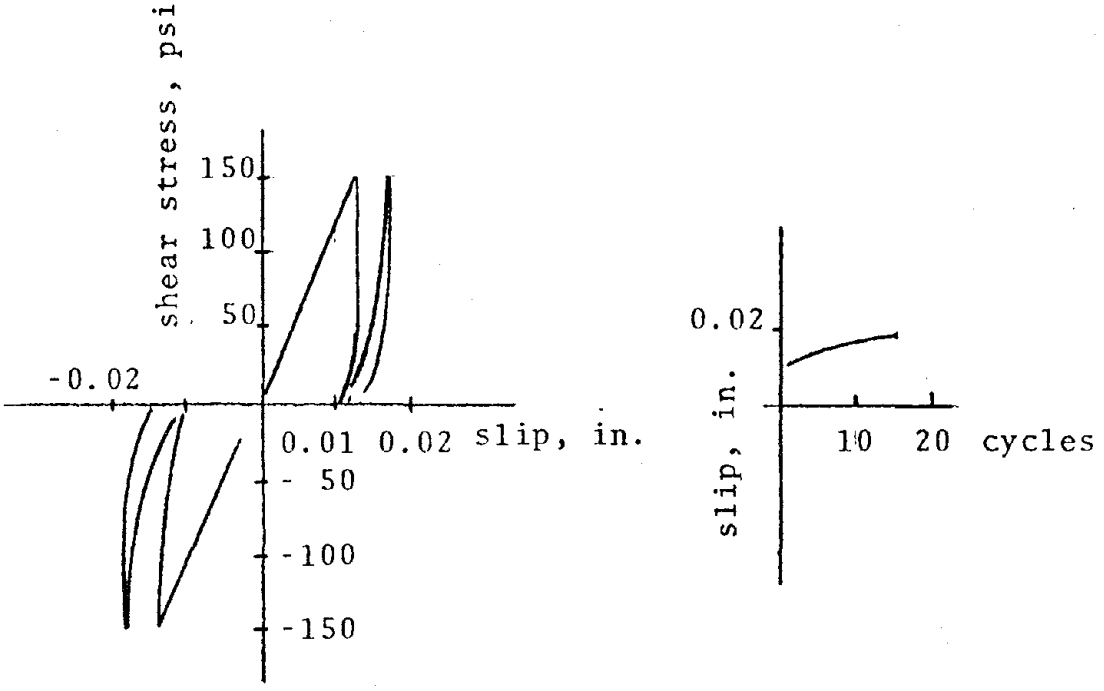

(a) small scale specimen IST1, 15 in^2 shear area

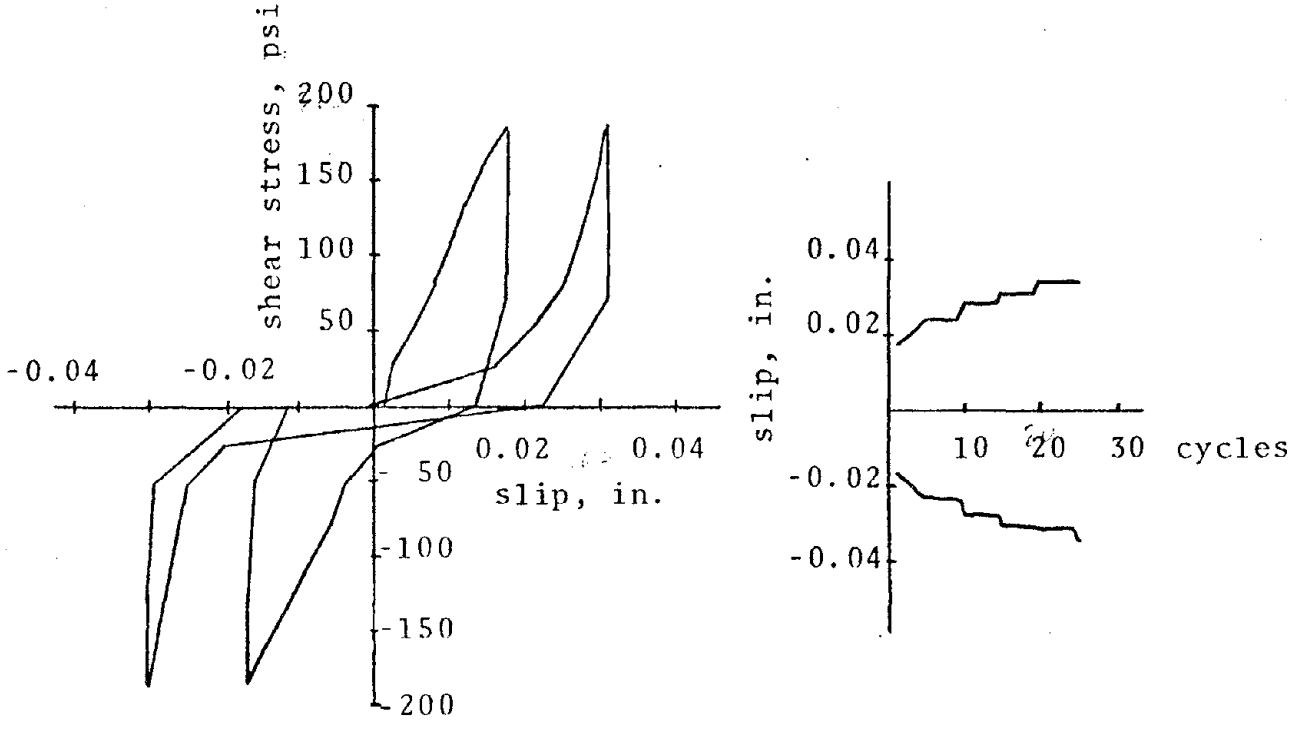

(b) large scale specimen J3, 300 in^2 shear area

Fig. A2 - variation of slip with shear stress and with cycling, interface shear transfer

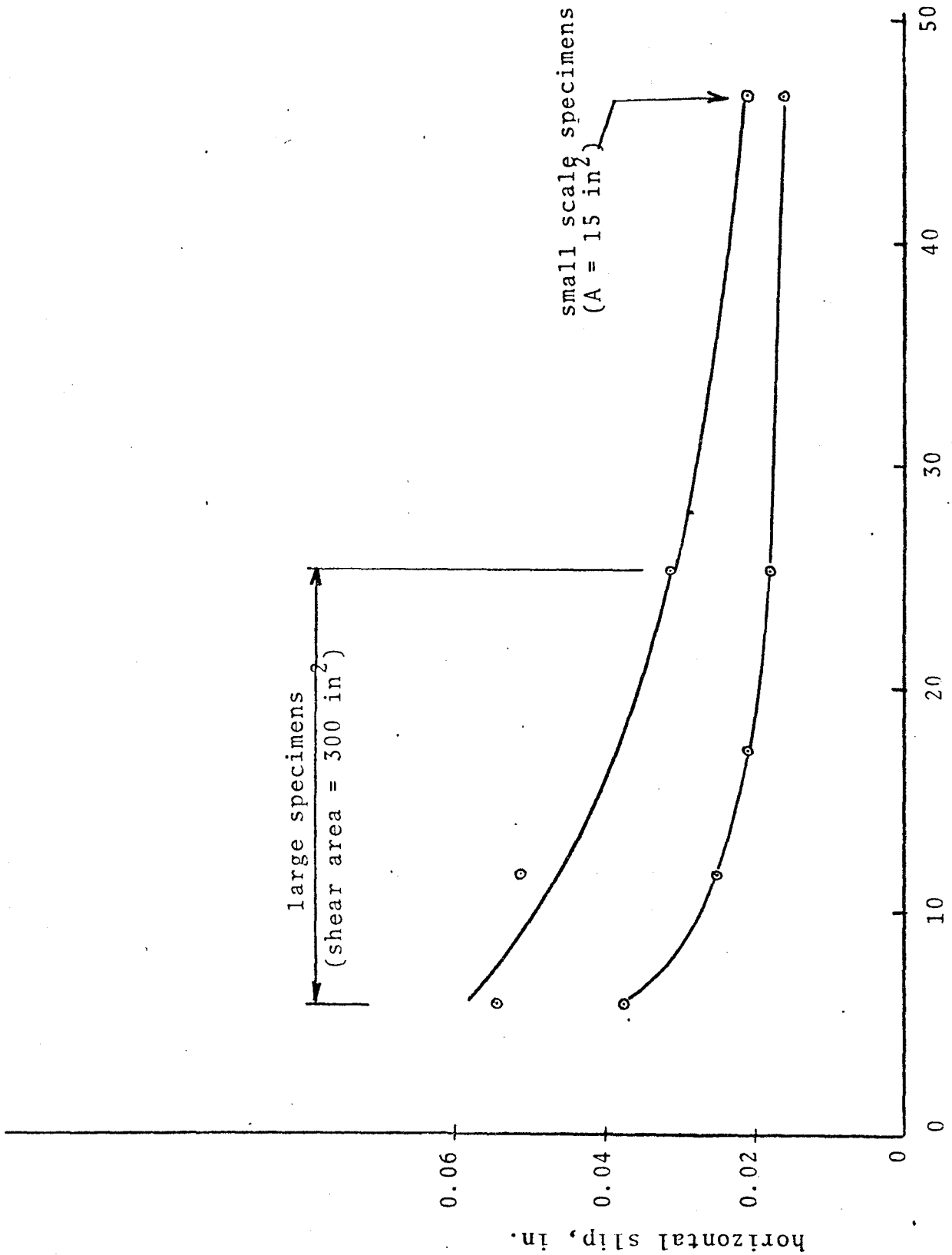

Fig. A3 - shear slip vs. restraint system stiffness

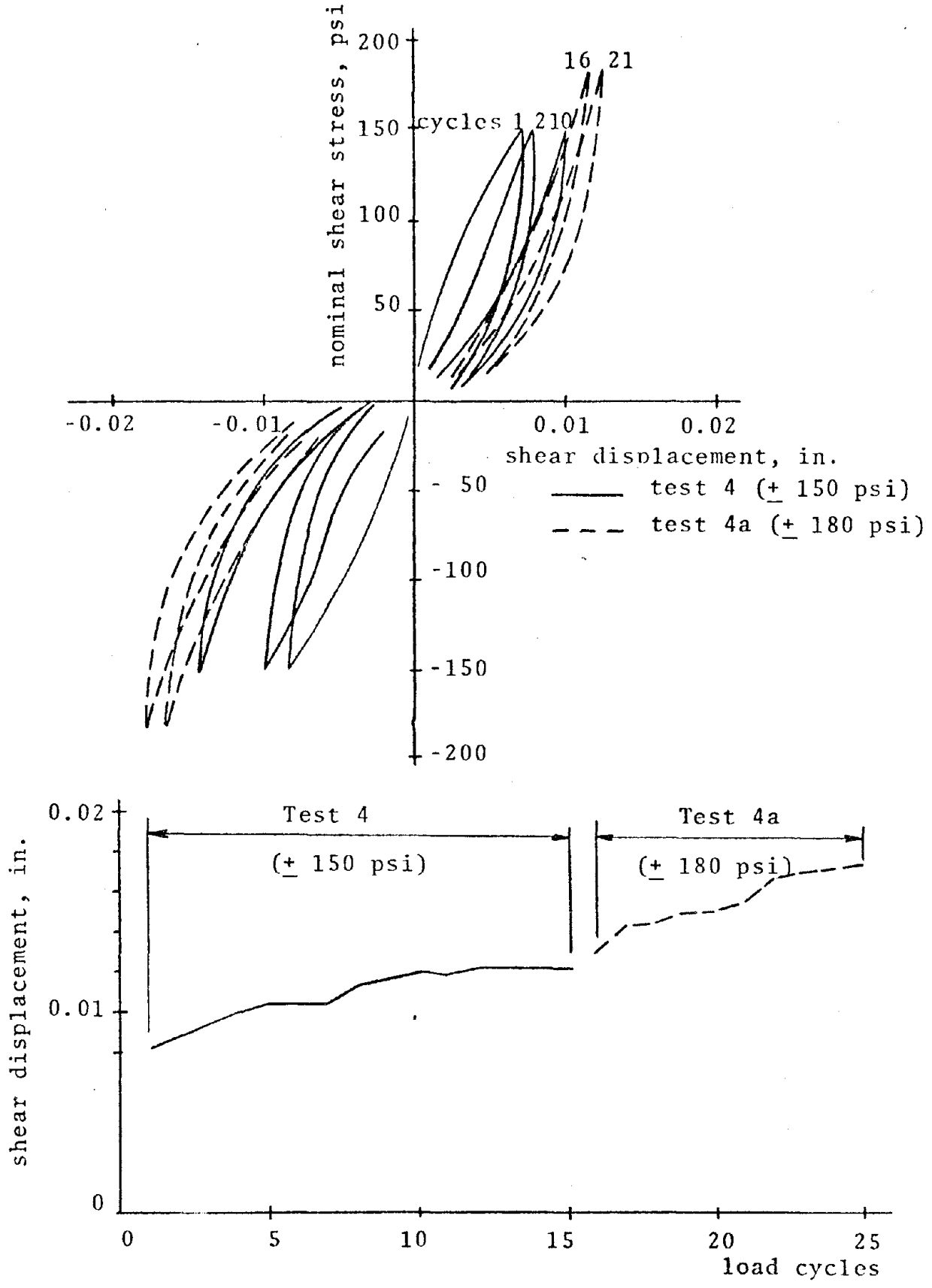

Fig. A4 - dowel action, #4 bar, axial stress $f_t = 0$

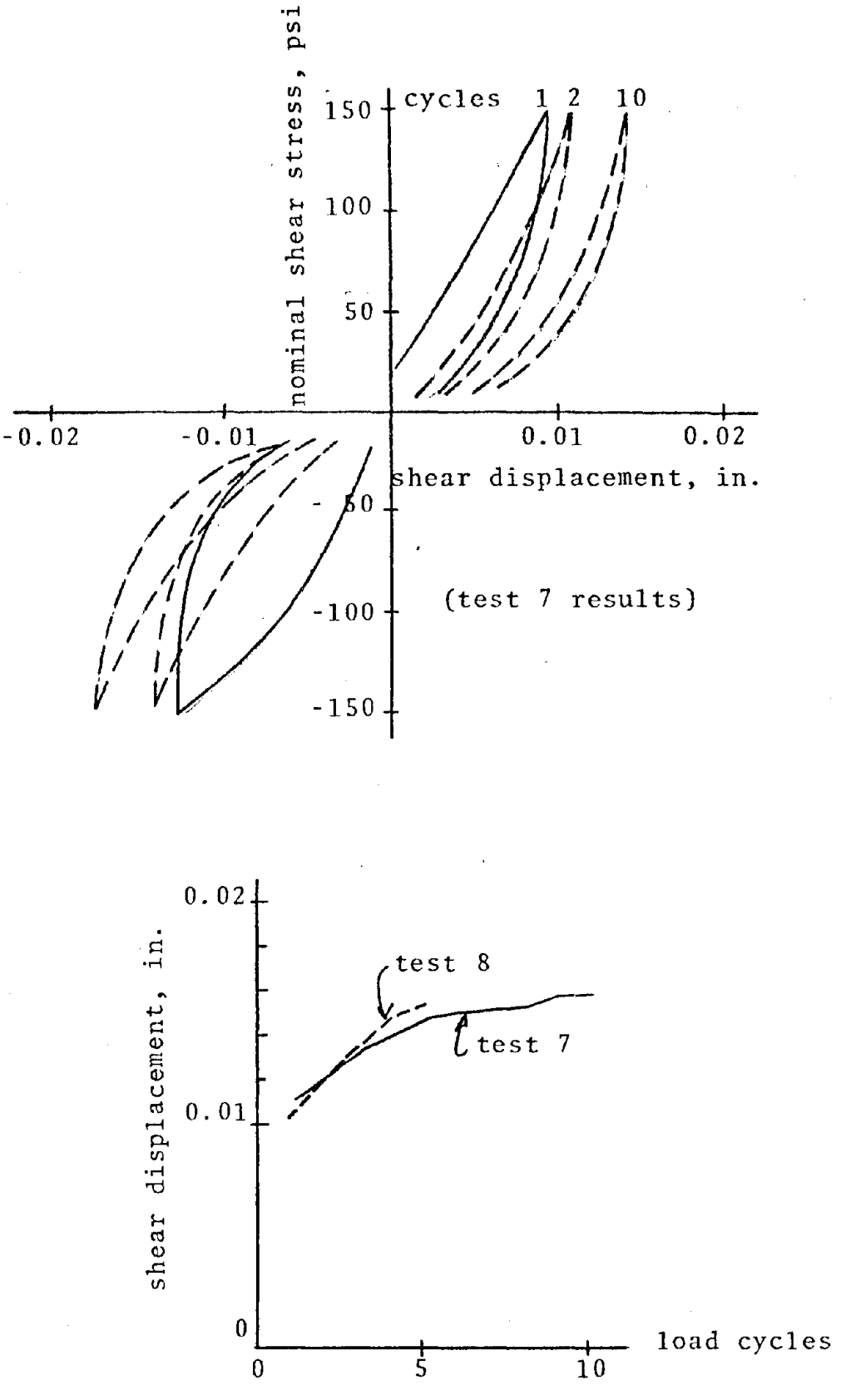

Fig. A5 - dowel action, #6 bar, axial stress $f_t = 0$

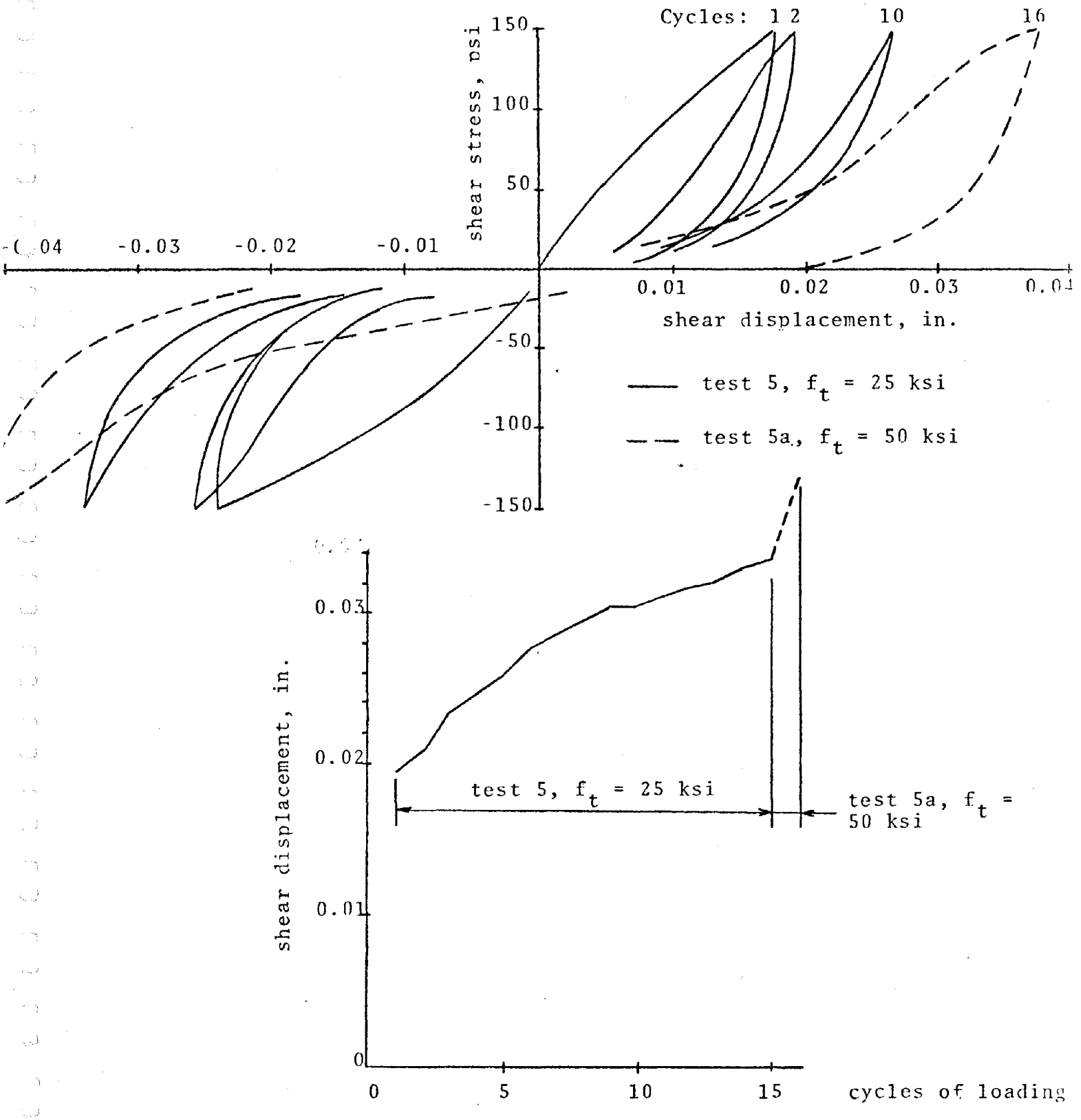

Fig. A6 - effect of axial stress on dowel action, #4 bar

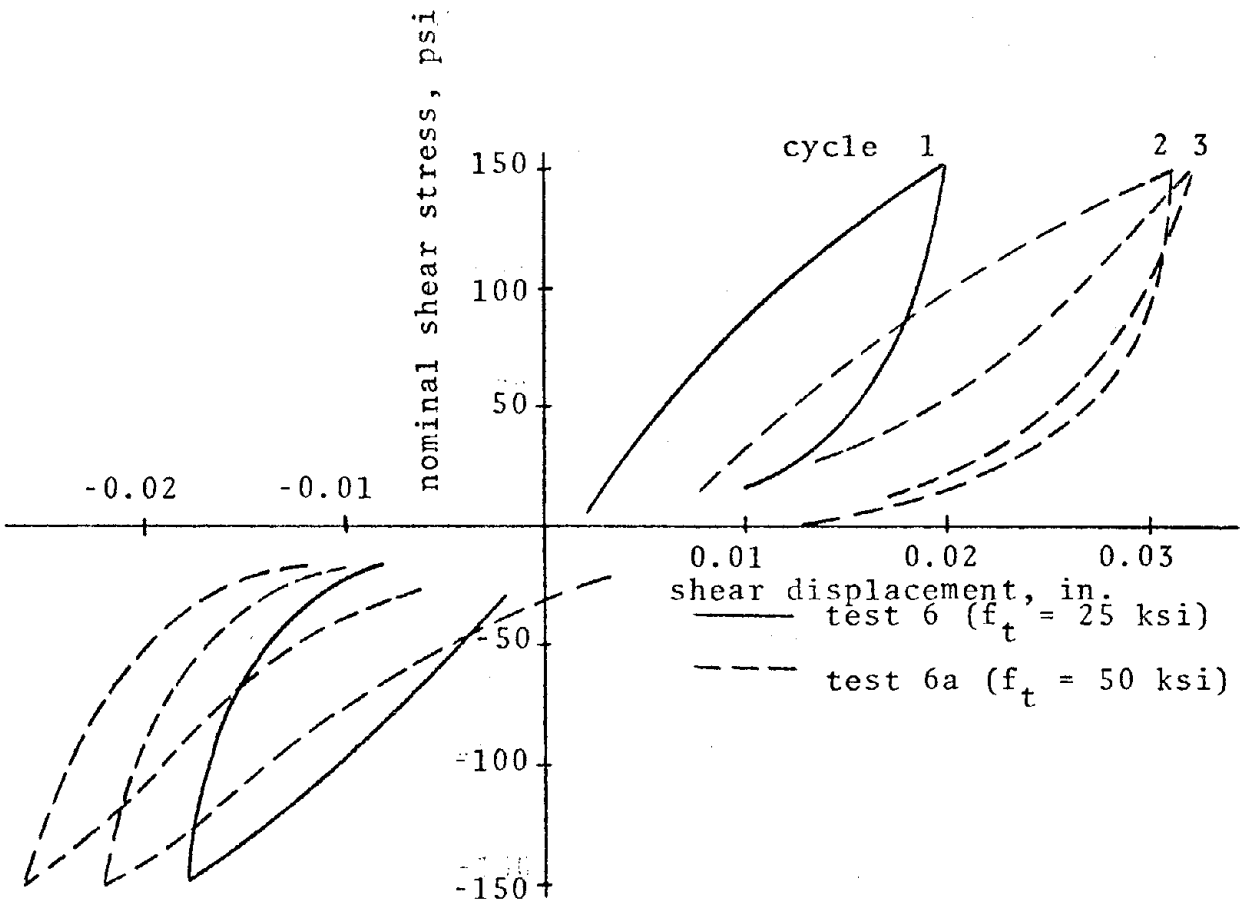

Fig. A7 - effect of axial stress on dowel action, #4 bar

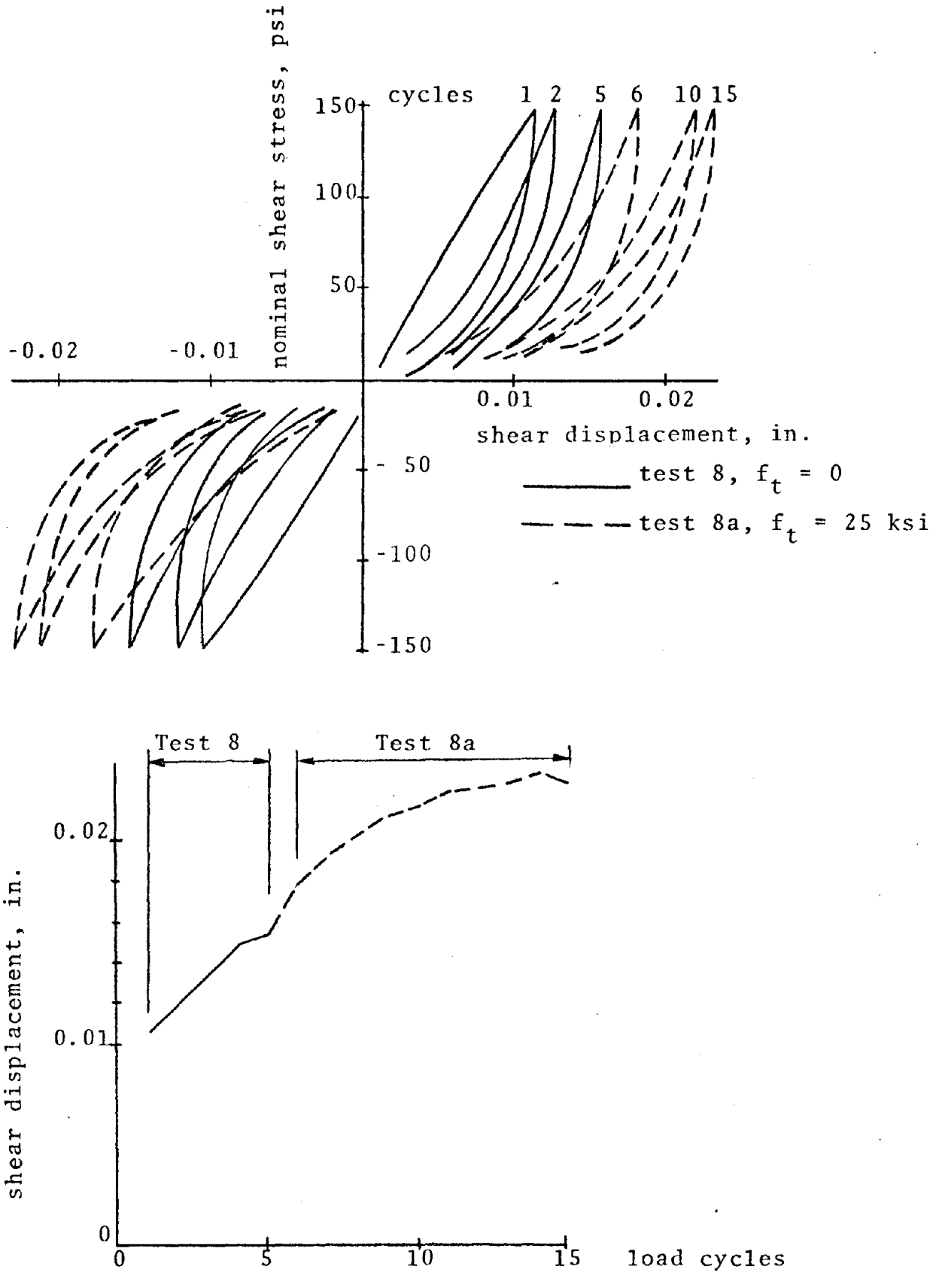

Fig. A8 - effect of axial stress on dowel action, #6 bar

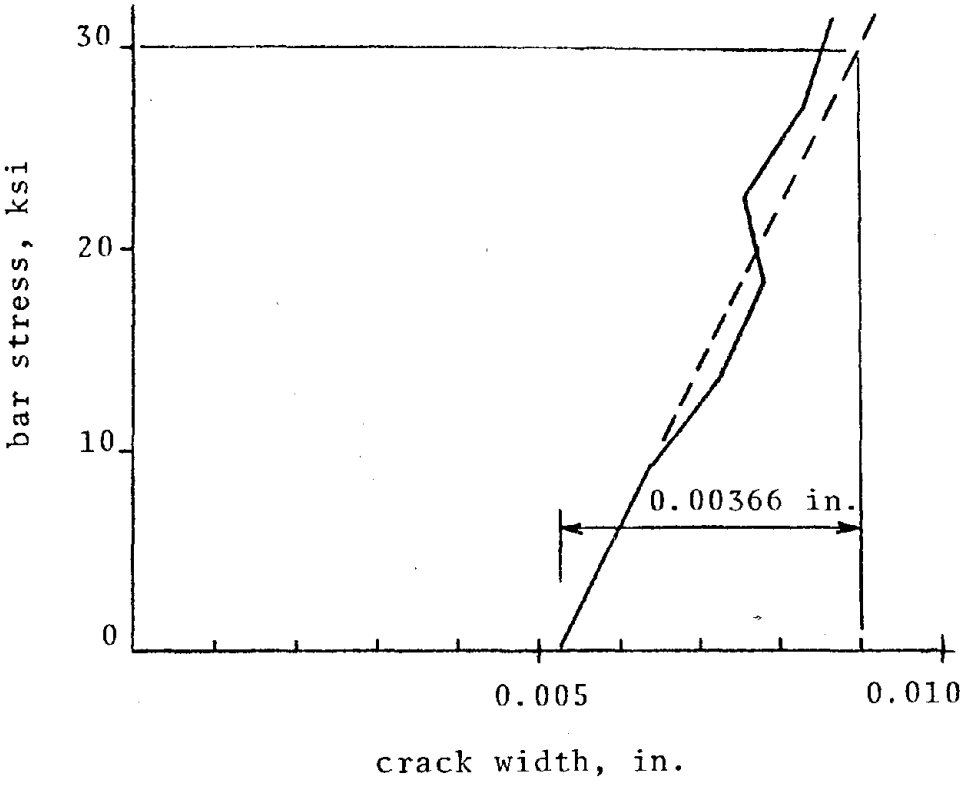

Fig. A9 - measurement of normal restraint stiffness of #6 bar after cycling

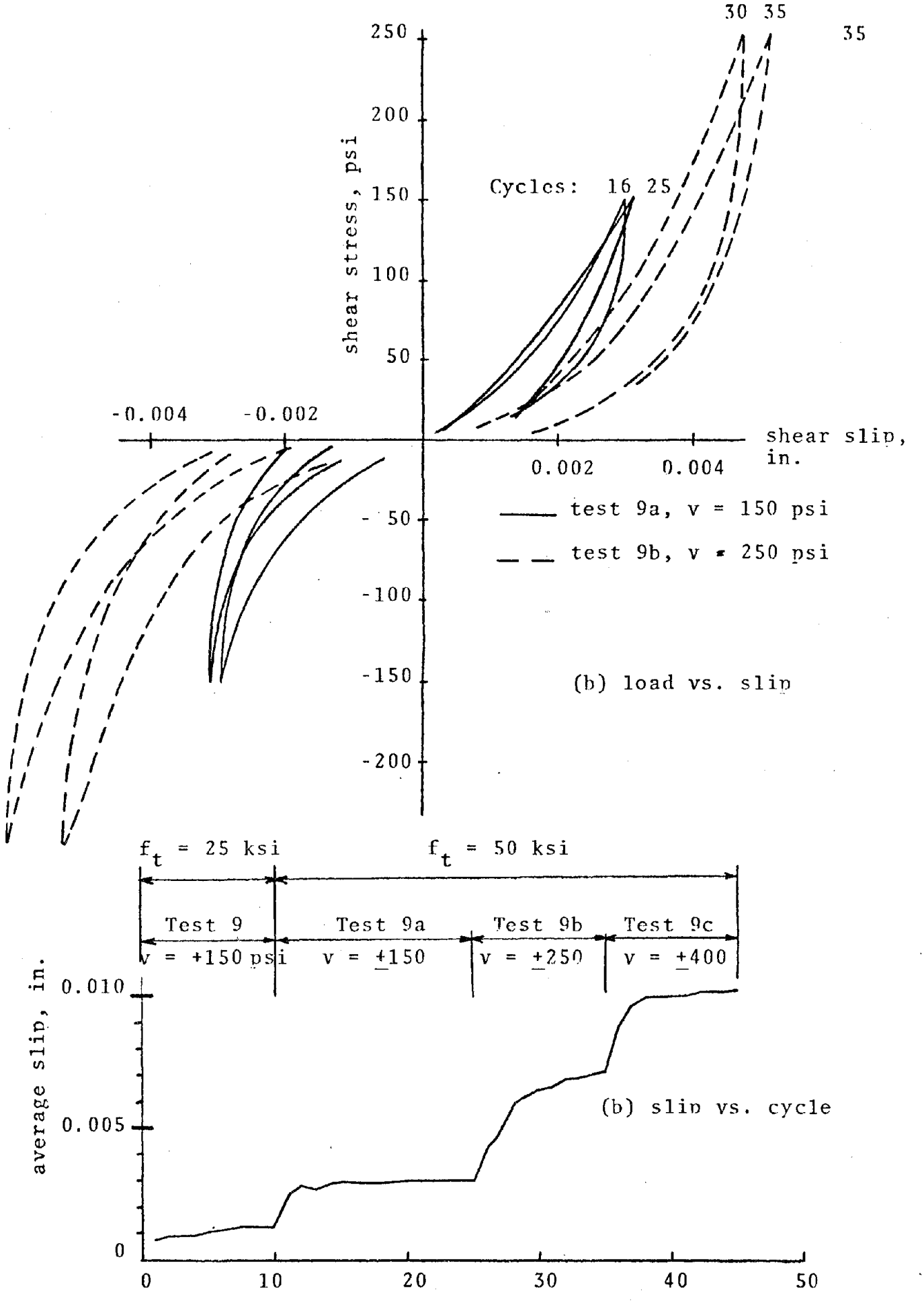

Fig. A10 - tests 9, 9a, 9b, 9c

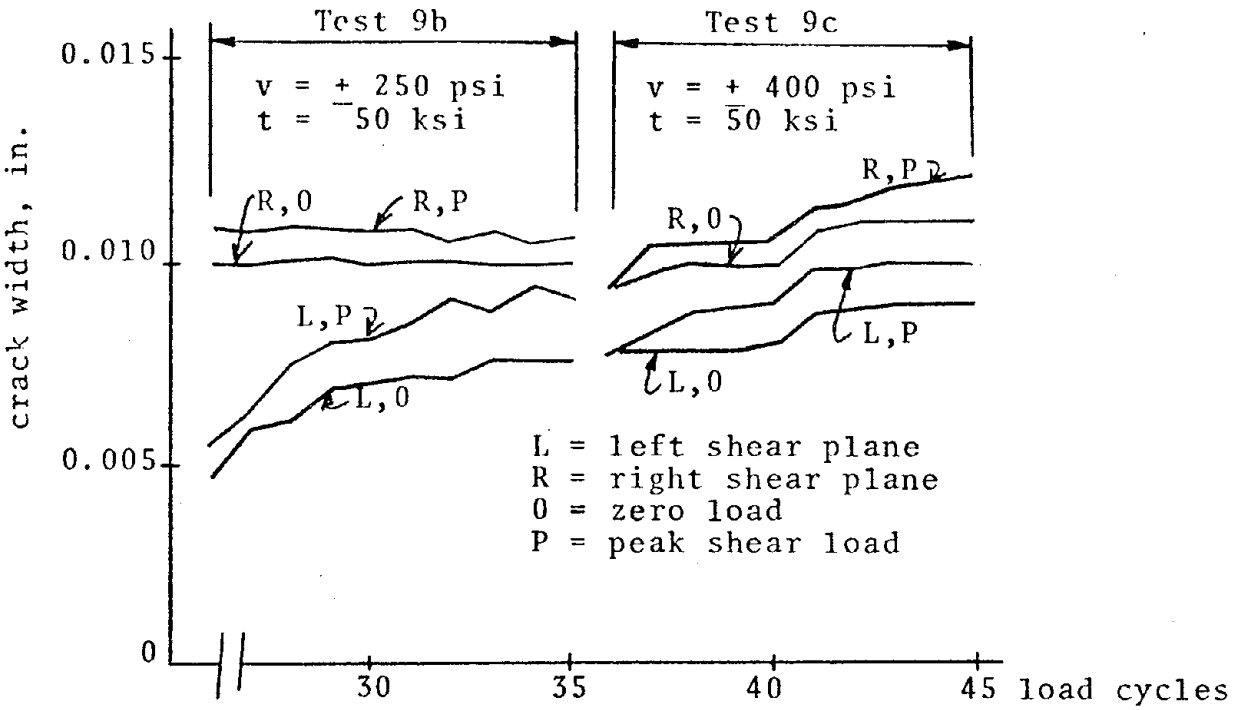

(a) crack widths for each shear plane at zero and peak shear loads

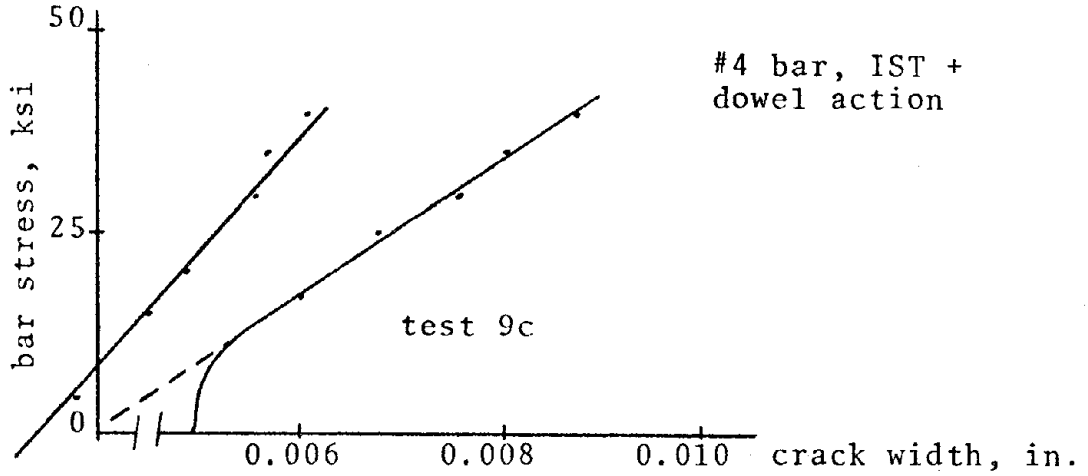

(b) bar stress vs. crack width

Fig. A11 - crack width variations, tests 9b and 9c

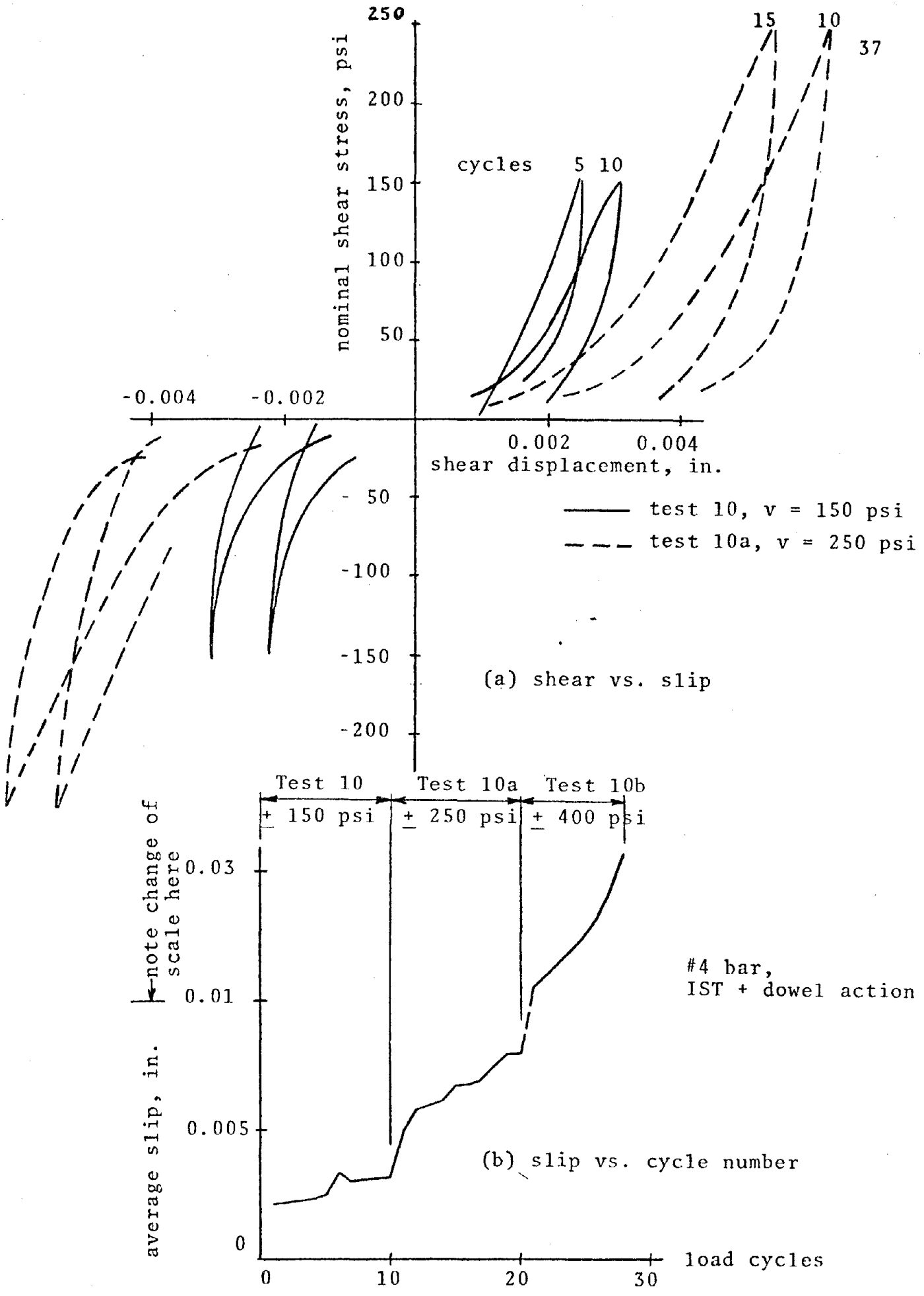

Fig. A12 - slip behavior, combined IST + dowel action, #4 bar

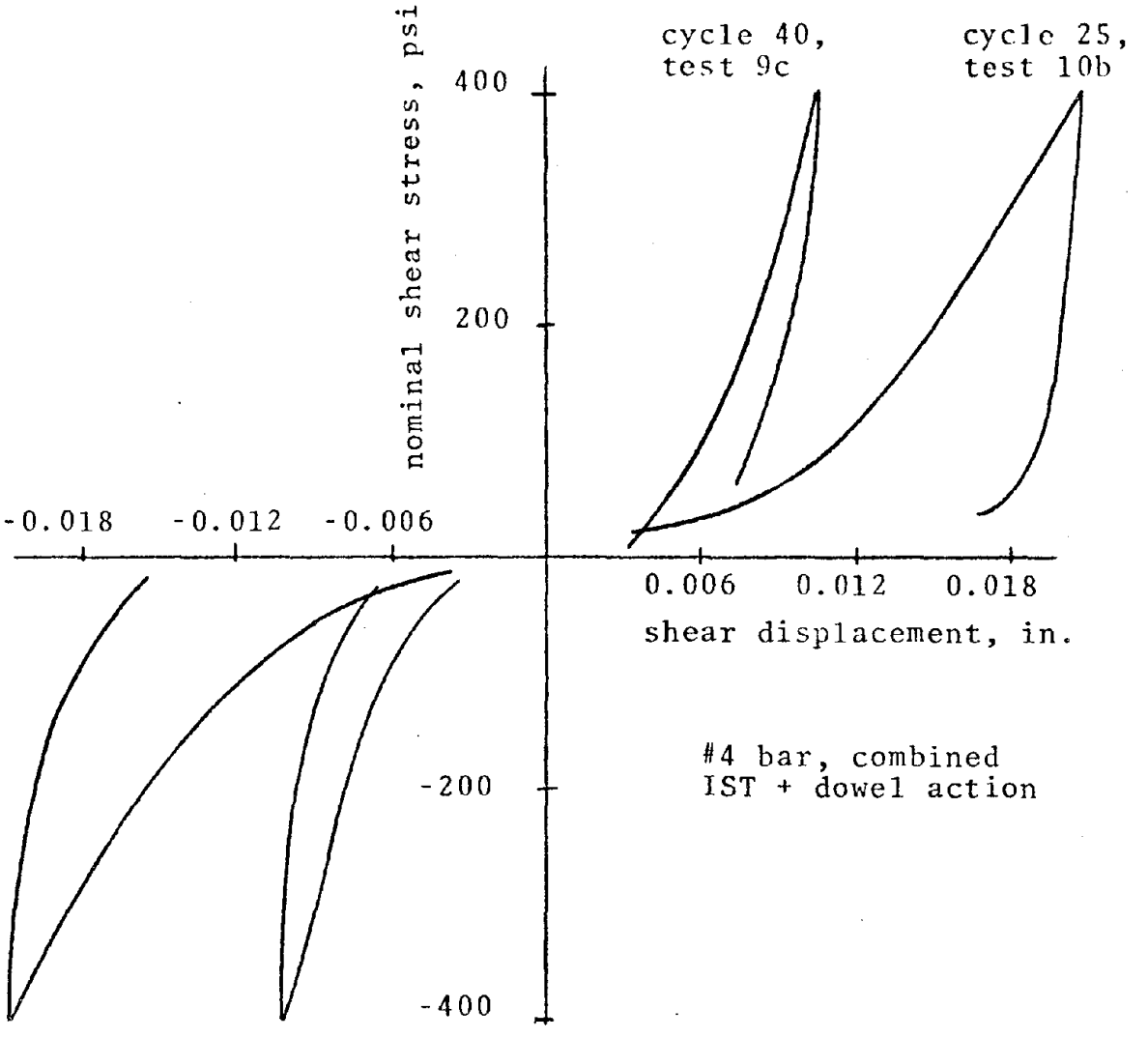

Fig. A13 - shear displacement during 5th cycle at $v = \pm 400$ psi, $f_t = 50$ ksi, for tests 9c and 10b.

B. DOWEL ACTION AND DYNAMIC RESPONSE OF CONTAINMENT VESSELS

1. Dynamic Response of Cracked Containment Vessels

The response to earthquake motion of structures that display a nonlinear hardening, hysteretic stiffness is presented in this section. Such stiffness characteristics are typical of nuclear reactor containment vessels after they have been cracked by internal pressurization.

The idealized load-slip relationship for cracked reinforced concrete subjected to cyclic shearing stress is shown in Fig. B1, where the values of stiffness are taken from experimental studies at Cornell. The structure idealization is given in Fig. B2. Five lumped masses and five hysteretic springs are used, along with rotational and translational springs on the foundation mass. The effects of several important variables are assessed here by considering the results of five separate dynamic analyses of a typical containment vessel. These variables include earthquake input, crack stiffness properties, crack spacing, and soil conditions.

The analysis program performs a numerical integration of the equations of motion of the spring-mass system, utilizing the Wilson "theta" method of integration. The latter technique is an extension of the well-known linear acceleration method, but it has the advantage of being unconditionally stable for linear systems. The nonlinear system analyzed here is considered to be linear over any time step.

The matrix form of the equations of motion are

$$[M]\{\ddot{u}\} + [K]\{u\} = \{P\}$$

where $M =$

$$\begin{bmatrix} M_5 & & & & \\ & M_4 & & & \\ & & \cdot & & \\ & & & M_0 & \\ & & & & I_T \end{bmatrix}, \qquad u = \begin{bmatrix} u_5 \\ u_4 \\ \cdot \\ \cdot \\ u_0 \\ \theta \end{bmatrix}$$

$$\{P\} = \begin{Bmatrix} F^*_{45} \\ F^*_{34} - F^*_{45} \\ \vdots \\ -F^*_{01} \\ -(F^*_{45}\, h_5 + \ldots F^*_{01}\, h_1) \end{Bmatrix} - \begin{Bmatrix} M_5 \\ M_4 \\ \vdots \\ M_0 \\ 0 \end{Bmatrix} \ddot{x}_5$$

and the matrix [K] is given in Fig. B3. This formulation is identical to that for a linear system except for the terms in F* in the forcing function. Thus standard procedures for integrating linear equations can be used, provided that the F* terms are evaluated at the end of every integration step and then included in the new forcing function at the start of the next step.

The major problem met in the analysis is in making the change from one stiffness to another on the hysteresis loop. This is accomplished by treating the continuous nonlinear curve as a series of linear steps and iterating to the new stiffness value (Fig. B4). Very small time steps, as low as 0.0025 sec, are used where necessary, and an automatic time step expansion of up to 0.01 sec is programmed into the analysis to better cover the time history where stiffness changes are not occurring. This approach cuts off some small areas of the hysteresis loops, but the lost area at the falling stiffness change is partially balanced by the gained area at rising stiffness changes, and the total error generated is less than several percent. The full program and additional details on its operation are given in Ref. B1.

The structure analyzed is typical of containment vessels for large (750-1000 MW) nuclear plants. The effective shearing area of the cylindrical wall was taken as 3/4 the total cross-sectional area (halfway between thin-walled elastic shell theory and rigid body translation at the crack).

Run 1 was a control run with the following variables:

Number of degrees of freedom	5
Masses (each)	12100 kips
Segment heights (each)	504 in
Shear area	213000 in^2
Crack spacing	60 in
G (Concrete)	1540 ksi
Viscous damping	0%
Basic time step	0.01 secs
Crack stiffnesses:	
initial (elastic)	3.17 ksi/in
subsequent (hysteretic)	16.45, 143, 1.2, ksi/in
Earthquake	N65E component of Parkfield (1966)

The control earthquake was 4 seconds of the N65E component of the Parkfield shock of June 1966 (maximum ground acceleration of 0.51g). The standard hysteresis loop was an idealization of tests results from Laible (Ref. B2) which included both dowel action and interface shear transfer (IST) with an initial crack width of 0.01 in. Crack spacing in Run 1 was 60 in. No soil-structure interaction was used in Run 1.

Run 1 - Critical displacements of masses 1, 3, and 5 are plotted in Fig. B5. The structure was extremely stiff and maximum response occurred about 0.05 sec after maximum ground acceleration. Maximum values of displacement, slip at the crack, and shear stress for each of the masses are tabulated in Table 1. A typical hysteresis loop is shown in Fig. B6.

Run 2 - 4 secs of the NS component of the El Centro 1940 earthquake was used, with a maximum ground acceleration of 0.35g. Response was similar to Run 1 results except the values ranged from about 10% to 35% less. Maximum values are listed in Table 1.

Run 3 - The Parkfield earthquake was used for this run, but the crack stiffness properties were changed to simulate those of a rather "soft" construction joint; the stiffness values were initial elastic = 0.862 ksi/in and subsequent hysteretic = 5.27, 46.75, and 0.184 ksi/in. Response for this structure with its sharply reduced stiffness was markedly different from the first two runs.

Maximum stress and maximum slip occurred closer to the middle of the vessel (see Table B1) and peak response values occurred near the end of the earthquake input in most cases. The hysteresis loop was far from stable (Fig. B7). The general behavior was that of a violent lurch in one direction, followed by about a half second of small amplitude vibrations centered about a point of large slip, followed by a violent lurch in the opposite direction.

Run 4 - The Parkfield earthquake and regular cracks at 15 in. spacing rather than 60 in. spacing were used for this run. The maximum response values in Table B1 show slips of the same order of those of the control run, but the stresses were only 50-80% of the control run values. The increased flexibility produced by the greater number of cracks produced response more like that of Run 3, with maximum response near the middle of the structure and hysteresis loops exhibiting the same patterns as in Run 3. Maximum response occurred within 0.2 sec of the maximum ground acceleration.

Run 5 - This run was similar to Run 1 except two extra elastic degrees of freedom were added to simulate the soil-structure interaction, and viscous damping was included for these two degrees of freedom. Soil properties were density = 125 lb/ft^3 and shear wave velocity = 750 fps. Calculated stiffness and damping properties were:

Stiffness (translational)	60000 k/in
Stiffness (rotational)	2.5×10^{10} k-in/rad
Damping (translational)	3685 k/in/sec
Damping (rotational)	3.43×10^{10} k-in/rad/sec

The foundation had a mass of 26546 k and an inertia of 13856×10^6 $k\text{-}in^2$.

The increased displacements and decreased shear stresses for this flexible system are evident in Table B1. Displacements without soil-structure interaction were determined from the analysis results and they were found to be 65-75% of the displacements found in Run 1. Since the soil properties assumed are for a rather poor soil, it is felt that the results of Run 5 represent a limiting condition, with Run 1 being the limit at the other end

of the stiffness possibilities.

Critical response values for the five cases are summarized in Table B2. The analyses indicate that the only parameter that might threaten the integrity of the vessel (actually the integrity of the liner because of excessive slips at a crack) is the presence of a poorly done construction joint with excessive flexibility and poor shear transfer characteristics. The maximum shear stress for any of the runs was 280 psi. It remains to be seen if this level of shear would produce dowel splitting or other undesirable effects in the typical containment vessel.

2. A Mathematical Model of Dowel Action

Dowel action of reinforcing bars in cracked, thick concrete sections is treated by considering the dowel as a beam on elastic foundation (Fig. B8a). Since the very high contact stresses in the concrete near the slip plane produce some crushing action, a portion of the bar with half-length b (Fig. B8a) is considered free to flex. The foundation modulus provided by the concrete is determined by cutting the concrete section into thin slices (Fig. B8b) and then analyzing a typical slice by plane stress elasticity methods. The loading on each slice is shown in Fig. B9 and is cosinusoidal in nature. The solution to this problem, given in detail in Ref. B1, provides foundation modulus values as well as giving stresses in the concrete around the dowel. It is considered an adequate solution up to the time of tensile cracking in the concrete; after cracking there may be a considerable adjustment in load carrying in both the dowel and concrete.

Values of circumferential tensile stresses in the concrete are

$$\sigma_\theta = 0.344 \left(\frac{2P}{\pi a}\right) \text{ at } \theta = 0$$

$$\sigma_\theta = 0.637 \left(\frac{2P}{\pi a}\right) \text{ at } \theta = \frac{\pi}{2}$$

Thus the tensile stress in the direction of the dowel force is highest, and the tensile force normal to the dowel force, which tends to produce a wedging action splitting, is only 54% of the maximum.

The foundation modulus k was determined from the average displacement (in the direction of the load) over the 60° sector of $\pm \frac{\pi}{6}$.

The behavior of the dowel in Fig. B8a is governed by

$$EI \frac{d^4y}{dx^4} + ky = \text{loading}$$

The load V is applied at x = -b, and the total displacement at the slip-plane is determined by solving the equation for y and adding the bending and shearing deformations of the free half-length b; it is

$$y_{(-b)} = \frac{V}{EI} \left[\frac{1+b\beta}{2\beta^3} + \frac{b(1+2b\beta)}{2\beta^2} + \frac{b^3}{3} + \frac{ba^2(1+\nu)}{2}\right]$$

where V = applied shear

EI = EI of the reinforcing bar

b = free half-length where concrete is crushed

$\beta = \sqrt[4]{\frac{k}{4EI}}$

k = foundation modulus

a = bar radius

The corresponding dowel stiffness is simply $V/2y_{(-b)}$.

The last term, $\frac{ba^2(1+\nu)}{2}$, in the above equation is the shearing deformation component. It can be shown that the effect of shear strain is limited to about 4% of the maximum displacement, regardless of bar size (Ref. B1).

Dowel stiffness values for one #11 bar (1 3/8 in. diameter) as a function of β and free half-length b are plotted as solid lines in Fig. B10. When b = 0, the stiffness reduces to

$$K = EI\beta^3 = a \sqrt[4]{\frac{\pi E k^3}{4}}$$

and the stiffness varies linearly with bar diameter 2a. This result is very different from the result obtained by assuming that the bar is fully fixed at both ends, in which case the stiffness varies with the fourth power of bar diameter.

The β value of 0.618 in Fig. B10 is for a 15 in. wide concrete specimen with one #11 bar and 4000 psi concrete strength. β decreases to 0.49 for a #14 bar and 0.39 for a #18 bar; the stiffness of one #18 bar is shown as a dashed line. Other concrete strengths would change β by the factor $\sqrt{\frac{f_c'}{4000}}$

The rather sharp decrease in dowel stiffness with increasing free half-length is evident in Fig. B10.

The next step in the analysis is to combine the elasticity analysis for concrete stresses with the beam on elastic foundation solution. Assuming that concrete cracking initiates at a tensile stress of $7.5\sqrt{f_c'}$, a #11 bar with $\beta = 0.618$, $b = 0$, and $f_c' = 4000$ psi gives $V_{cracking} = 650$ lbs. Similarly, equating peak radial stress to the compressive strength of the concrete, f_c', the value of shear is $V_{crushing} = 3500$ lbs. for a #11 bar with the same properties as above. This result is quite approximate since the true stress level at which the concrete shows crushing is not known. Comparisons of analysis with test results will be given in the next section of this report.

Bar bending stresses also may be computed from

$$f = M/S = --EI \frac{d^2y}{dx^2}/S$$

where $M_{max} = -\frac{V}{\beta} e^{-\beta x_1} \sqrt{\frac{1}{2} + \beta b + (\beta b)^2}$

For a typical case of $f_c' = 4000$ psi, one #11 bar, $\beta = 0.618$, $b = 0.5$ in., and $V = 25$ k, the value of M_{max} is 25 in-kips and the corresponding elastic bar stress is 100 ksi, which means the bar will yield at the slip plane.

3. Experimental Study of Dowel Action Under Cyclic Shearing Forces

Five specimens with the geometry given in Fig. B11a were loaded with cyclic shear across planes where the shear force was carried by dowel action alone in a single reinforcing bar. The shearing forces were applied as shown in Fig. B11c and d, where the solid arrows indicate load in one direction (defined here as positive) and the dashed arrows represent a reversal of load direction (negative). Specific questions considered were: how the stiffness of dowel bars changes with increasing cycles of load, and what failure mode is to be expected.

Each specimen had a single #11 bar with greased 16 gage steel sheets separating the block into three sections. The loading for specimens 4 and 5 minimized the minor bending effects present in the first three tests. Specimens 1, 2, and 3 had no reinforcing other than the #11 dowel bar. Specimens 4 and 5 had transverse reinforcement, as detailed in Fig. B12, to assess its effect on delaying and restraining splitting effects produced by the dowel forces.

Slip of one block relative to the other was measured at each shear plane. Opening and closing tendencies of the "crack" were also measured. The major difficulty met in testing these specimens was the tendency for twisting to occur about the axis of the bar. The two ends of the specimens were seated in Hydrostone prior to loading, but some minor twisting action was still observed in some specimens. Twisting is highly undesirable because it may damage the concrete immediately surrounding the reinforcing bar. The cyclic loading sequence for the five specimens is given in Table B3. Specimen 1 was loaded in small increments from 5 k to 55 k. The other specimens were started at higher loads. Specimen 4 failed prematurely by local crushing at the 2 1/2 in. wide bearing plates used to support the specimen.

Discussion here will focus on Specimens 3 and 5; the complete results are given in Ref. B1. The increases in shear slip with load cycling are shown in Fig. B13 for the two specimens. In both specimens, cycling at loads of 30 or 35 kips (shear forces of 15 or 17.5 kips on each shear plane) produced only small increases in shear slip, while higher loads increased slip rather sharply. As

in all specimens, the slips produced by negative loads were slightly larger than those from the positive loads.

Specimen 3, with no transverse reinforcement, failed by splitting along a warped vertical surface through the bar at P = 70 k (Fig. B14a) while Specimen 5, with transverse steel, failed at P = 60 k by splitting horizontally along the dowel (Fig. B14b). Specimen 5 showed first cracking on the 6th load cycle, with horizontal cracks beginning at the shear plane and extending out about 3 in. in the plane of the bar.

Load-shear slip relations for Specimens 3 and 5 are given in Figs. B15-B17. In all cases the shear load per bar is half the total applied load. The basic shapes of these curves are similar to those obtained on smaller dowels by Elleiott, and have a strong resemblance to the load-slip curves for interface shear transfer alone. However, the transverse stiffness of the dowel after "free slip" has occurred does not increase significantly with cycling as does the post-free slip stiffness of the interface shear transfer mechanism. The average width of the hysteretic loop increases slightly with higher cyclic load levels, thus implying a higher percentage of equivalent viscous damping at high shear load levels.

The complete splitting failure of Specimen 3 permitted good inspection of damage to the concrete around the bar at the shear plane. A funnel-shaped volume of crushed concrete was observed, with visible damage extending about 1 in. in each direction from the slip plane. Similar damage was observed in Specimen 2, and other specimens must have suffered the same damage. It is believed that the higher shear slips in Specimen 5 (as compared to Specimen 3) were produced by the increased damage to the lower strength concrete of Specimen 5 (3000 psi in #5 vs. 4000 psi in #3).

The transverse reinforcement used in Specimen #5 had negligible influence on specimen strength.

4. Discussion of Results and Design Implications

Several important points from Ref. B1 are presented here, including: (a) comparison of the dowel action analysis with results obtained from Fajardo's specimens and from interface shear transfer specimens, (b) prediction of dowel forces, bar stresses, and slips in typical containment vessels, and (c) overall conclusions.

Fajardo tested #11 bars in combined dowel action and interface shear transfer with a pre-defined unbonded length of bar at the slip plane. His specimen with a 1 in. unbonded length on each side of the shear plane had an average dowel shear stiffness after initial cycling of about 900 k/in, where the average stiffness is defined as the applied peak shear divided by the average of the peak positive and negative slips. This dowel stiffness value of 900 k/in was obtained by subtracting out the interface shear transfer stiffness of a specimen that had similar crack width and resisted shear by interface shear transfer alone.

The corresponding dowel force on each bar was then about 11 k. The analysis of Part 2 of this section can be applied with a free half length of 0.55 in. to get a predicted dowel stiffness of 580 k/in for each bar, as compared to the 900 k/in. obtained by subtracting out the IST stiffness from Fajardo's Specimen #1. While the results are not conclusive they are quite encouraging.

An analysis for slips and bar forces in a typical containment vessel is given in Ref. B1. A 4.5 foot wall thickness with ρ = 1.39% for vertical #18 bars was assumed, and f'_c = 4000 psi was used. For an initial crack width of 0.015 in. and an applied maximum shear stress of 100 psi, the following results are obtained for various assumed free half-lengths of each bar at the crack:

free half-length, in.	0	0.5	1	2	4	6
shear force per bar, k	11.2	8.5	6.4	3.7	1.5	0.7
% of shear carried by dowel	39	30	22	13	5	2
axial stress in bar, ksi *	30.2	30.4	30.6	30.8	30.9	31.0
bending stress in bar, ksi	8	9	9	8	6	4
shear stress in bar, ksi	2.8	2.1	1.6	0.9	0.4	0.2
slip at crack, thousandths of in.	5	6	6.5	7	8	8

*Obtained from 28.8 ksi due to pressurization, plus the axial force generated by over-riding in the IST mechanism.

A second analysis was done for the case of a maximum shear stress of 300 psi, which is the upper limit on dynamic shear stresses calculated earlier in Section B1. The free half-length is estimated at 1.63 in., which gives a dowel force of 13.9 k/bar, a peak bar bending stress of 25 ksi, and a slip of 0.021 in. at the crack. The dowel load is less than the load needed to produce splitting in the #11 dowel tests reported here, but the latter specimens did not have tensile stress superimposed on the dowel forces, nor was the concrete in biaxial tension as it would be in a containment.

Several conclusions may be drawn from this work:

a. the maximum seismic shear to be expected in a typical reinforced concrete containment vessel is on the order of 300 psi for earthquakes similar to the Parkfield 1966 and El Centro 1940 shocks.

b. combined stress effects in reinforcing bars at crack locations may be appreciable and should be considered in design.

c. potential splitting effects from dowel action must be accounted for in design. They appear to be much more dependent on shear stress level and on bar axial tension than on number of load cycles. Biaxially tensioned specimens are needed to resolve the many unanswered questions about dowel effects in containment structures.

REFERENCES

B1. Stanton, John, "The Dowel Action of Reinforcement and the Nonlinear Dynamic Analysis of Concrete Nuclear Containment Vessels", M.S. Thesis, Cornell University, May 1976.

Run	Segment	Displacement, in	Slip, in	Shear stress, psi
1	1	1.41	0.0256	252
	2	1.19	0.0286	228
	3	0.91	0.0263	226
	4	0.62	0.0259	263
	5	0.32	0.0267	280
2	1	1.22	0.0233	207
	2	1.01	0.0254	195
	3	0.75	0.0244	194
	4	0.49	0.0246	176
	5	0.24	0.0205	193
3	1	4.59	0.0826	214
	2	3.92	0.0996	221
	3	3.10	0.138	218
	4	2.03	0.138	227
	5	1.12	0.125	207
4	1	4.14	0.0203	126
	2	3.64	0.0232	185
	3	2.91	0.0294	175
	4	2.12	0.0360	193
	5	1.10	0.0311	167
5	1	5.97	0.0213	70
	2	4.90	0.0310	111
	3	3.76	0.0305	129
	4	2.60	0.0233	113
	5	1.49	0.0256	123

Table B1 - Maximum Response Values for each Segment, Runs 1-5

Run	Description	Peak accel	Maximum Dis.	Rel.Dis.	Slip	Stress
1	Control	.51g	1.4"	0.315"	.0267"	280
2	El Centro	.35g	1.2"	0.264	.0254"	210
3	Crack at Constr. Jt.	.51g	4.5"	1.20"	.12"	230
4	Crack at Spacing 15"	.51g	4.13"	1.25"	.03"	190
5	SSI	.51g	5.969	0.28	.031	129

Table B2 - Summary of Maximum Response Values, Runs 1-5

Note: Loads below are twice the shear force on the #11 bar.

CYCLE NO.	SPECIMEN				
	1	2	3	4	5
1	5 k	30 k	20 k	45 k	30 k
2	10	35	35		30
3	15	35	35		30
4	20	35	35		30
5	20	45	35		30
6	20	65	35		30
7	25	65	35		30
8	30	65	35		30
9	35	80	35		30
10	35		45		30
11	35		50		40
12	40		70		40
13	45				40
14	55				40
15					40
16					60

Table B3 - Load sequence for dowel action tests

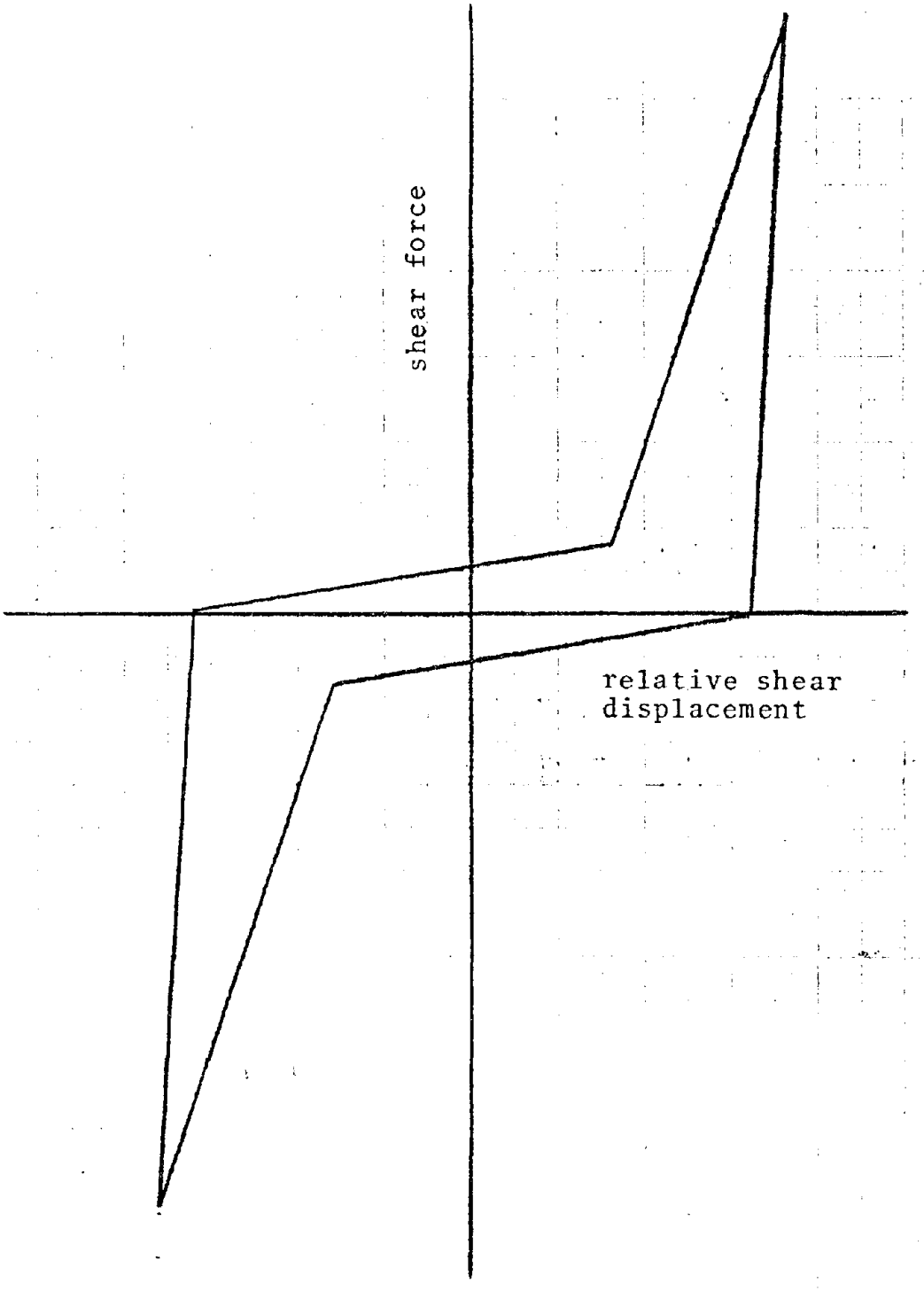

Fig. B1 - idealized load-slip relationship

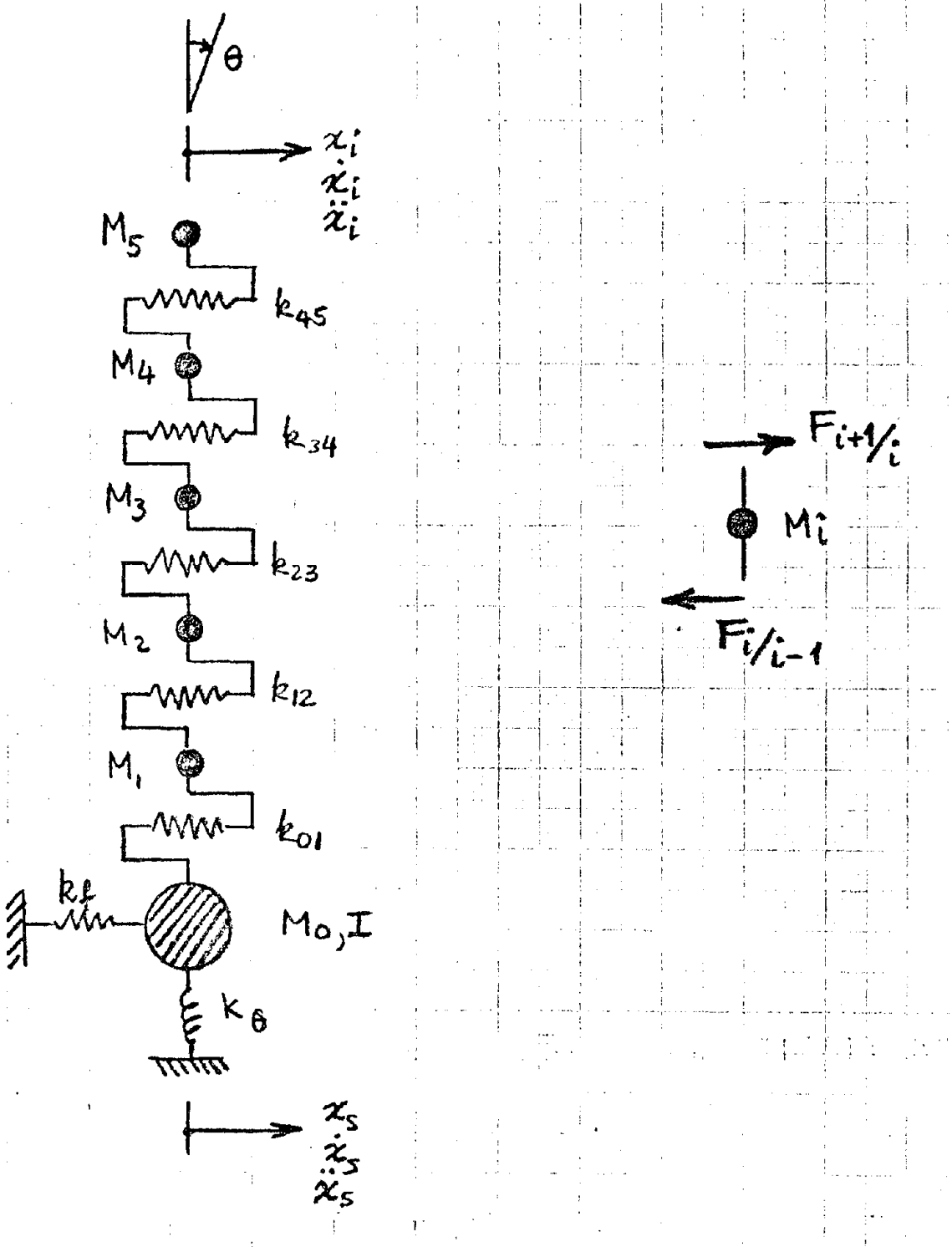

Fig. B2 - structural idealization for dynamic analysis

	5	4	3	2	1	0	θ
5	k_{45}	$-k_{45}$	0	0	0	0	$-h_5 k_{45}$
4		$k_{45}+k_{34}$	$-k_{34}$	0	0	0	$h_5 k_{45} - h_4 k_{34}$
3		Symmetric	$k_{34}+k_{23}$	$-k_{23}$	0	0	$h_4 k_{34} - h_3 k_{23}$
2				$k_{23}+k_{12}$	$-k_{12}$	0	$h_3 k_{23} - h_2 k_{12}$
1					$k_{12}+k_{01}$	$-k_{01}$	$h_2 k_{12} - h_1 k_{01}$
0						$k_{01}+k_{ST}$	$h_1 k_{01}$
θ							$h_5^2 k_{45} + h_4^2 k_{34} + h_3^2 k_{23} + h_2^2 k_{12} + h_1^2 k_{01} + k_{SR}$

Model:

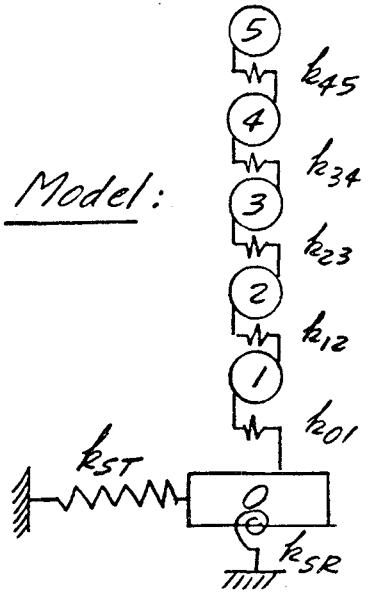

$$\begin{bmatrix} M_5 & & & & & & \\ & M_4 & & & & & \\ & & M_3 & & & & \\ & & & M_2 & & & \\ & & & & M_1 & & \\ & & & & & M_0 & \\ & & & & & & I_T = \Sigma I_m \end{bmatrix}$$

Mass matrix

all $h = 504$ in.

NOTES:
1. If soil properties are not included, use stiffness matrix in dashed brackets.
2. kst and ksr were taken to be elastic; k_{01} thru k_{45} were hysteretic.
3. Program was set up to include a (viscous) damping matrix.

Fig. B3 - dynamic model idealization

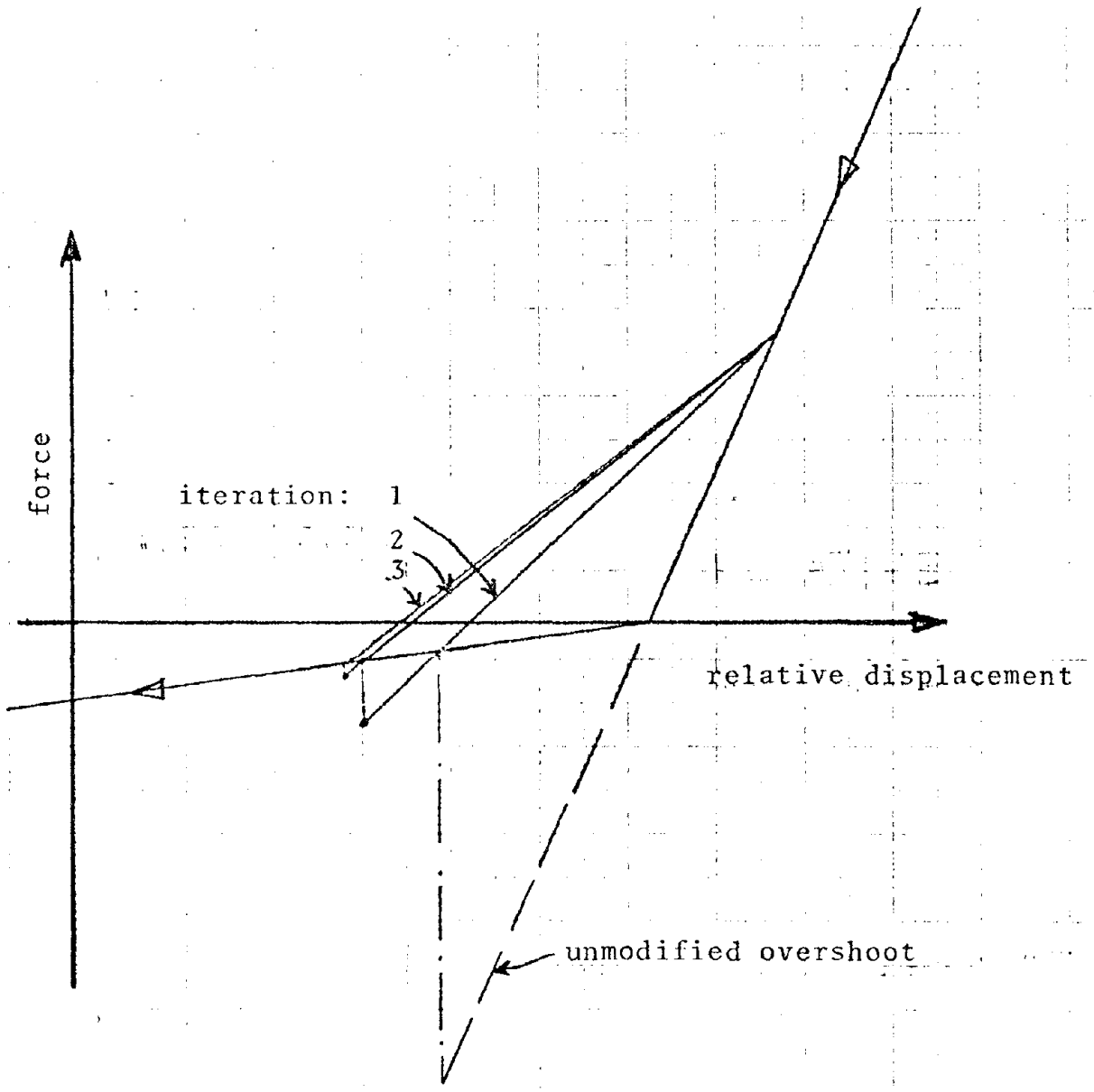

Fig. B4 - cornering technique

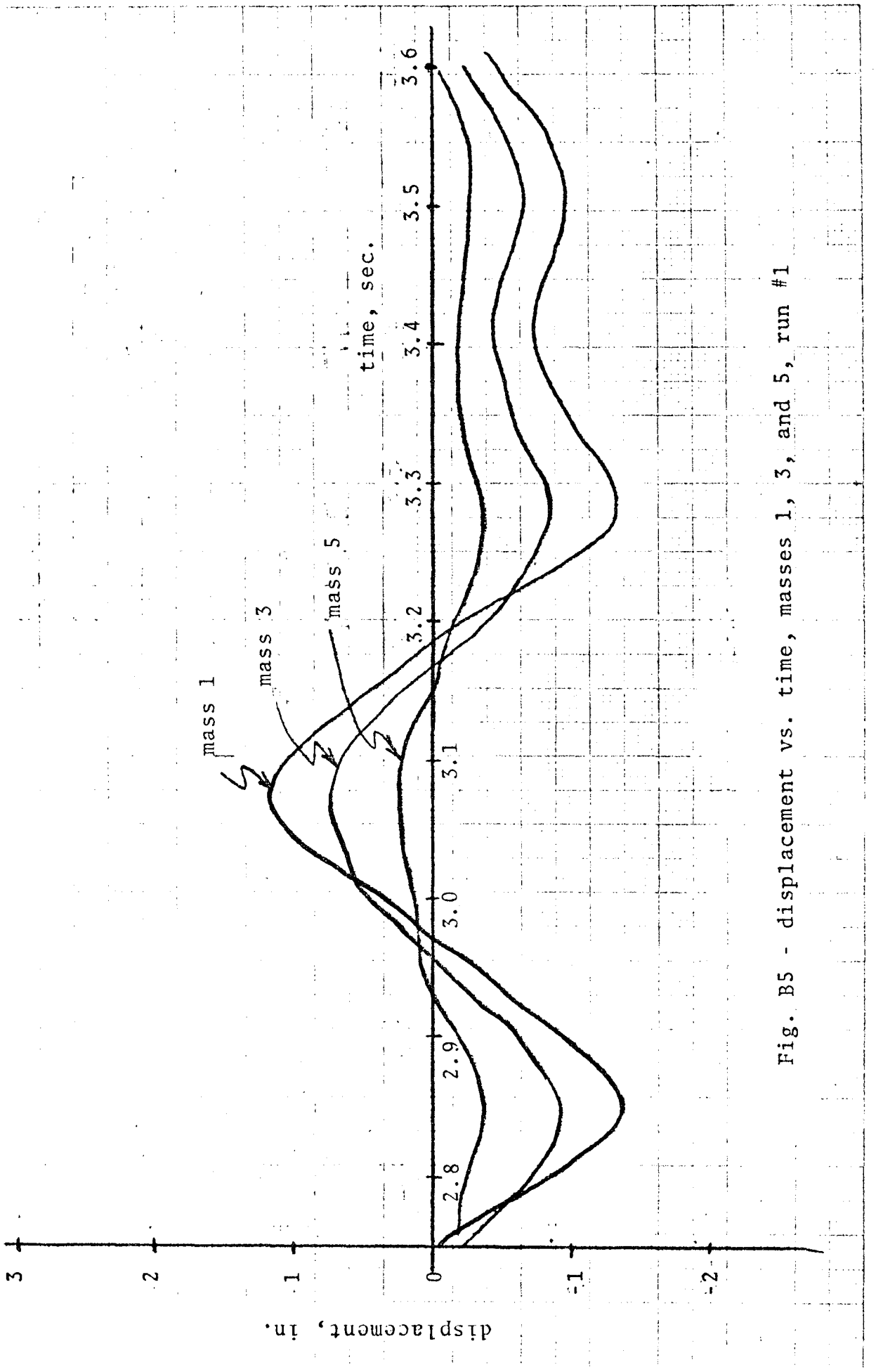

Fig. B5 - displacement vs. time, masses 1, 3, and 5, run #1

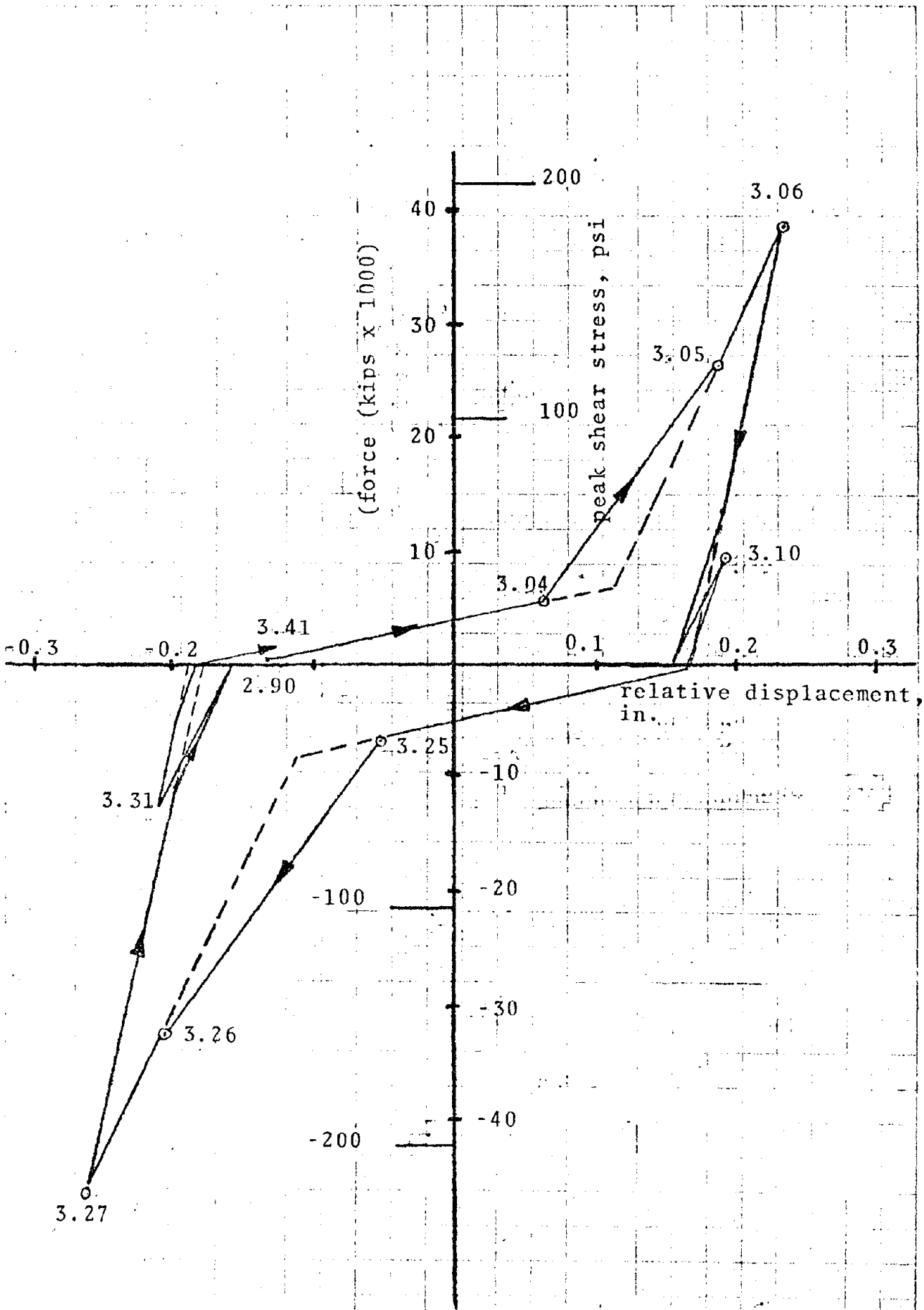

Fig. B6 - force vs. relative displacement, mass 1, run #1

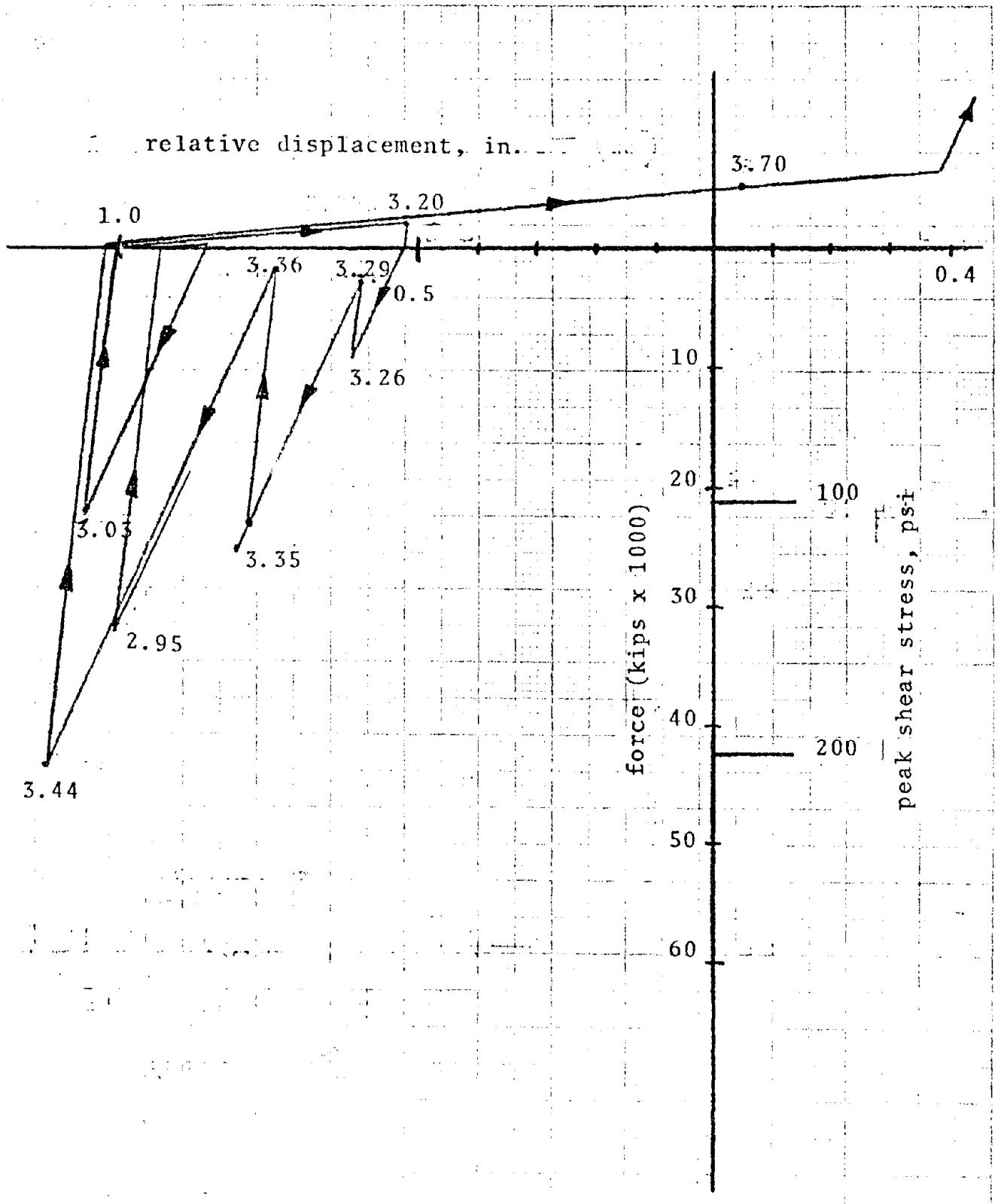

Fig. B7 - force vs. relative displacement, mass 5, run #3

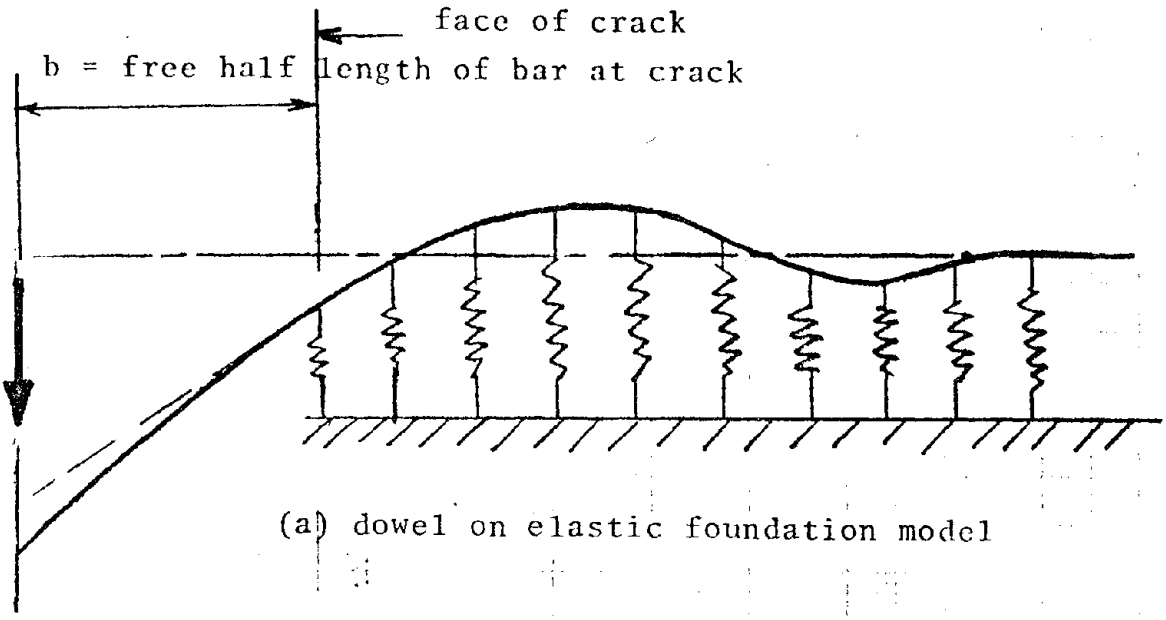

(a) dowel on elastic foundation model

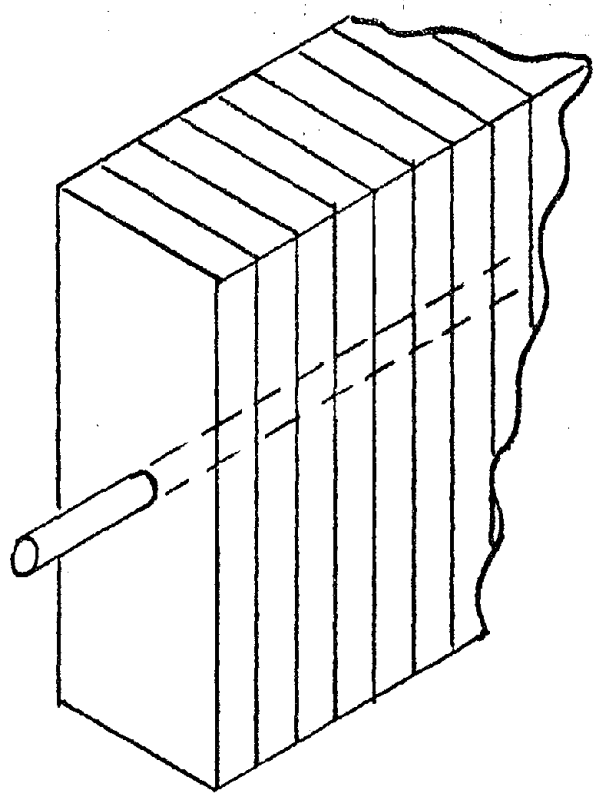

(b) longitudinal slices of concrete

Fig. B8 - idealized model for dowel action analysis

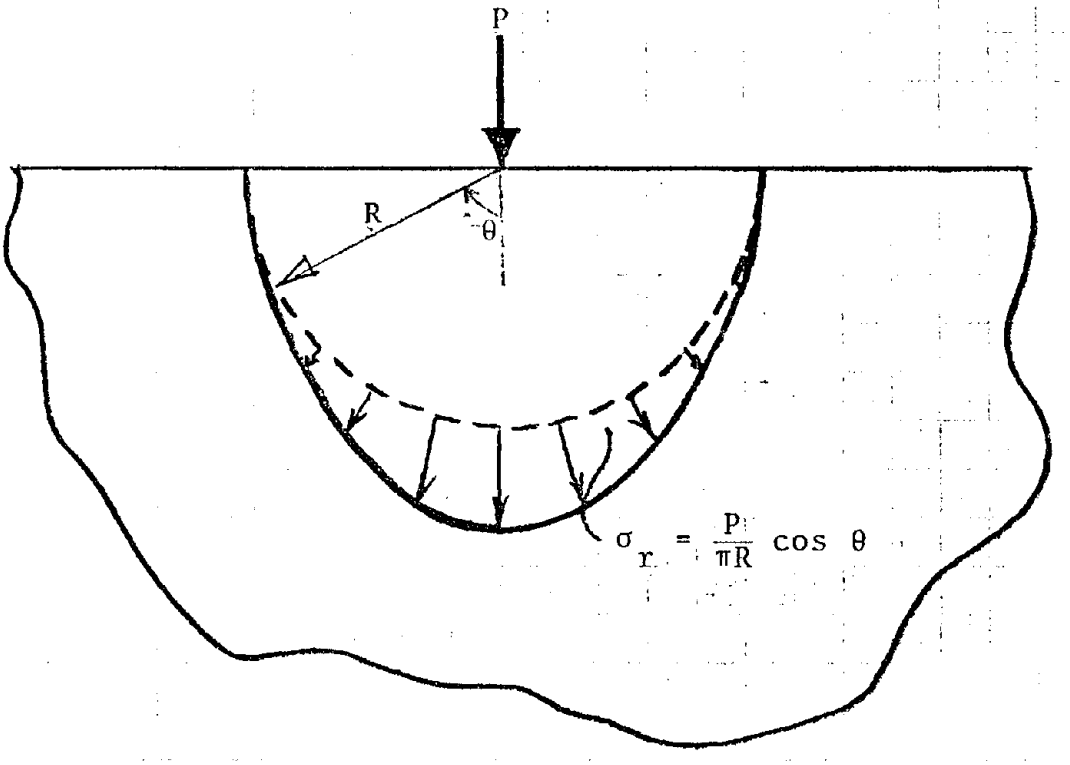

Fig. B9 - action of dowel of concrete

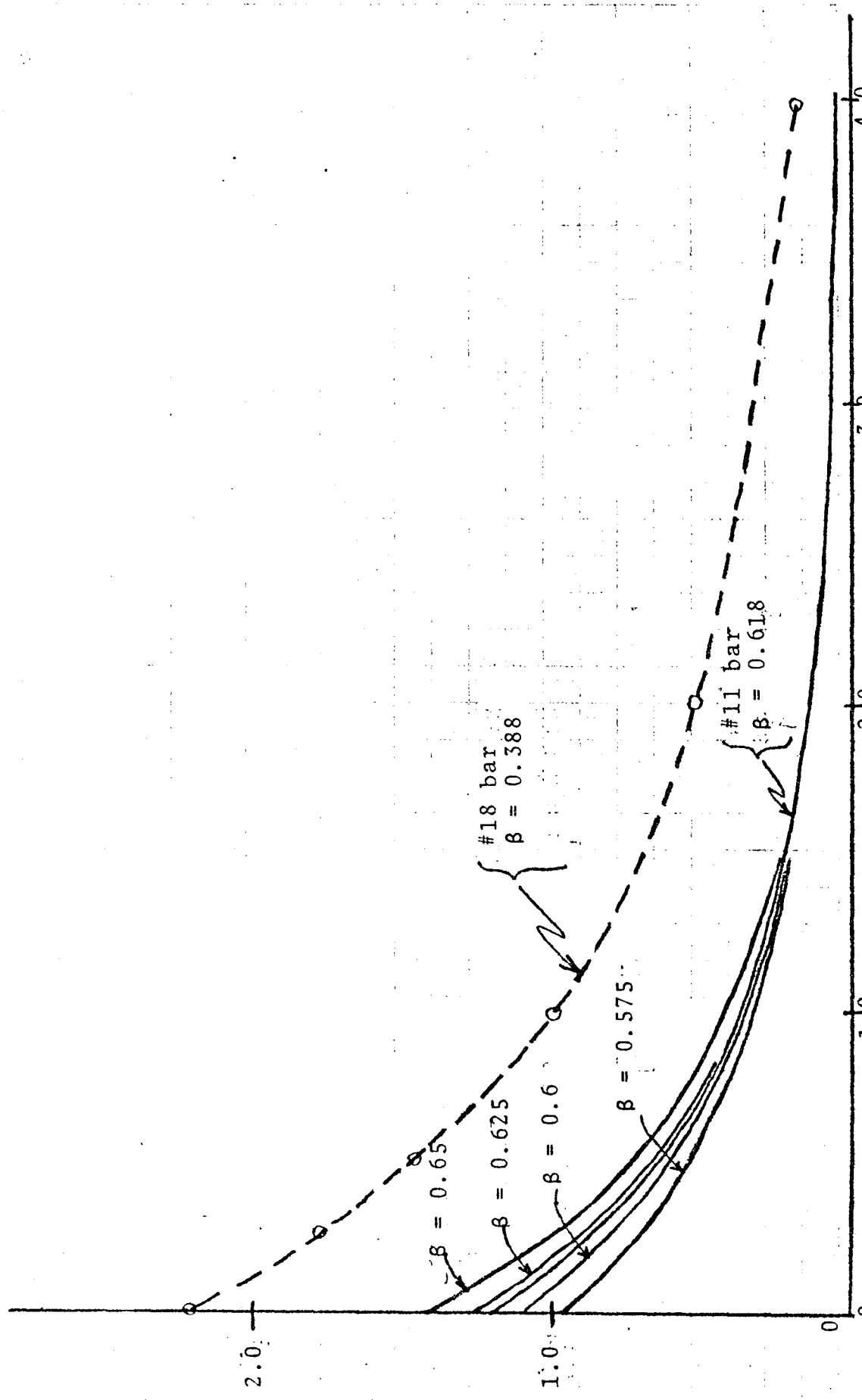

Fig. B10 - dowel stiffness as a function of free half-length

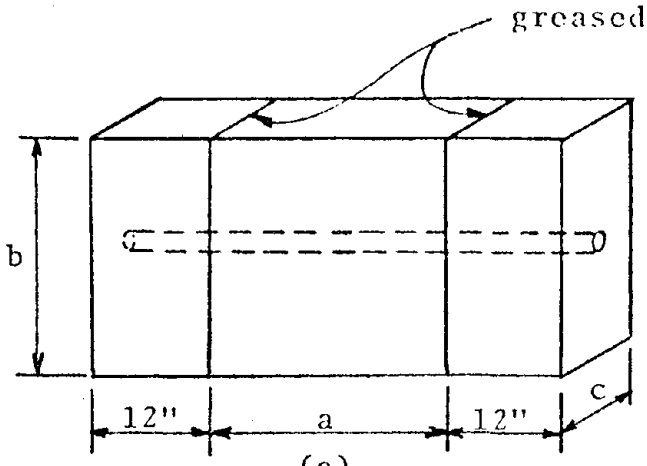

(a)

Spec.	a,in.	b,in.	c,in.	f'_c,psi
1	24	24	8	4020
2	12	24	12	4130
3	12	24	8	4080
4	24	20	$7\frac{1}{2}$	3200
5	24	20	$7\frac{1}{2}$	3080

(b)

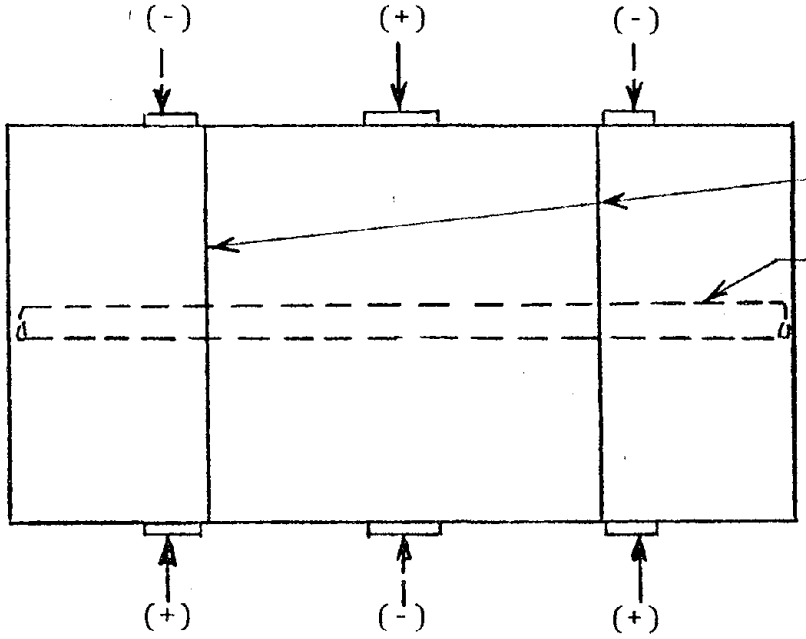

(c) specimens 1-3

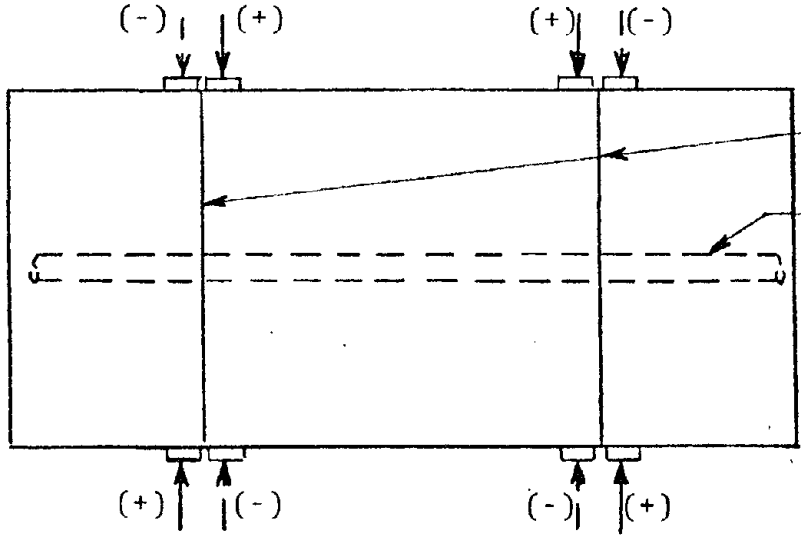

(d) specimens 4 & 5

Fig. B11 - dowel specimen geometry

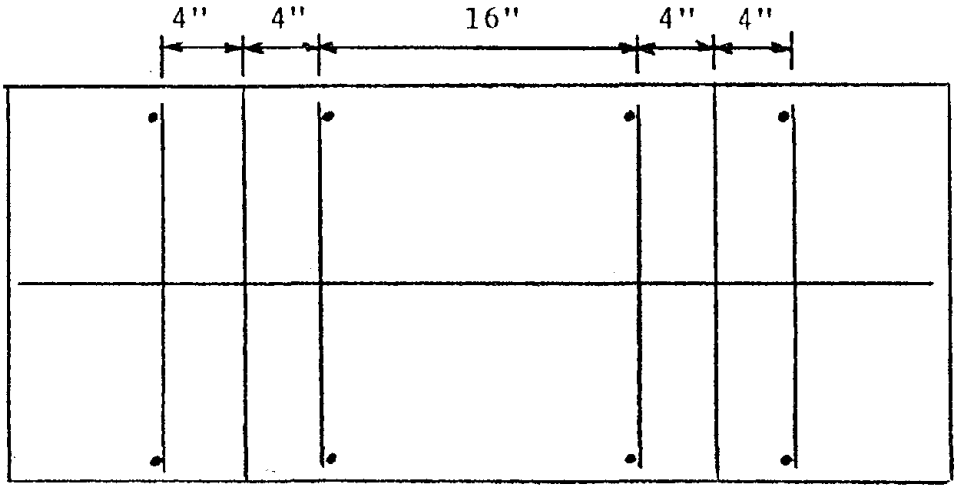

specimen 4

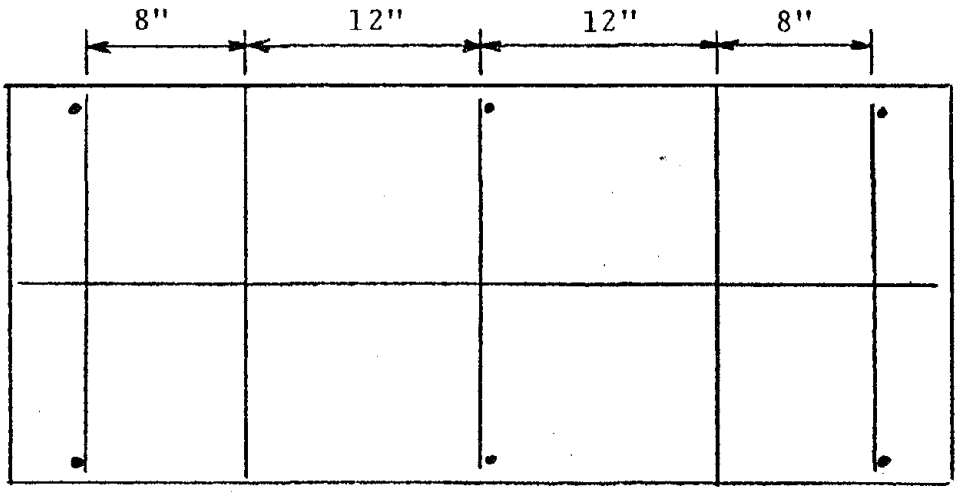

specimen 5

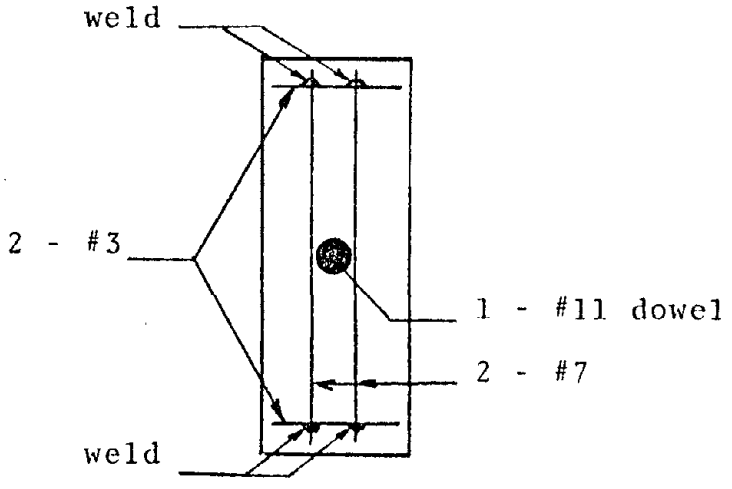

Fig. B12 - details of transverse steel in specimens 4 & 5

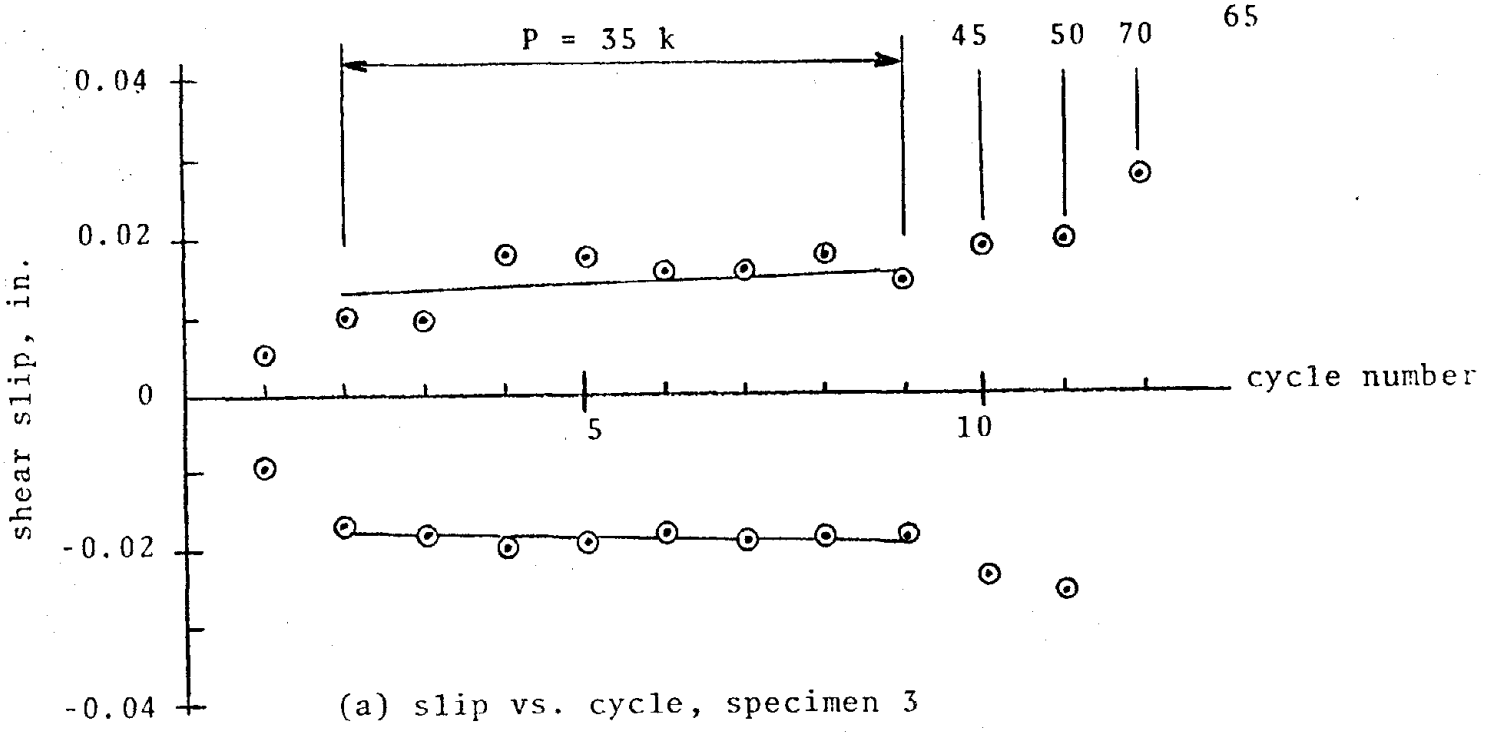

(a) slip vs. cycle, specimen 3

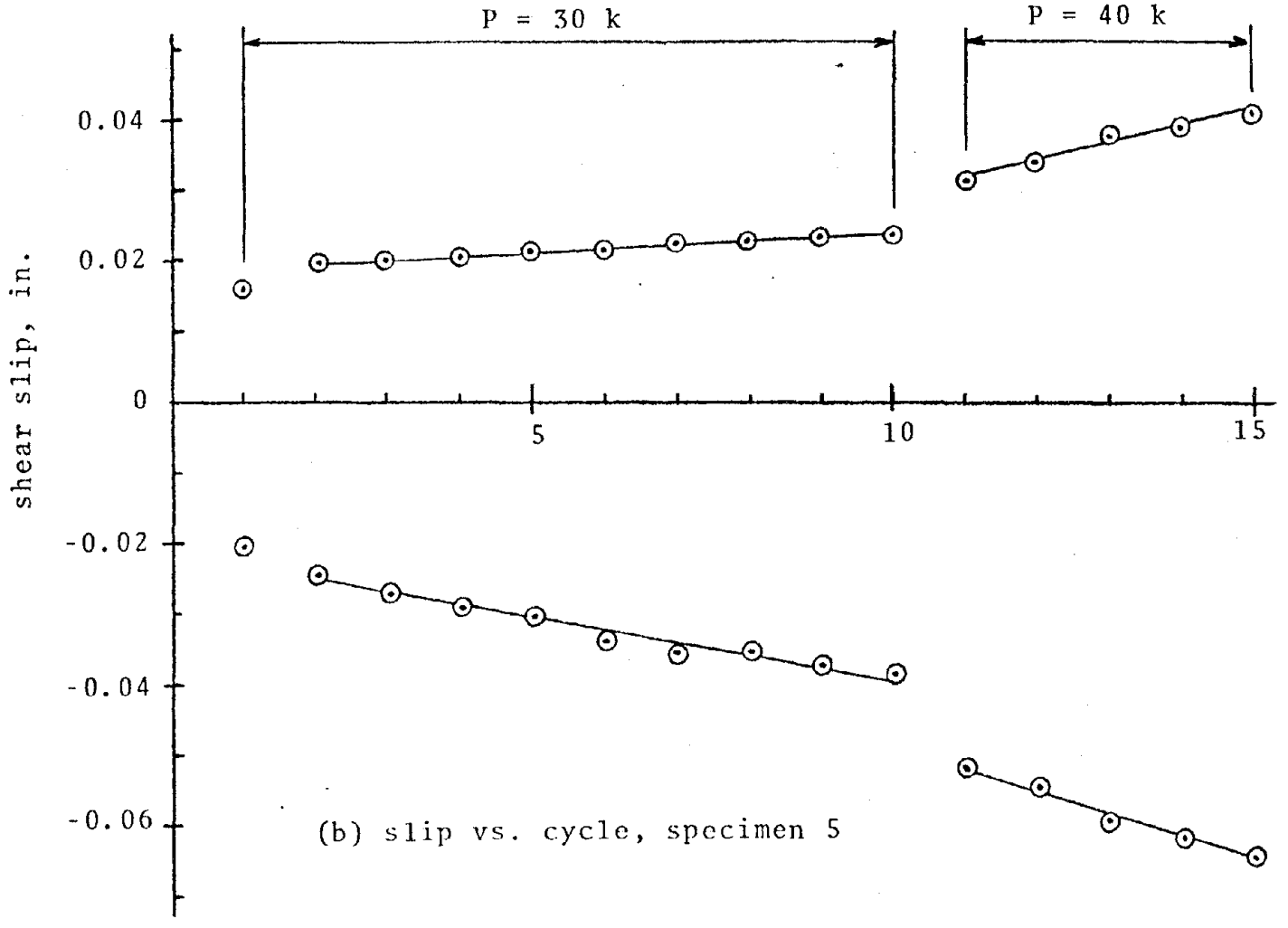

(b) slip vs. cycle, specimen 5

Fig. B13 - slip as a function of cycling, specimens 3 & 5

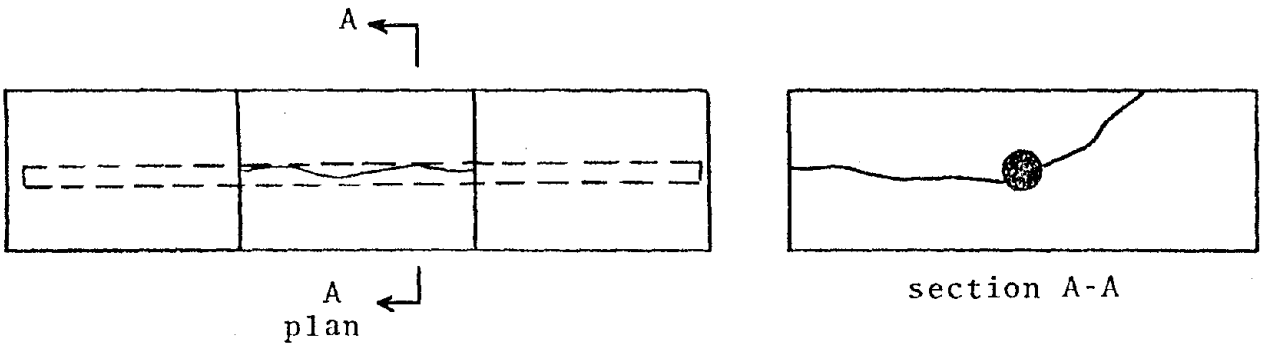

(a) specimen 3

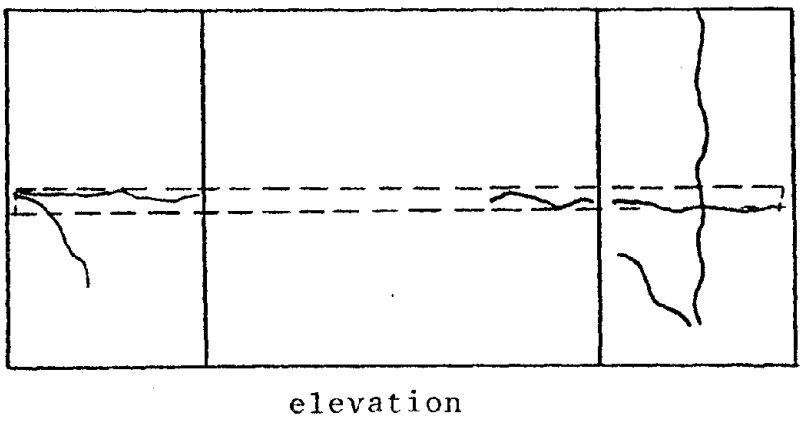

(b) specimen 5

Fig. B14 - failure modes of specimens 3 & 5

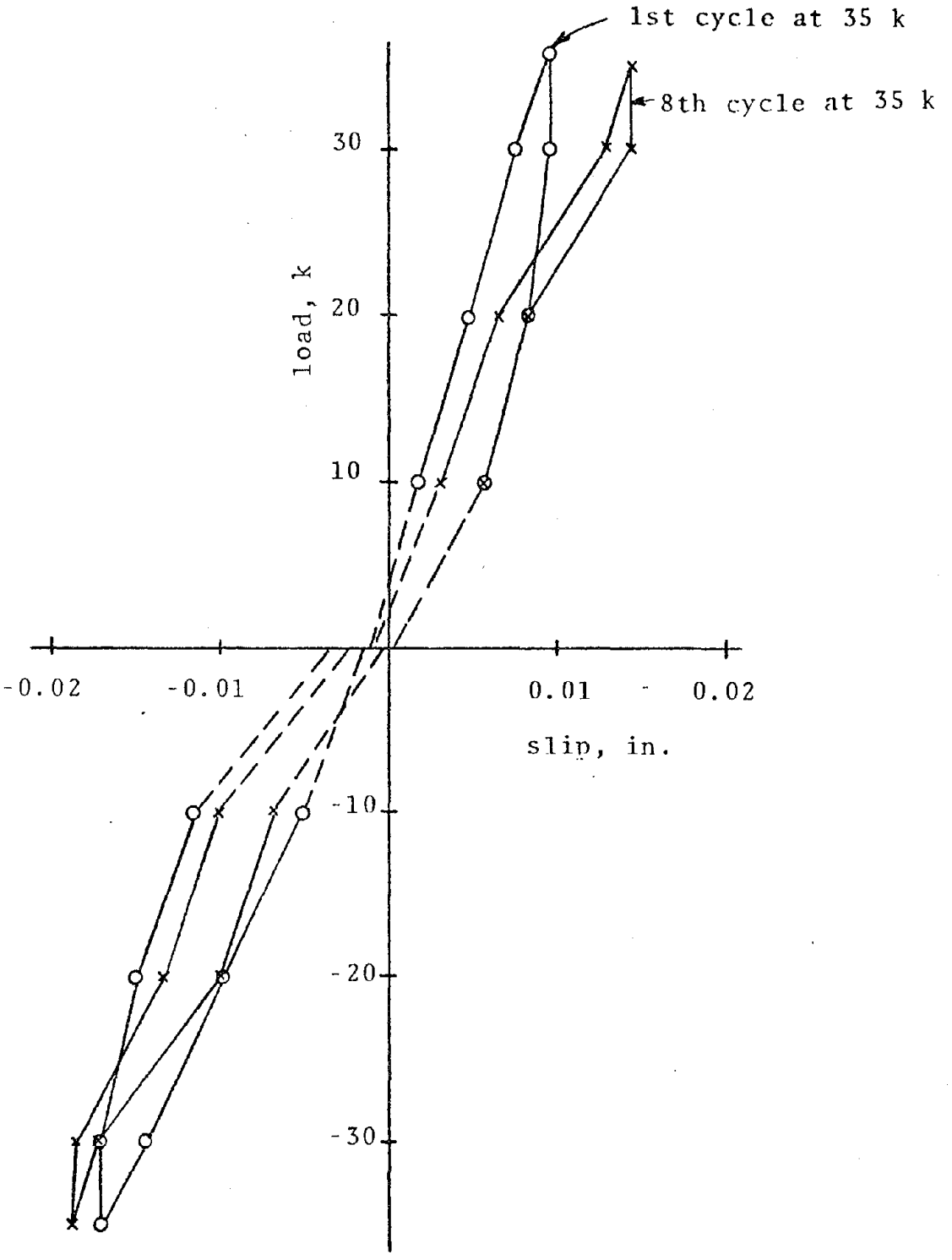

Fig. B15 - load vs. slip, specimen 3

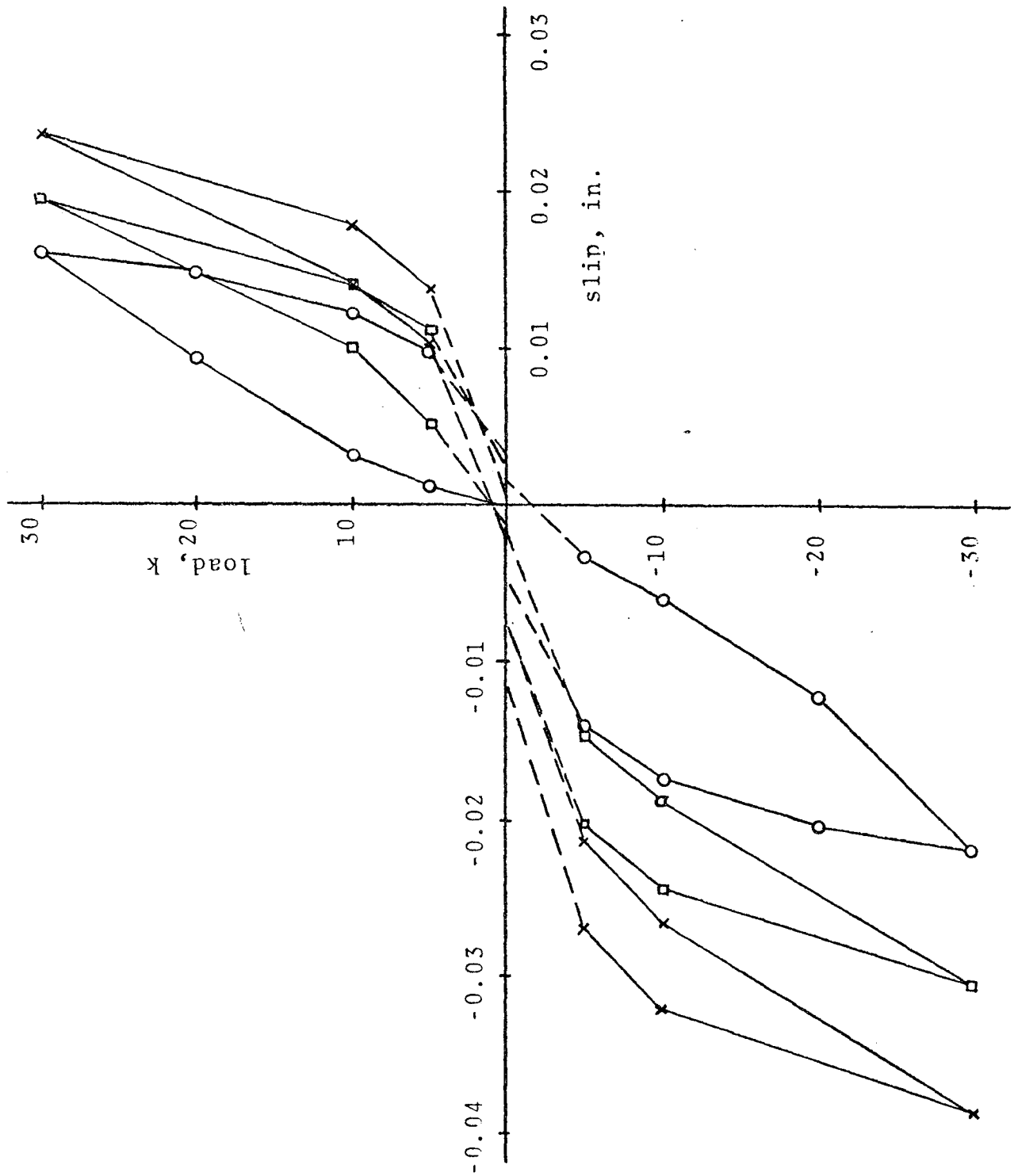

Fig. R16 - load vs. slip, specimen 5, cycled at ± 30 kips

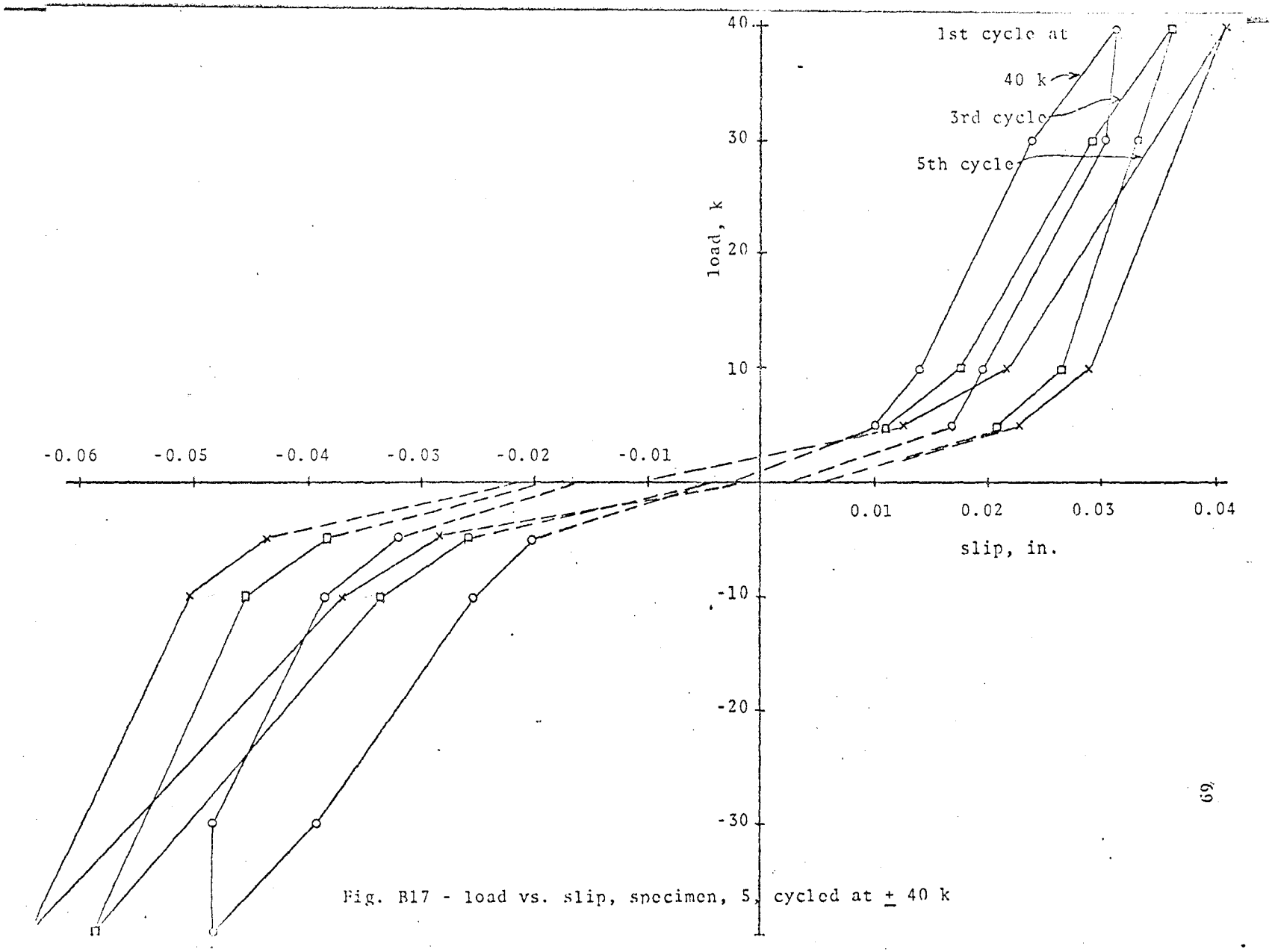

Fig. B17 - load vs. slip, specimen, 5, cycled at ± 40 k

C. LARGE-SCALE TESTS WITH COMBINED AXIAL TENSION AND DOWEL EFFECTS

The experimental program involving large-scale specimens was continued during the past year. In addition to the interface shear transfer and dowel force mechanisms, the effects of axial tension in the bars was studied. Such tension would occur in vertical bars of a nuclear containment vessel when internal pressure develops. Dowel bars are also in tension in other applications, such as in tall shear wall structures under severe seismic loads.

Two types of tests were used in this study. One was the same setup (Fig. C1) as employed from the beginning of the research, except the embedded #9 bars were tensioned to a certain stress level or until the initial crack width reached the desired magnitude. Two such block-type specimen tests are reported here.

The second type of test was essentially a large beam loaded transversely by two forces in such a manner that a plane of zero moment existed, (Fig. C5(a)). The specimens were precracked at this plane by tensioning the #14 longitudinal bar using an external force system. The transverse loads applied reversed cycling shear forces at the crack plane. Four specimens were tested.

Block Tests with Axial Tension

In the beam-type tests reported in the next section, the self-weight of both the specimen and the axial loading system made it difficult to achieve a uniform crack width at the shear plane before the iniation of the cyclic shear test. This problem was met by shifting away from the beam tests and using the modified block test setup shown in Fig. C1. In this test an independent frame is used to sustain the vertical tensile stresses applied to the reinforcing bars. A vertical beam distributes the applied horizontal load (shearing force) in the required proportions to the top and bottom concrete blocks. By moving the beams in the vertical plane, the shear stress acting in the shear plane is reversed. There is no moment at the crack location.

The specimen cross-sectional shearing area was 225 in^2. Four #9 reinforcing bars (ρ = 1.78%) extended through the 24 in. high specimen and were locked off against the independent stressing frame. The shear plane at mid-height of the specimen was formed

by tensioning the reinforcing bars. A crack-initiating groove formed into the specimen during casting controlled the crack location. The reinforcement was instrumented with internal strain gages, 3/8 in. gage length, placed 1 in. above and below the shear plane. The axial load induced in the reinforcement was measured by external strain gages.

After aligning the specimen in the loading frame, the crack at the shear plane was produced and an axial stiffness test was conducted to determine the reinforcement stress necessary to impose the desired crack width. Subsequently, the specimen was cycled for 25 cycles, of which cycles 1, 15, and 25 were loaded incrementally for detailed measurements of slip and reinforcing bar strains. An axial stiffness test was also conducted at the end of the cycling.

The results of two tests conducted on specimens with equal percentages of reinforcement (ρ = 1.78%) but different initial crack widths are presented.

The first specimen had an initial crack width of approximately 0.02 in. that was formed by tensioning the bars. The bars were stressed to 33.1 ksi during the simultaneous shear loading of $\pm$ 160 psi. In Fig. C2(a), the average horizontal slip is plotted against the applied shear stress for cycles 1 and 15. The shape of both curves may be roughly characterized by a bilinear relationship. Peak values of slip as a function of cycle number are shown in Fig. C3(a). Observations include:

a. The load at which "hardening" of the load-slip relationship is observed, decreases with increased cycling.

b. After the 15th cycle, there is no appreciable increase in the horizontal slip of the specimen (Fig. C3(a)).

c. The ability of the specimen to absorb energy decreased with increasing number of cycles.

The initial crack width of 0.02 in. did not increase measurably with increasing shear stress in any of the cycles, nor did it change with cycling (Fig. C3(a)). It was found, however, that maximum strains recorded by several internal strain gages were of the order of 2500 micro-in/in. (Fig. C4). The shape of the strain vs. shear load curve is very similar to that observed for horizontal

slip vs. shear load. The magnitude of the strains on the surface of the reinforcing indicates that the bars were partially plastic at 1 in. from the shear plane.

Specimen 2, also reinforced with four #9 bars, was tested with an initial crack width of 0.01 in. and an applied axial load during shear loading of 21.4 ksi. The horizontal slip is plotted against the applied shear stress in Fig. C2(b) for cycles 1 and 15, and maximum slip values for each cycle are given in Fig. C3(b). Comparing load-slip curves for specimens 1 and 2 (Figs. C2(a) and (b)), the following observations can be made:

a. For specimen 2, the shear stiffness during cycle 1 remains essentially constant up to maximum load, and it is higher than in specimen 1.

b. The horizontal slip attained at cycle 15 is approximately equal to that obtained in cycle 1 for specimen 1, showing the rather substantial reduction in slip as the initial crack width decreases.

The earlier observations (b) and (c) made for specimen 1 are also valid for specimen 2. As for specimen 1, there is little difference in crack width variation with increased cycling (Fig. C3(b)).

Further tests are underway to evaluate the effects of several important variables, namely, reinforcement diameter, level of axial stress in the reinforcement, concrete cover, and level of shear stress. Such tests are imperative to fully understand dowel action and interface shear transfer under cyclic loading.

Beam Tests

The beam-type specimen shown in Fig. C5(a) was loaded through two steel beams that reacted against the concrete specimen through rollers. With only the two rollers designated as (+) in position between the specimen and each loading beam, the shear and moment along the beam are as shown in Fig. C5(a). This load system produces shear but no moment at the critical shearing plane (neglecting dead weight effects). The direction of shear is reversed by removing the (+) rollers and loading through the four (-) rollers.

Each of the four beam-type specimens had a 225 in^2 shearing area with a single #14 reinforcing bar centrally located in the

specimen. The longitudinal bar was stressed until a crack occurred at the shear plane at mid-length. The weight of the beam and the tensioning frame produced variations in the crack width over the depth of the specimen. This configuration, which theoretically seems fine, was in reality very difficult to work with, particularly for the case of a single bar in the middle of the concrete.

In Specimen 1 the average crack width was about 0.020 in. and the axial force in the single #14 bar was 26 kips, or 12 ksi stress. At a shear stress of 100 psi the slip was 0.008 in. and the crack width increased by about 0.002 in. Unfortunately, the secondary reinforcement (which was about 4 in. away from the crack) was insufficient, and flexural cracks and subsequently large diagonal tension cracks developed because of the combined effect of tension and shear in the concrete. At a shear stress of 450 psi the test was discontinued. The inclination of the major diagonal crack was somewhat less than 45° from the axis of the beam and passed through the intersection of the bar axis and the shear crack.

Specimen 2 was identical to Specimen 1 and also had an average crack width of about 0.02 in. It was cycled twice at $\pm$ 100 psi shear stress with a bar tension of 16 ksi. Then four cycles at the same shear stress but with a bar tension of 29 ksi were applied, followed by two cycles at $\pm$ 125 psi and a bar tension of 29 ksi. In the latter stages, with the bar stressed to 29 ksi, the average peak crack width increased to about 0.026 in. The failure mode was similar to that in Specimen 1 and occurred at an applied shear stress of about 350 psi.

Fig. C6 shows the shear-slip relationships for cycling at 100 psi and 125 psi peak shear stress when the bar stress was 29 ksi tension. It can be seen that these curves are similar to those obtained in the block-type tests. However, comparison of the behavior of Specimen 2 with that of a block specimen with external reinforcing rods (no dowel action possible) shows that for the same level of loading, the former had slips about one-third those measured in the latter. This sharp reduction in slip is due to two causes: (a) dowel force in the #14 bar, and (b) increased effective axial stiffness of the bonded #14 bar as compared to the long external restraint bars of the block specimen. The relative magnitude of each contribution remains to be determined.

Specimens 3 and 4 had additional web reinforcement away from the shear plane and on either side of the level of the steel to prevent premature diagonal tension failure but not to restrict possible splitting along the steel. Strain gages were attached to the #14 bars at the shear crack.

The crack width was nonuniform in Specimen 3, 0.014 in. on top and 0.042 in. at the bottom at the beginning of the shear loading. Large slips occurred at low shear stresses, and cracking developed at a shear of 150 psi, as shown in Figure C7. The stress in the bar was about 28 ksi throughout the loading, measured outside the specimen. The internal gages were affected by local bending and the somewhat inconsistent readings have not yet been fully evaluated. The strains in the bars outside the specimens tend to decrease when shear is applied because of the overriding and crack width increase at the shear plane.

Specimen 4 is considered the most reliable since the initial crack width was uniform (0.025 in.) across the depth of the specimen. Accordingly, the results and discussion presented here are drawn mainly from this specimen. The axial stress applied to the bar was 28 ksi, and the loading history was:

a. cycles 1-15 at $\pm$ 100 psi shear stress
b. cycles 16-25 at $\pm$ 125 psi
c. cycles 26-30 at $\pm$ 150 psi

Major cracks appeared only in the 20th cycle, although several earlier cracks were caused by the axial tension alone. At 150 psi the cracks became very large (Fig. C8) and the test was stopped after the 5th cycle at this stress level.

Shear stress is plotted against slip in Fig. C9 and against crack width in Fig. C10. The behavior of each is similar to that observed in other tests. The rate of increase of peak slip values and crack width at peak loads are plotted in Fig. C11, where it is evident that behavior in the last 5 cycles (with 150 psi shear stress) was substantially different from the earlier cycles at lower stress levels. This may have been caused by additional internal cracking that was not visible, but that greatly decreased the effective axial stiffness of the bar and thereby increased the crack width, thus leading to larger slips. Or the reinforcing

bar could have undergone considerable yielding near the crack, which would increase the crack width and the level of slippage during shearing.

The results of these tests will be included in more detail in Fajardo's thesis, along with further analysis and discussion of these and other results.

3. Comparison of Various Test Results

Load-slip curves for several types of specimens are summarized in Fig. C12 (Ref. C1). Each curve was obtained during the 15th cycle of shear loading at the indicated stress levels. Curves A, B, and C were obtained from specimens with external restraint rods to give results for interface shear transfer alone (no dowel action with the condition of rather low axial stiffness. Curves D and E were measured on specimens that were cracked, separated to produce an initial crack width of 0.030 in., and then had four #11 reinforcing bars grouted in place with either 1 in. or 4 in. unbonded length at the shear plane. This eliminated most of the dowel action and also increased the axial stiffness of the restraining reinforcing that acts to prevent the crack from opening. Curve F is combined interface shear transfer and dowel action and was obtained from a beam-type specimen with parameters as indicated.

The basic shapes of both loading and unloading branches of all the curves in Fig. C12, B16, and A8 are quite similar for the three cases of interface shear transfer alone, dowel action alone, and combined interface shear transfer and dowel action. A rational model of shear transfer that incorporates all important parameters is under development. The effects of biaxial tension in the specimen may alter the behavior substantially because of the cracking that is expected to occur under these more severe stress conditions.

REFERENCES:

C1. Gergely, P., Stanton, J., and White, R.N., "Behavior of Cracked Concrete Nuclear Containment Vessels During Earthquakes", Proceedings, 1975 U.S. National Conference on Earthquake Engineering, June 1975.

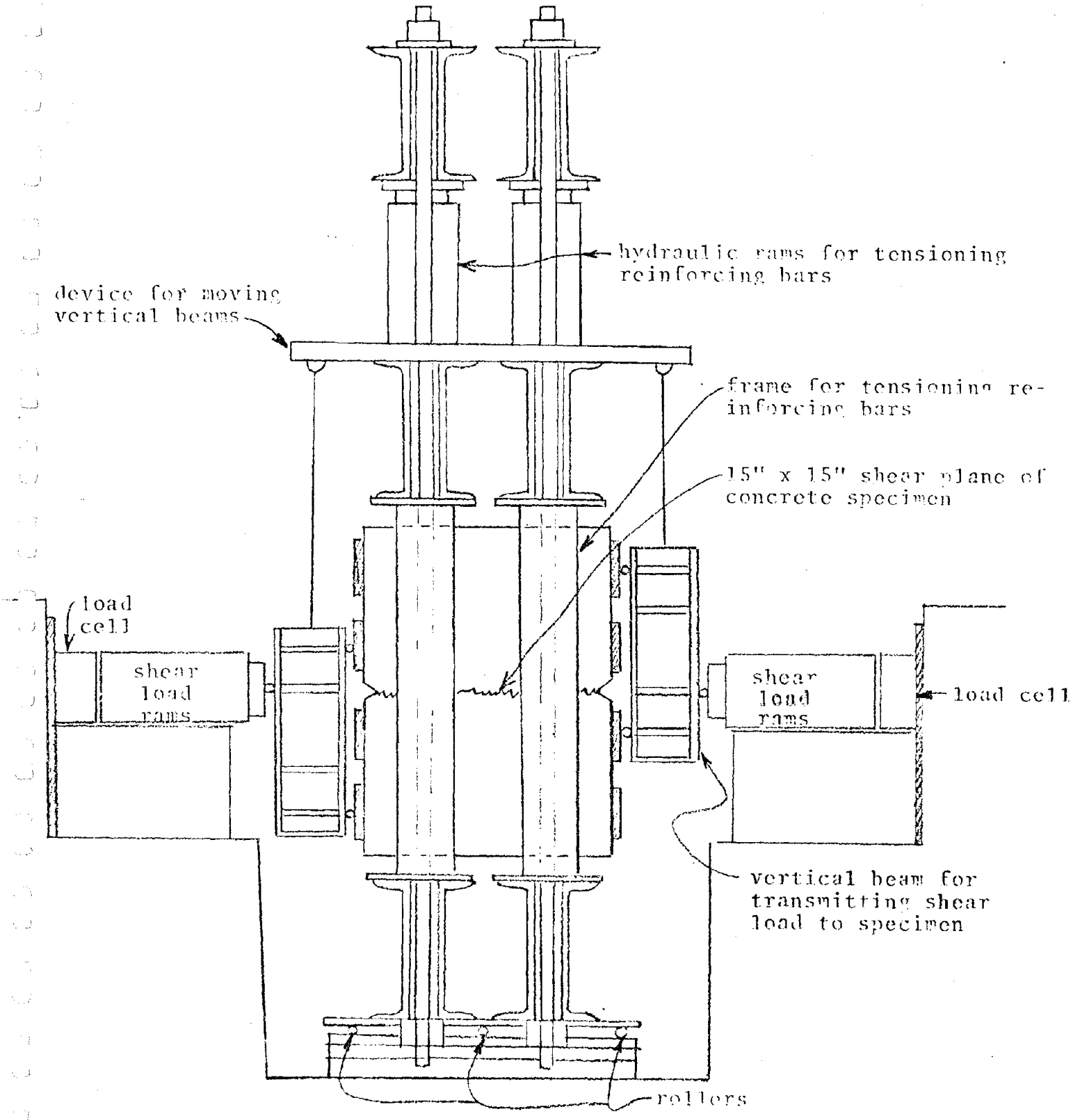

Fig. C1 - test specimen (reinforced with 4 - #9 bars)

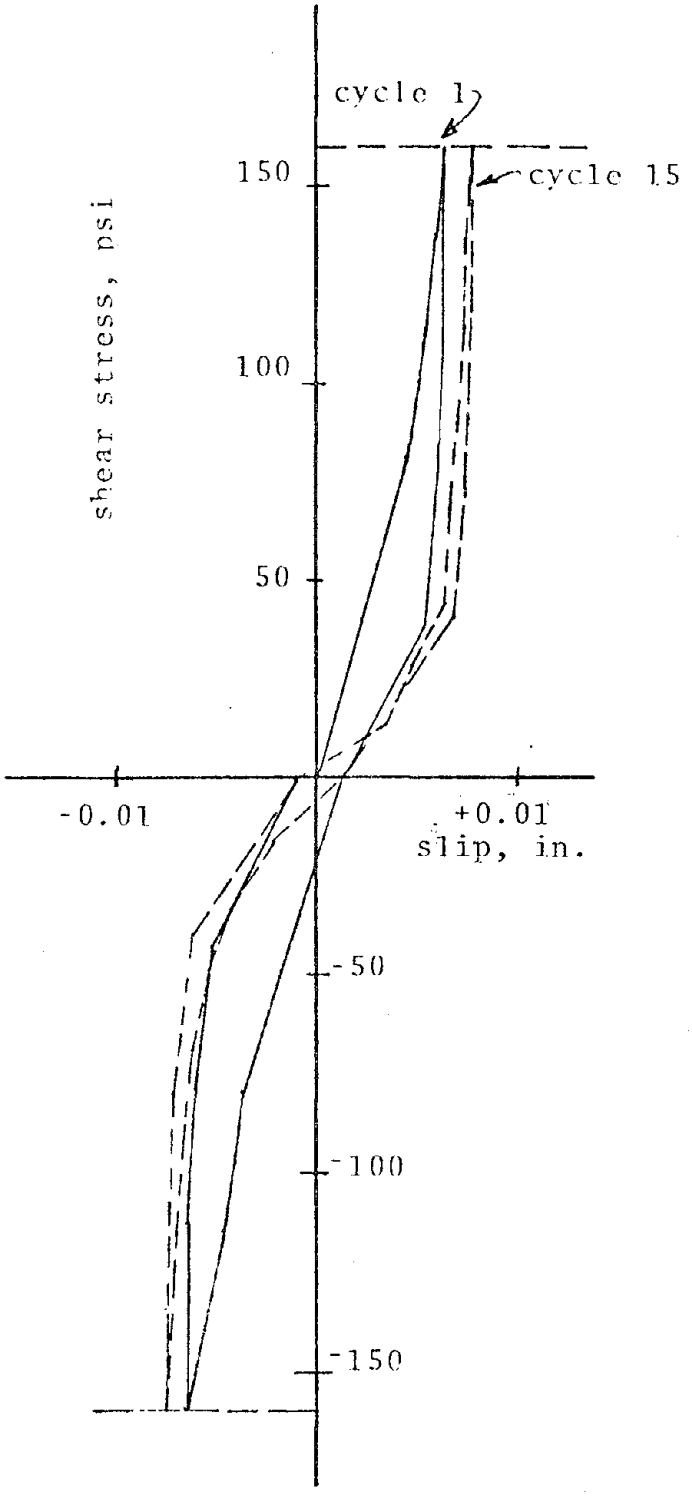

(a) specimen 1; initial crack width = 0.02 in.

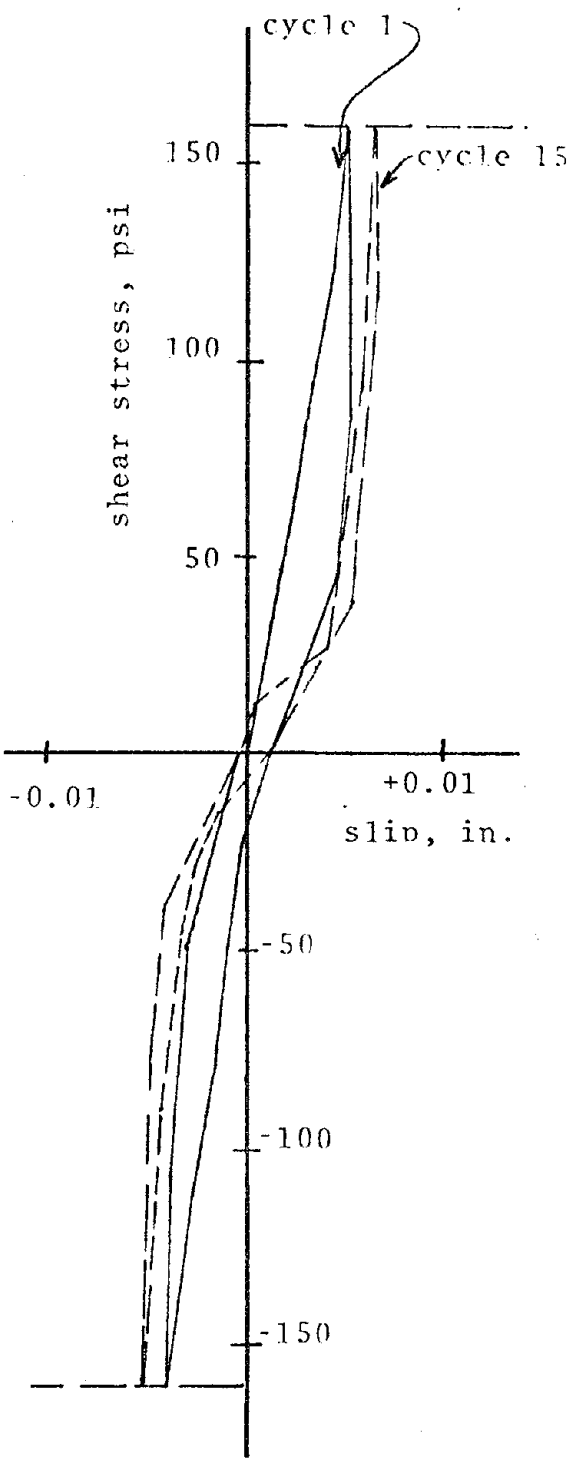

(b) specimen 2, initial crack width = 0.01 in.

Fig. C2 - load-slip curves

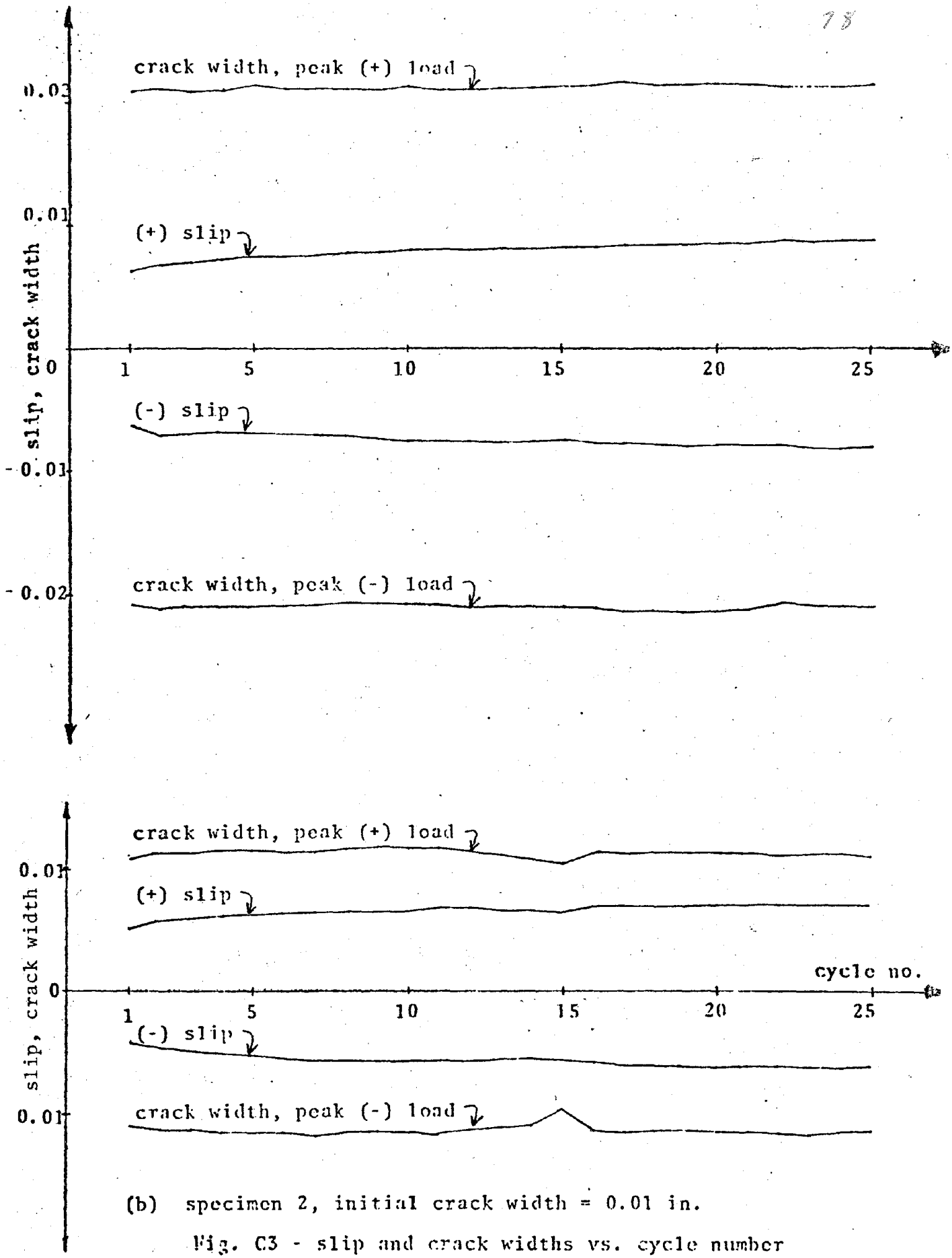

(b) specimen 2, initial crack width = 0.01 in.

Fig. C3 - slip and crack widths vs. cycle number

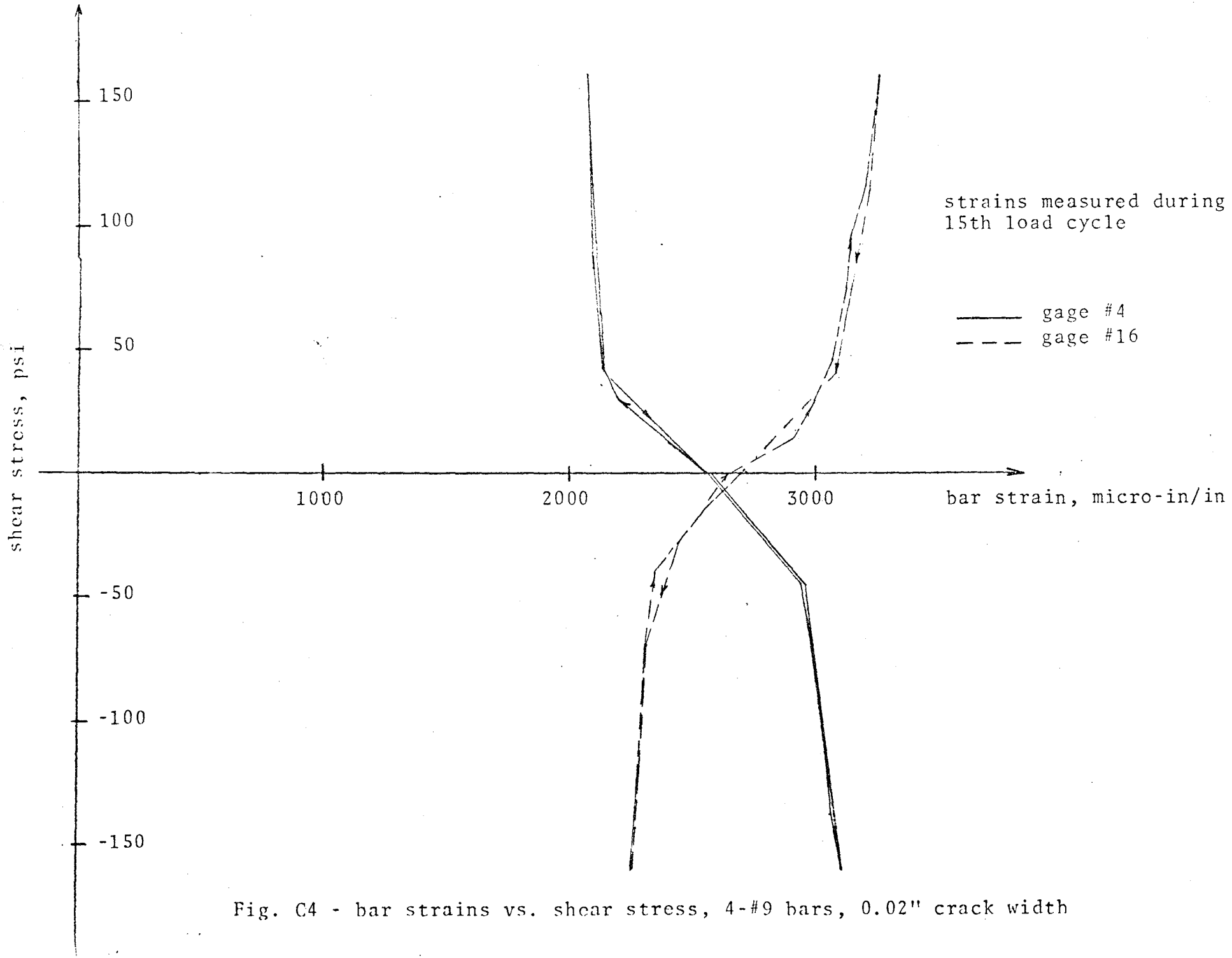

Fig. C4 - bar strains vs. shear stress, 4-#9 bars, 0.02" crack width

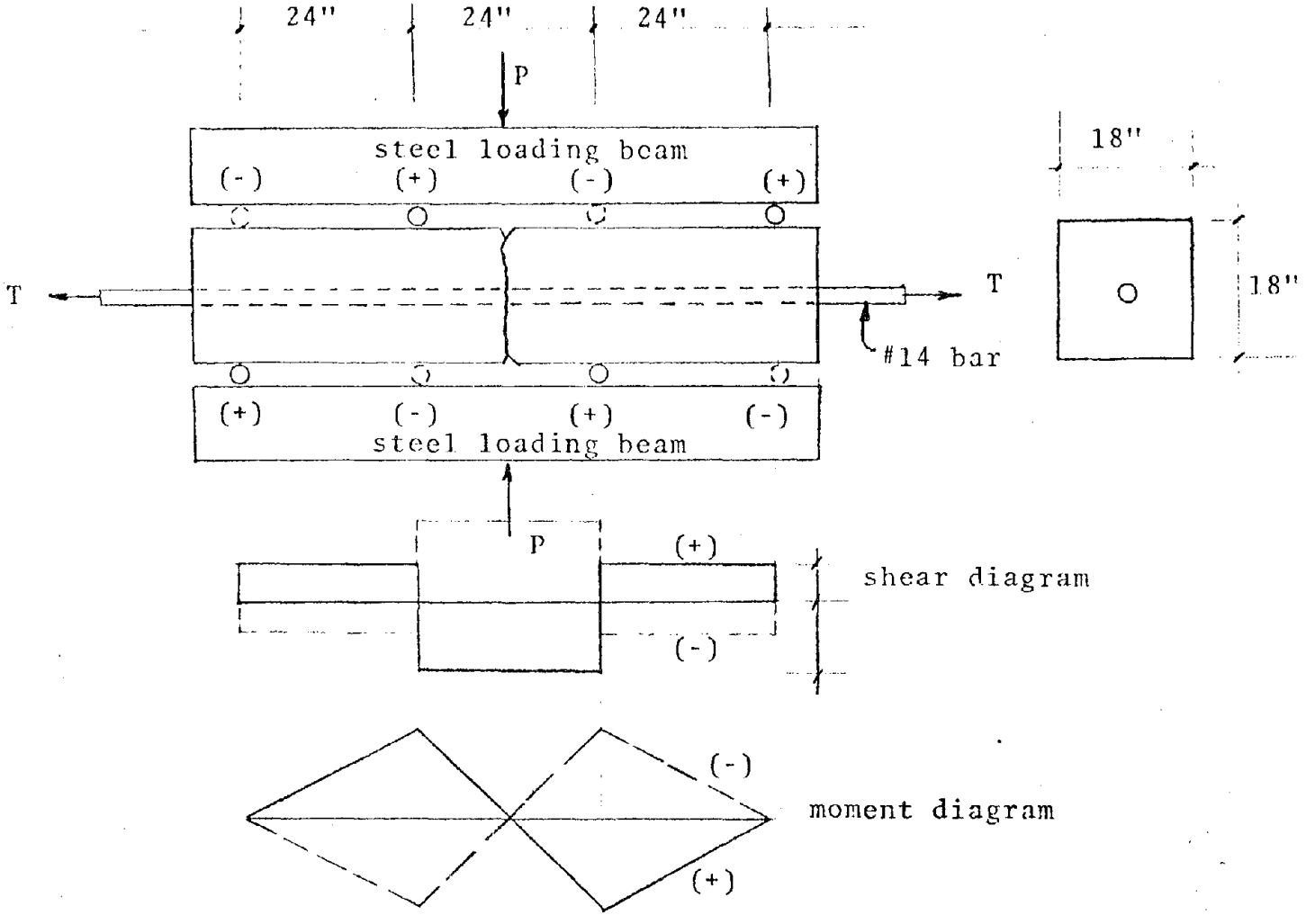

(a) loading system to induce cyclic reversing system

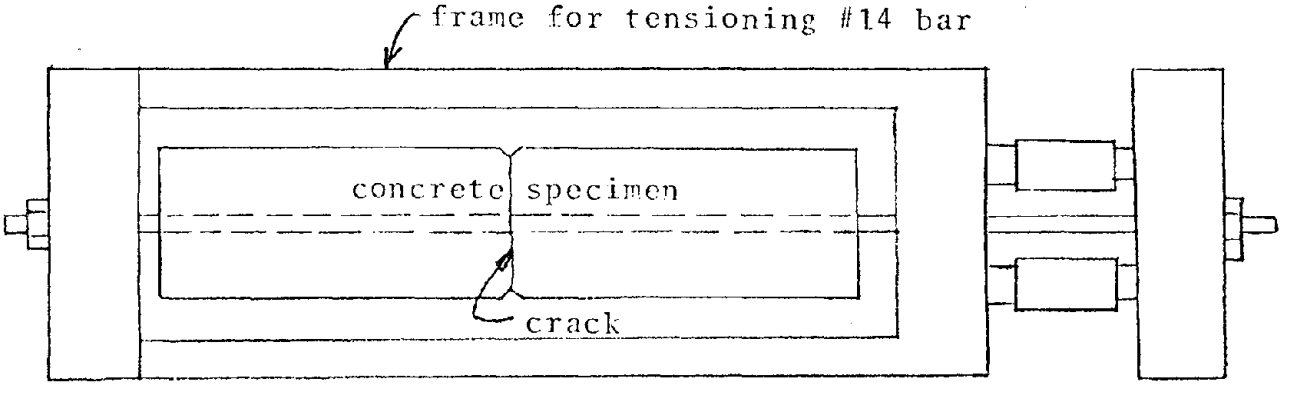

(b) plan view of test specimens and frame

Fig. C5 - beam-type specimen

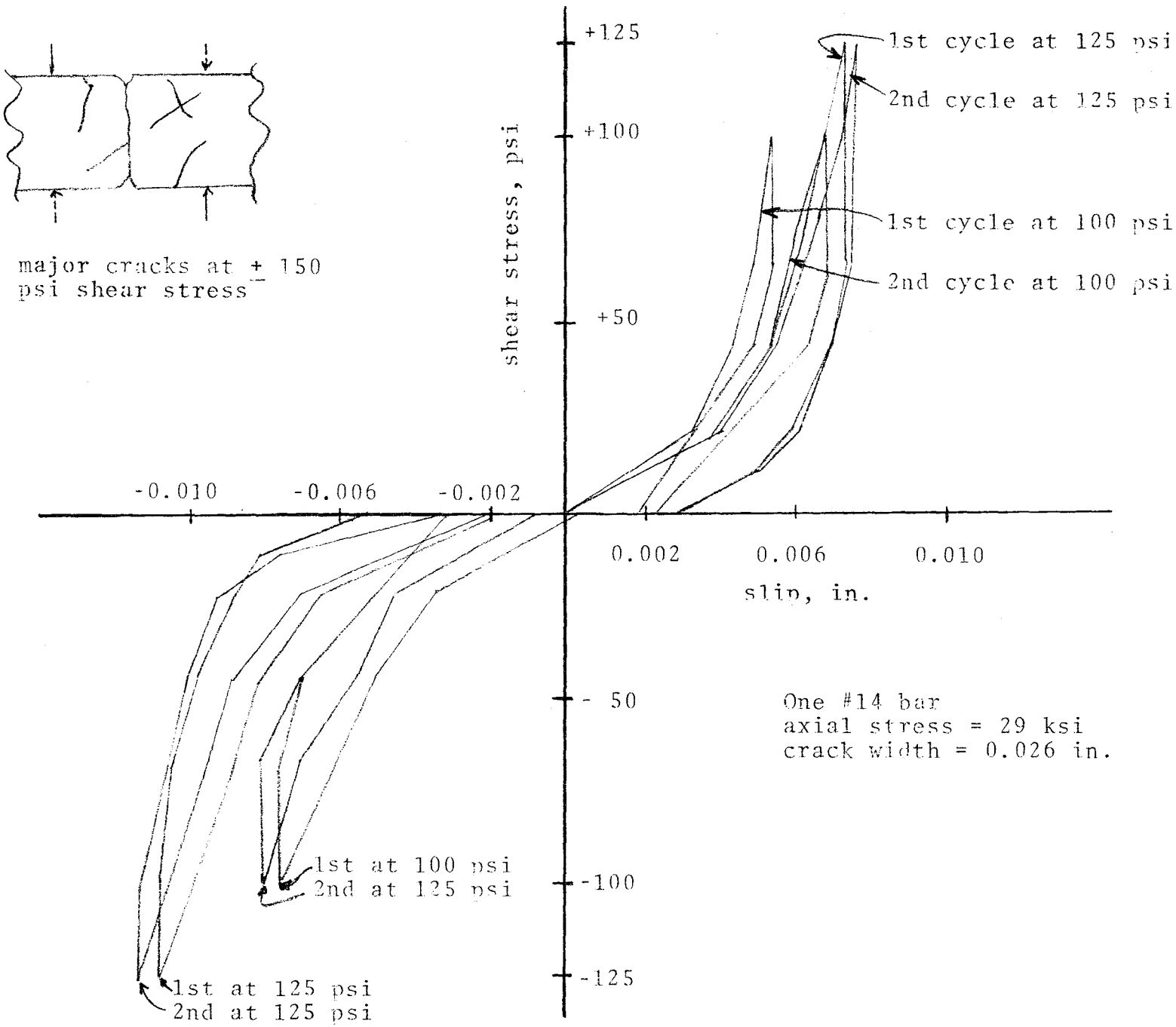

Fig. C6 - load-slip relationships, beam #2

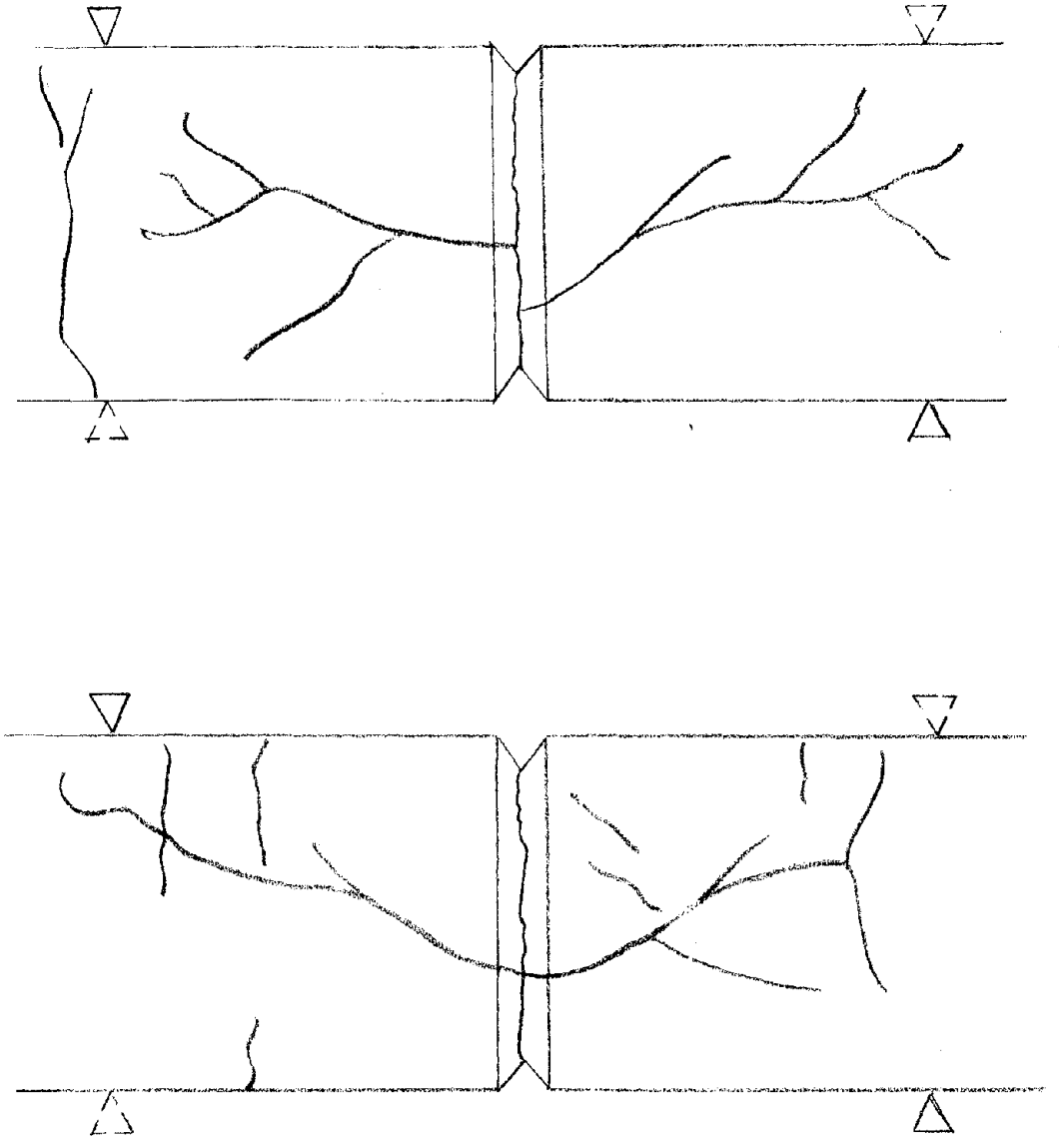

Cracks developed after 2 cycles at 150 psi (point at which test was stopped).

Fig. C7 - cracking patterns, beam 3

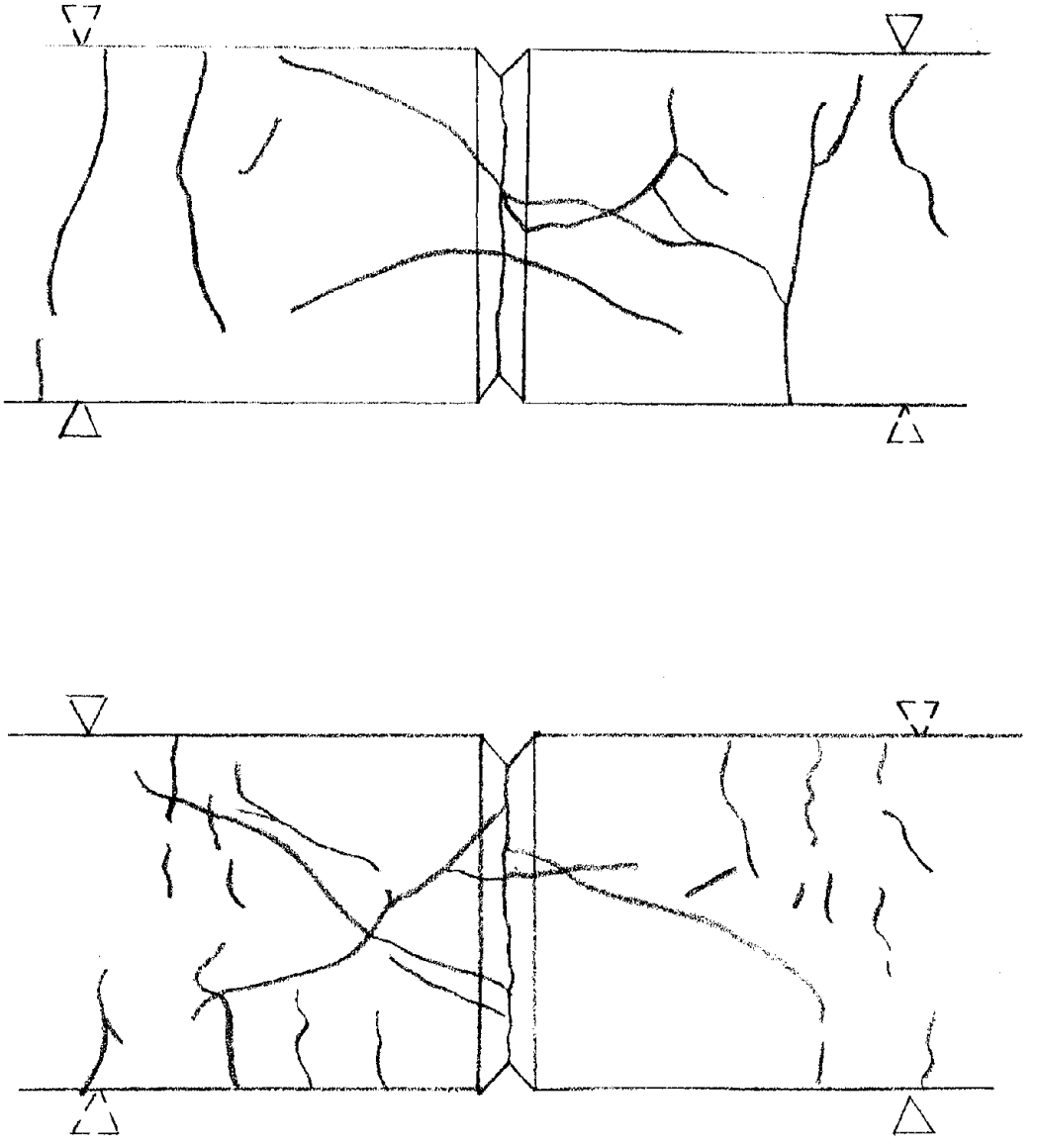

Cracks developed after 5 cycles at 150 psi (total of 30 loud cycles).

Fig. C8 - cracking patterns, beam 4

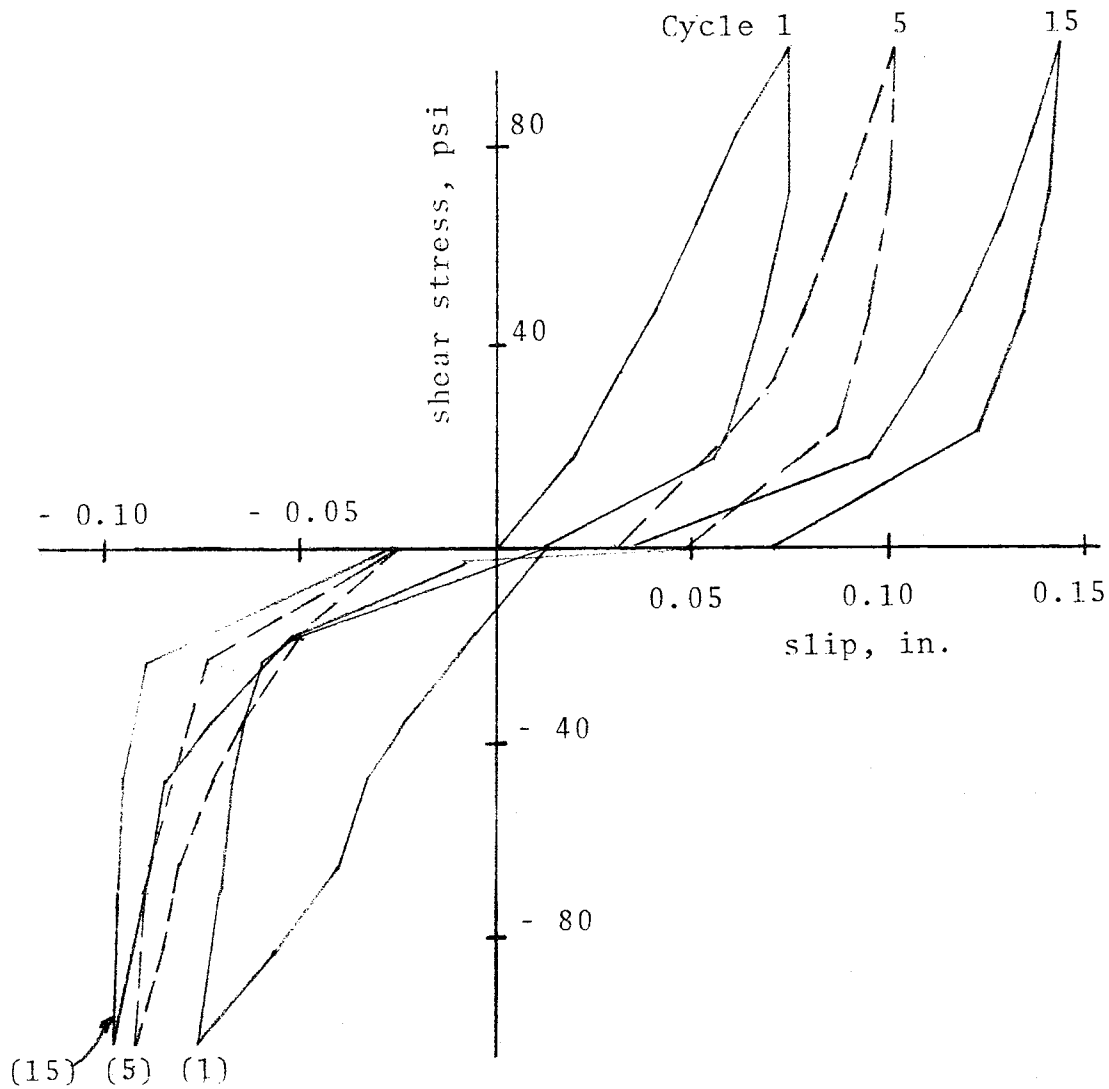

Fig. C9 - slip vs. shear load, beam 4 (cycles 1, 15, and 25)
(see also next sheet)

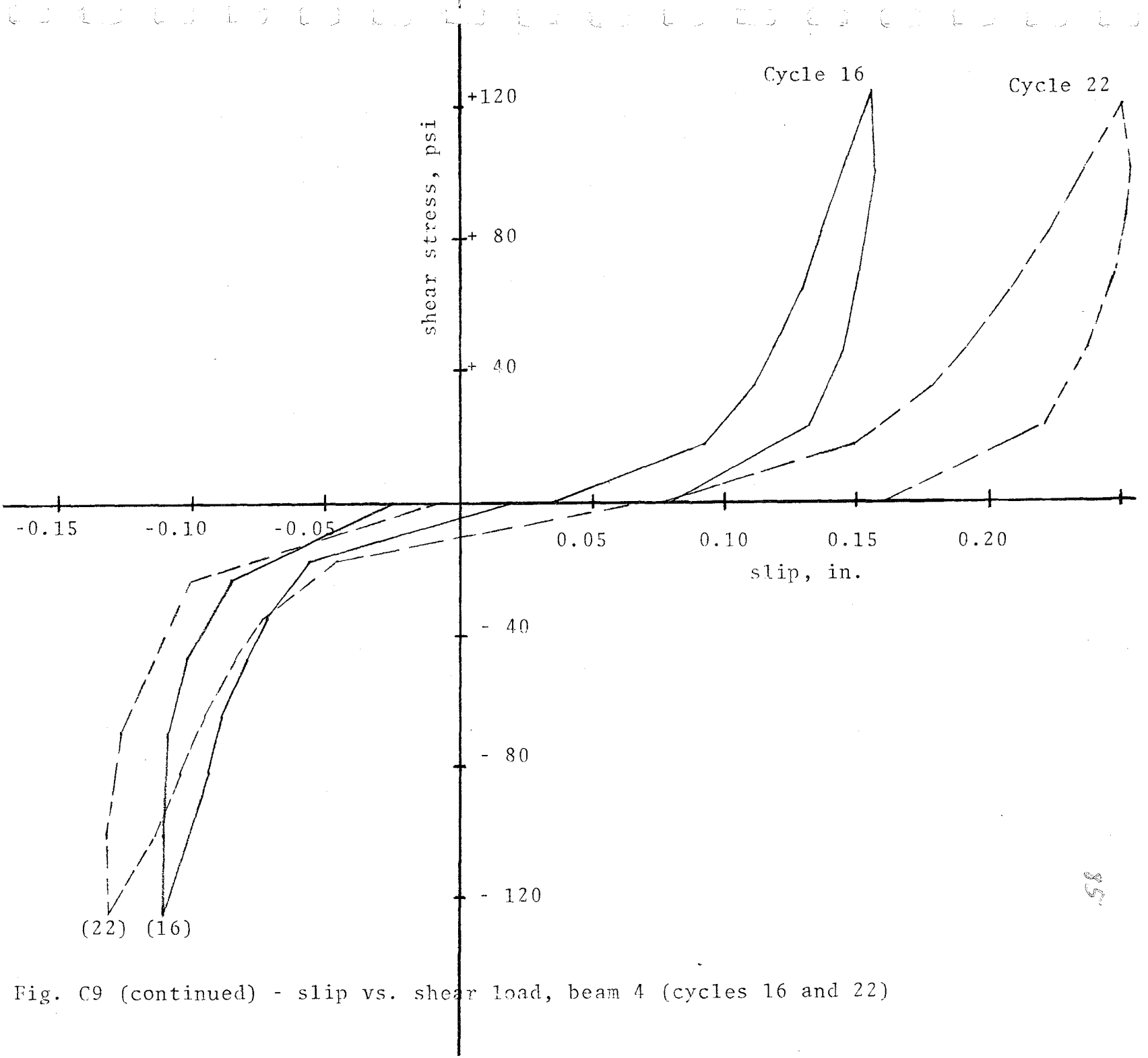

Fig. C9 (continued) - slip vs. shear load, beam 4 (cycles 16 and 22)

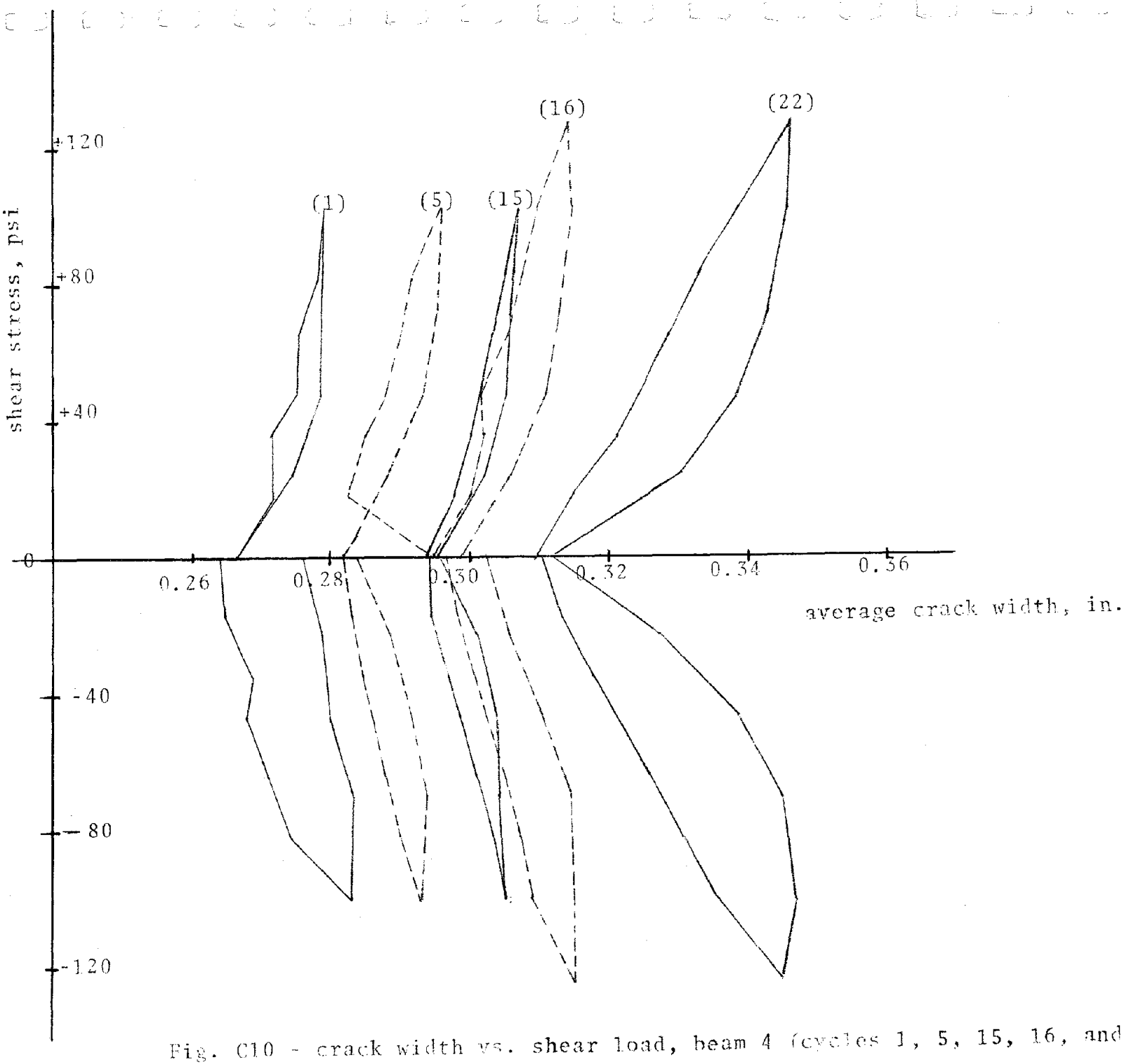

Fig. C10 - crack width vs. shear load, beam 4 (cycles 1, 5, 15, 16, and 22).

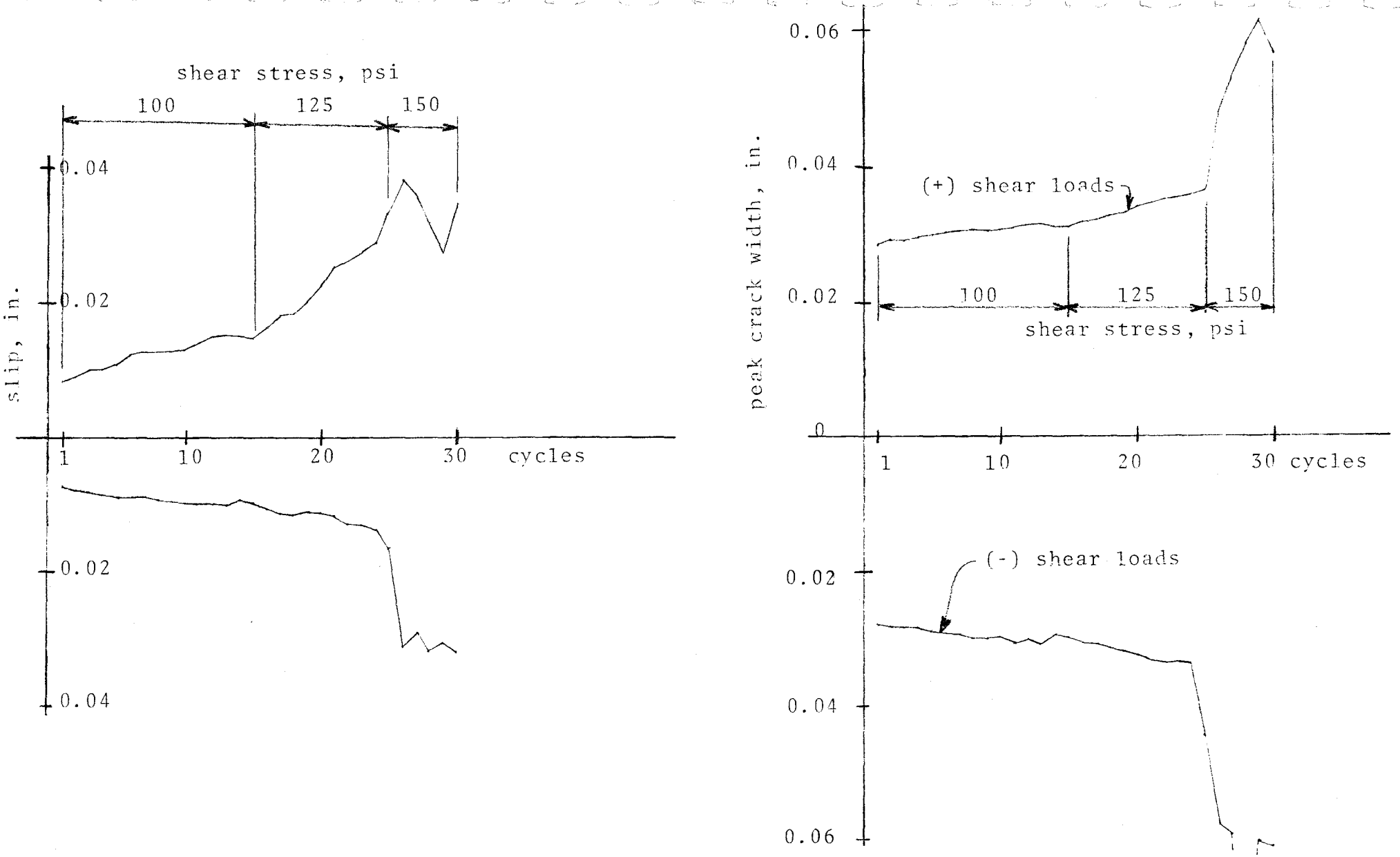

Fig. C11 - slip and crack width vs. cycle number, specimen 4

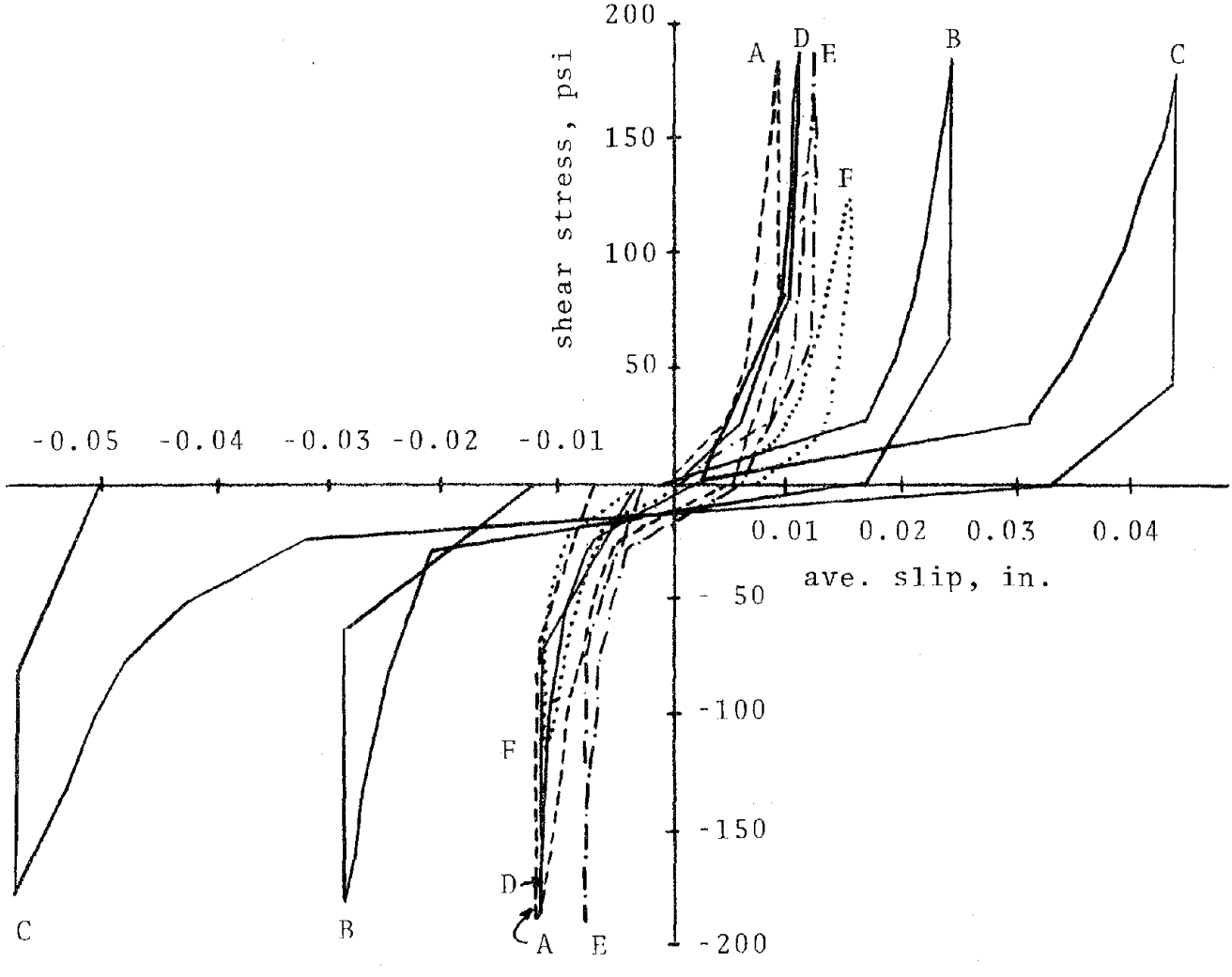

legend

A. 0.010 in. initial crack width
B. 0.020 in. initial crack width
C. 0.030 in. initial crack width
} external restraint bars

D. Four #11 embedded bars, 0.030 ICW and 1 in. unbonded length
E. Four #11 embedded bars, 0.030 ICW and 4 in. unbonded length
F. One #14 embedded bar, 28 ksi tension, 0.030 in. ICW

Fig. C12 - typical hysteresis curves during 15th load cycle